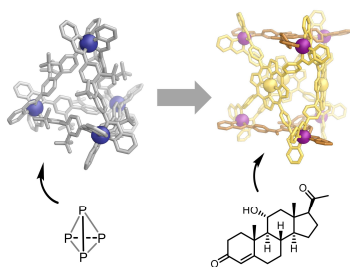# Beyond Platonic: How to Build Metal-Organic Polyhedra Capable of Binding Low-symmetry, Information-rich Molecular Cargoes

Charlie T. McTernan,[§] Jack A. Davies,[§] Jonathan R. Nitschke*

Yusuf Hamied Department of Chemistry, University of Cambridge, Lensfield Road, Cambridge, CB2 1EW, United Kingdom

§ = CTM and JAD contributed equally to this manuscript.

* jrn34@cam.ac.uk

Contents:

1. Introduction

1.1 Overview

The field of metallosupramolecular chemistry has advanced rapidly in recent years. Much work in this area has focused on the formation of hollow self-assembled metal-organic architectures and exploration of the applications of their confined nanospaces.[1-5] These discrete, soluble structures incorporate metal ions as 'glue' to link organic ligands together into polyhedra. Their hollows have found applications in binding and sensing guests,[6-8] stabilizing reactive molecules,[9-13] and catalyzing reactions as enzymes do.[14-19] Most of the architectures employed thus far have been highly symmetrical, as these have been the easiest to prepare (Figure 1).[20] An understanding of the design principles underpinning the formation of high-symmetry metal-organic cages,[1] such as tetrahedra,[21-24] cubes[25-28] and octahedra,[29-34] has enabled their synthesis and application.[35-38] Modification of these structures, either before or after assembly,[39-41] can imbue them with new functions.[42] Such functions include the modulation of guest-binding properties,[43-46] phase-transfer (whereby a capsule and its cargo are induced to move between phases),[47,48] and enabling the formation of higher-order metal-organic cage-based materials.[49-56]
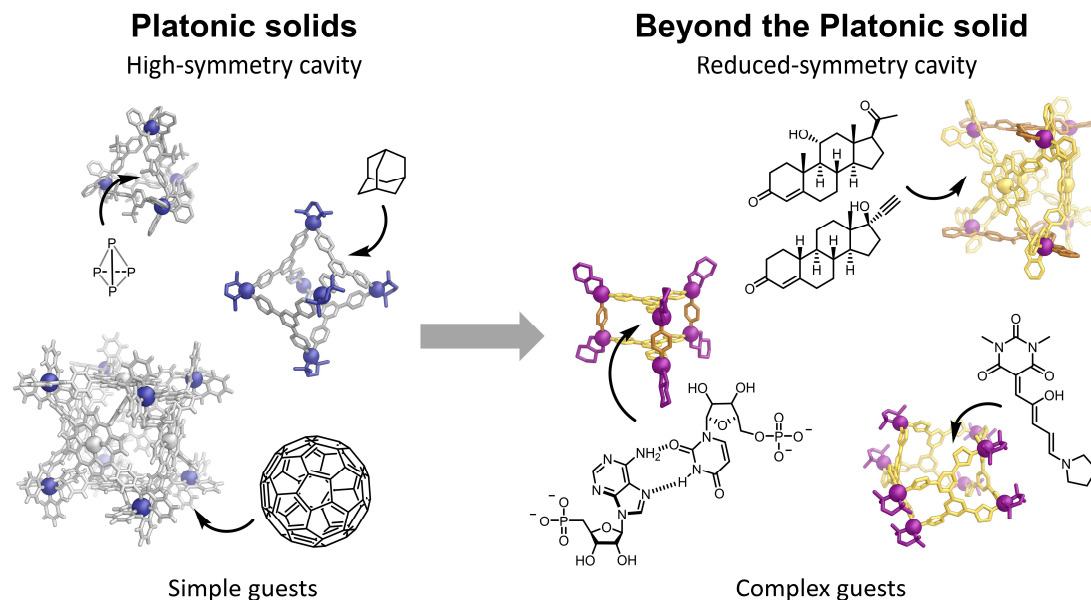
Figure 1. Examples of coordination cages with structures corresponding to Platonic solids, which are well-adapted to pseudo-spherical guests, contrasting with more complex 'beyond Platonic' cages, which are primed for binding anisotropic guests.[25,35,36,59,62-64]

Such high-symmetry structures contain pseudo-spherical cavities, and so bind roughly spherical guests optimally,[25,35-38] although asymmetric guests can also be encapsulated.[10,12,20,57-59] In some cases more than one smaller guest is bound within a relatively large cavity,[57] or the flexibility of a guest enables it to adopt a folded conformation with a complimentary size and shape for the cage cavity.[18,59,60]

Biomolecules and high-value synthetic compounds are rarely isotropic, highly-symmetrical species.[61] To bind, sense, separate, and transform such substrates, new, lower-symmetry, metal-organic cages are needed. In response to this need, recent work has focused upon the construction of metal-organic cages with interior cavities of reduced symmetry.

Many early examples of lower-symmetry structures were discovered serendipitously. Only a limited number of structure types beyond the Platonic solids were prepared using established

design principles. The great promise of lower-symmetry structures to bind lower-symmetry guests selectively (Figure 1) has motivated efforts to decipher the rules underpinning the formation of complex architectures.[62-64] Herein we will outline different approaches, which taken together form the first draft of a handbook for the design of higher-complexity, lower-symmetry, self-assembled metal-organic architectures.

1.2 Classification of Approaches

The design of metal-organic architectures has been discussed in terms of the following four strategies: the directional-bonding approach,[1] the symmetry-matching approach,[65] the molecular-paneling approach,[66] and the weak-link approach.[67-69] Each of these strategies has been employed to form metallomacrocycles or high-symmetry three-dimensional architectures, often with Platonic geometries. With careful consideration, these design strategies can also be employed to form lower-symmetry structures, deviating from the Platonic solids. However, in this review we have opted for a method of classification which deviates from the strategies noted above, because approaches enabling the formation of more complex metal-organic assemblies have recently been established that do not neatly fall within these categories. We focus instead upon the properties of the building blocks, along with reaction conditions. This organization lends itself to the aim of this review article - to act as a preliminary guide for the further design of complex self-assembled architectures.

Using this building-block/reaction condition-based classification, we have identified six broad categories of approach (Figure 2): *(1) Heteroleptic Assemblies, (2) Lower-symmetry Ligands, (3) Ligand Flexibility, (4) Complexity derived from Solvent, Anions and Templates, (5) Multimetallics: Heterometallic and Cluster-containing Architectures, and (6) Geometric Constraints*.
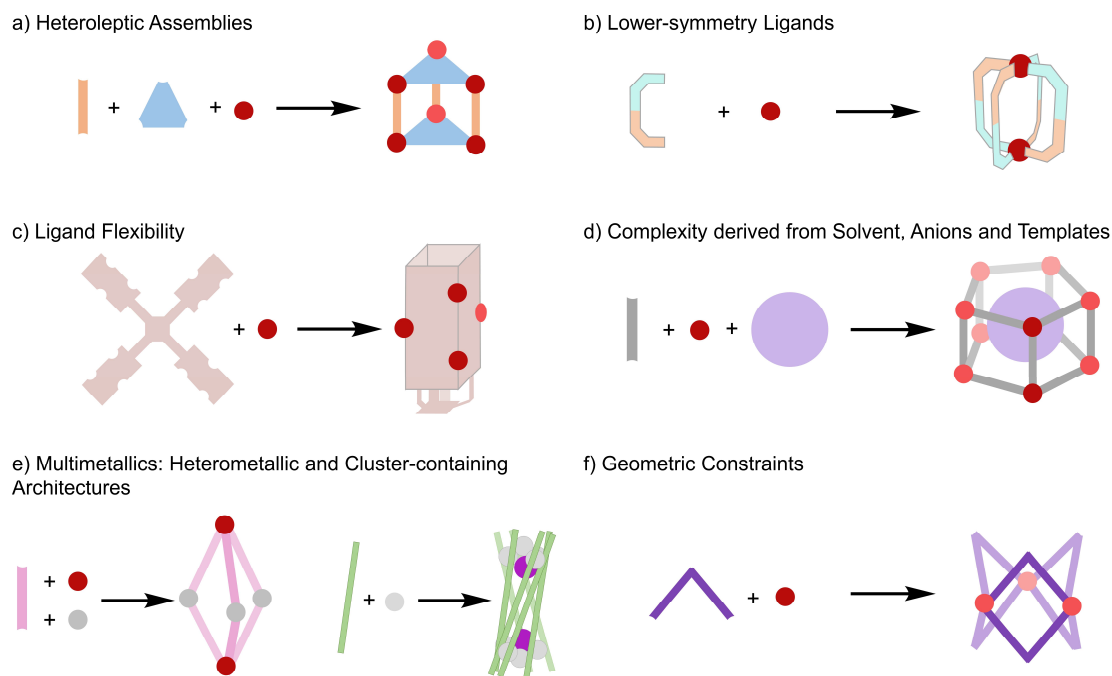
Figure 2. Categorization of approaches to forming complex metal-organic architectures.

Heteroleptic architectures incorporate multiple different ligands (Figure 2a). A particular challenge in this approach is to ensure that the different building blocks integrate into a single product, rather than segregating to form simpler structures that each contain only one type of building block. One strategy developed to overcome this challenge involves harnessing the enthalpic and entropic driving forces that govern self-assembly in order to favor a heteroleptic structure.

A similarly intuitive approach involves the use of ligands with greater structural complexity or reduced symmetry, which then translate to the assembly of more complex three-dimensional architectures (Figure 2b).

Flexibility is often incorporated within ligands by the addition of alkyl spacers. Such enhanced flexibility can increase the array of feasible structures, in comparison to the use of more rigid ligands, but also decrease the predictability of the self-assembly process (Figure 2c).

Complexity based upon solvent, anion and template effects relies upon altering the self-assembly reaction conditions in order to favor structural complexity (Figure 2d). This method is well-established for producing complex metal-organic architectures. However, as with enhancing ligand flexibility, predicting the outcome of self-assembly using this approach can be challenging.

Multimetallic architectures either contain more than one type of metal center, or have vertices that consist of homo-metallic clusters. Both cases can introduce co-ordinational flexibility, enabling the formation of architectures with increased structural complexity (Figure 2e).

The sixth approach to generating complex structures in a controlled and predictable manner is the incorporation of geometric constraints into ligands. These geometric constraints can act to frustrate the formation of simpler structures, thus favoring the construction of architectures with greater complexity (Figure 2f). Examples which use steric control or noncovalent interactions to form complex metal-organic structures are also highlighted in this section.

1.3 Scope of the Review

This review focuses on techniques used to prepare metal-organic architectures by self-assembly of organic ligands and metal ions. Some complex structures that form with metal-cluster cores, or with metal clusters as vertices,[70-72] are also included. The term 'complex structure' within this review generally refers to structures that deviate from a framework corresponding to one of the high-symmetry Platonic or Archimedean solids. Some examples of structures that outwardly resemble these simple polyhedra, but with reduced symmetry, are included, particularly when the source of the reduced symmetry can be determined.

Although a key motivation for this review is to aid those who might wish to design new lower-symmetry structures for new applications, we focus on construction principles as opposed to the utility and functions of these structures. As the field that we attempt to cover is wide-ranging and fast-moving, omissions in our coverage will be inevitable. We apologize for these in advance.

2. Heteroleptic Assemblies: Incorporation of Multiple Ligands Generates More Complex Architectures

The complexity of metal-organic assemblies can be increased through the use of combinations of multiple ligands, particularly those having different topicities, i.e. with different numbers of metal-binding sites per ligand. In principle, combinations of multiple ligands with different shapes can allow the emergence of unusual architectures with complex geometries. In practice, however, achieving the selective formation of a single structure from a range of possibilities can be challenging. This section explores ways in which this challenge has been overcome, focusing on approaches that may allow general routes to heteroleptic structures.

2.1. Heteroleptic Selectivity by Destabilization of Homoleptic Assemblies

The selective assembly of a single heteroleptic metal-organic architecture is often entropically disfavored. For example, a square planar metal vertex coordinated by two equivalents of two different ligands through monodentate donors (i.e. $ML^1_2L^2_2$) may co-exist with other mixed ligand (i.e. $ML^1_1L^2_3$, $ML^1_3L^2_1$) and homoleptic (ML^1_4, ML^2_4) vertices. One way to overcome this tendency is to build in an enthalpic driving force for heteroleptic assembly. Stang *et al.* found that the principle of charge separation could drive the assembly of less-symmetric structures.[73] This approach, shown in Figure 3, depends on the use of platinum(II) centers with two strong-field ligands in a *cis* configuration, and both pyridine (**1**) and carboxylate (**2**) donor ligands.
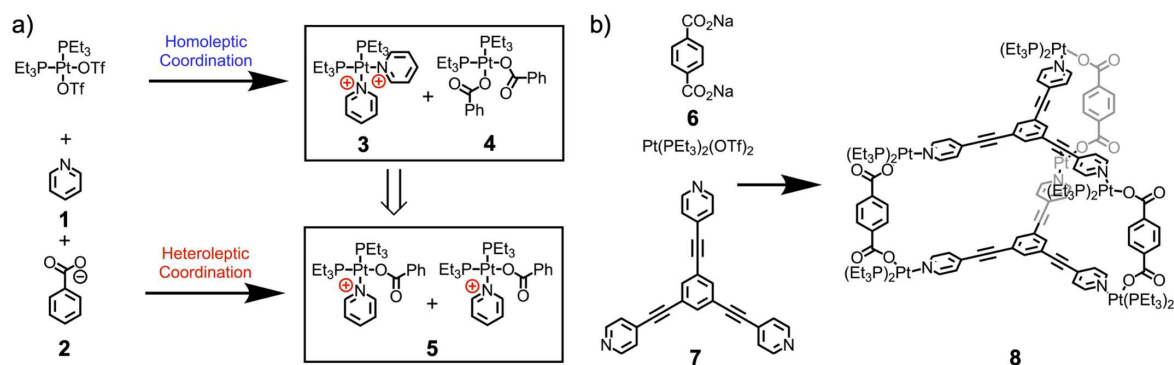
Figure 3. (a) Charge separation as a method for driving heteroleptic complex formation, (b) leading to the selective formation of mixed-ligand cages.[73]

After the coordination of a pyridine donor to platinum, the pyridine nitrogen atom bears a partial positive charge. When two pyridine donors are adjacent, they repel each other electrostatically (Figure 3, **3**). This repulsion is ameliorated when one of the pyridine donors is replaced by a carboxylate (Figure 3, **5**). This reduction in repulsion thus leads to the observed preference for heteroleptic coordination.

The Stang group has employed this concept extensively, for example to form an array of trigonal, tetragonal and hexagonal prisms, and other heteroleptic complexes, by combining cis-$Pt^{II}(PEt_3)_2(OTf)_2$ with 1,4-benzene dicarboxylate (Figure 3, **6**) and three-, four- or six-fold symmetric pyridine donors.[73-75] Figure 3 shows such a three-fold symmetric donor **7**, and 1,4-benzene dicarboxylate (**6**). In collaboration with the Huang group, this concept was extended to generate highly emissive platinum(II) metallacages, using a four-fold symmetric pyridine donor component that contains a fluorophore that undergoes aggregation-induced emission.[76] The strict spatial separation enforced by the metal-organic architecture preserved fluorescence under both high- and low-concentration regimes, allowing white-light emission. Similar principles were recently reported in a metallacycle where a high degree of intramolecular twist constrained the incorporated anthracenes, increasing emission intensity.[77] Furthermore, the same group, working with the Sun group, has shown that metal-organic capsules can self-assemble into soft superstructures of up to the millimeter scale.[78]

Combinations of nitrogen and carboxylate ligands have also been used to create molecular rectangles based on palladium.[79] The formation of cages containing perylene diimide panels, which can bind polycyclic aromatic hydrocarbons, has been reported recently by Zhang *et al*.[80] By combining the orange emission of the cage and blue emission of a captured guest, white-light emission was obtained. Differences in fluorescence quantum yield between the solid-

state and solution were also exploited to create hidden messages, revealed on exposure of the system to acetonitrile vapour.[80]

As shown in Figure 4, Severin *et al.* reported that strained homoleptic assemblies such as **9** rearrange following the addition of an extra ligand. Metallomacrocycle **9** is strained, and its strain is alleviated in heteroleptic assembly **11**, thus providing a driving force to counter the entropic cost of integrating more building blocks.[81] In homoleptic assembly **9**, one carboxylate at each metal center forms a four-membered chelate ring, the strain of which is relieved as these carboxylates become monodentate in flexible trigonal prism **11** following the addition of 2,4,6-tris(pyridine-4-yl)-1,3,5-triazine **10**. The resulting monodentate binding endows product **11** with a high degree of flexibility. In the absence of a guest, the trigonal prismatic framework of **11** collapses in the solid-state, forming a compressed structure without an interior cavity. However, when coronene is added, the trigonal prism expands to encapsulate two coronene guests in the solid-state. This work shows that flexible coordination cavities can be generated not just from flexible organic ligands, but also from coordinational flexibility about metal centers.
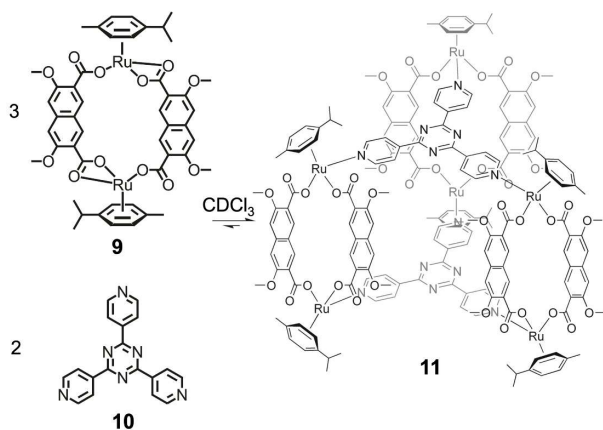
Figure 4. Selective assembly of trigonal prism **11** driven by the removal of a strained four-membered chelate ring in the homoleptic species. Reproduced with permission from ref 81. Copyright 2010 American Chemical Society.

Schmittel and co-workers have reported application of their 'heteroleptic terpyridine and phenanthroline metal complexes' (HETTAP) concept to generate myriad self-assembled structures, including nanoprisms. This approach relies on steric hindrance around the phenanthroline units to prevent homoleptic assembly.[82,83] By combining a three-fold symmetric bulky phenanthroline-based ligand (**12**) with linkers of different lengths (i.e. **13**, shown in Figure 5) the authors generate a series of trigonal prisms of differing heights of the general form $Cu^I_6L^1_2L^2_3$.
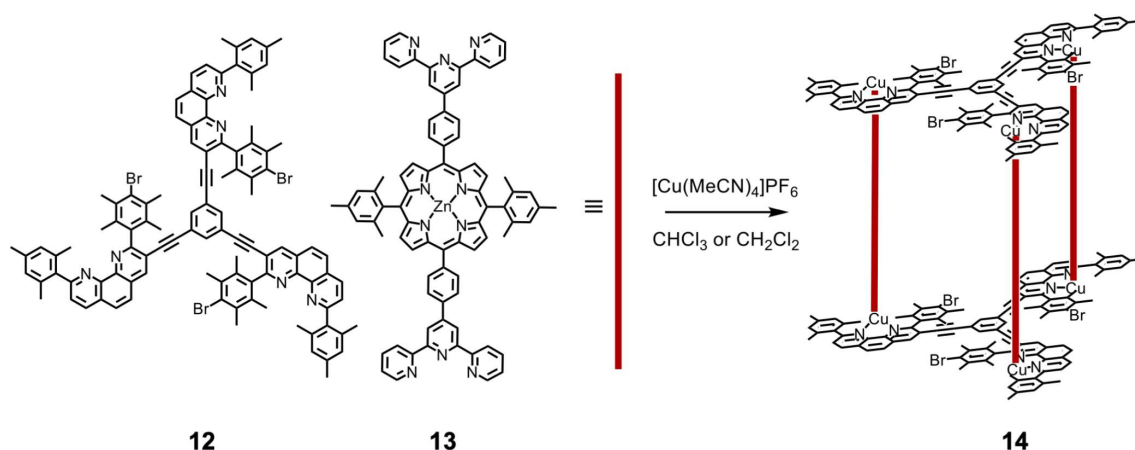
Figure 5. Selective assembly of heteroleptic trigonal prism **14** from precursors **12** and **13** driven by steric restriction involving hindered phenanthrolines (HETTAP).[82]

The heteroleptic architecture of **14** was further stabilized, eliminating minor by-products, by the addition of a suitable bridging guest capable of coordinating between the zinc centers in the porphyrins of the ditopic ligands. A planar tridentate pyridine ligand, which binds in the central belt of the three porphyrins, drives quantitative formation of the heteroleptic structure. Similar approaches, HETPHEN (heteroleptic bis-phenanthroline complexation) and HETPYP

(heteroleptic pyridine and phenanthroline complexation), have also been shown to selectively yield heteroleptic metal-organic complexes.[83]

A system may be guided towards heteroleptic assembly through the destabilization of alternative homoleptic products that would undergo steric clash. An early seminal example was provided by Yoshizawa and co-workers, who combined sterically hindered and unhindered ligands containing two pyridines to form heteroleptic trigonal prisms.[84] Similar approaches have been taken more recently by the Clever group, with steric bulk used to destabilize certain assemblies, favouring heteroleptic species.[85,86] We developed this concept during the selective formation of a copper(I) rhomboidal diporphyrin prism, shown in Figure 6.[87] Upon the mixing of four equivalents of bis(diphenylphosphino)benzene struts (**15**), eight equivalents of 2-formylpyridine (**16**), a guest (**17**), and two tetratopic zinc(II)porphyrin units (**18**), with copper(I), rhomboidal prism **19** forms. The offset between the porphyrins within **19** leads to its selective binding of 3,3'-bipyridine **17** between zinc centers.

The formation of a homoleptic $L_2Cu^I_4$ porphyrin copper(I) sandwich complex is disfavored by steric clashes between the phenyl groups, and the formation of copper(I) complexes involving the coordination of more than two phosphines is disfavored by the steric bulk of the phenyl groups on phosphorus. The simplest assembly that gives coordinatively-saturated copper(I) is thus prism **19**. The preference for heteroleptic assembly is likely reinforced by the known preference for copper(I) to selectively form mixed phosphine-pyridine complexes.[88]
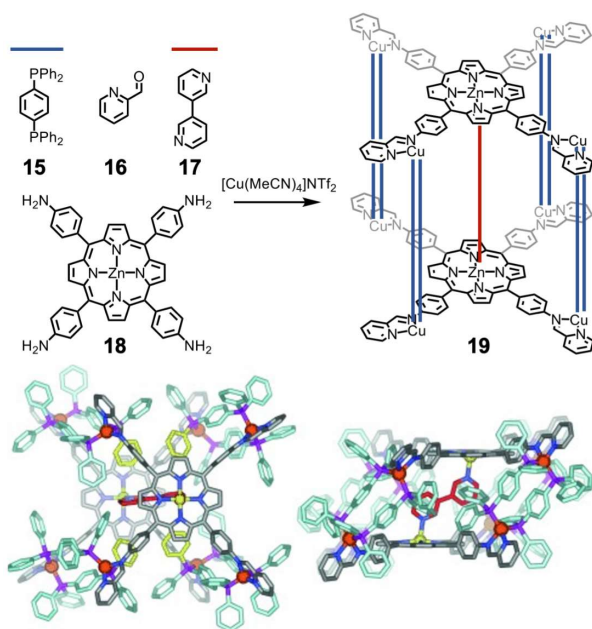
Figure 6. Formation of heteroleptic rhomboidal prism **19** by disfavoring the formation of homoleptic architectures. The offset between the zinc centers in the porphyrins leads to the selective incorporation of 3,3'-bipyridine (**17**). Adapted with permission from ref 87. Copyright 2015 Wiley-VCH Verlag GmbH & Co. KGaA, Weinheim.

The strategy of using ligands with donors of differing coordinative strength can also drive heteroleptic assembly in concert with the steric effects noted above. As shown in Figure 7, Lehn and co-workers have reported a series of cylindrical complexes based on combinations of linear oligo(bipyridine) ligands such as **20** with planar, three-fold symmetric hexaazatriphenylene (HAT) ligand **21**, and either silver(I) or copper(I).[89,90] The electron-deficient HAT ligands bind less strongly than bipyridines, and their phenyl groups generate steric clash when two HAT ligands bind around a single metal ion. Assemblies formed from HAT **21** alone would thus be relatively unstable, as well as polymeric in nature, and thus entropically less favored than the discrete cylindrical assemblies that are observed to form. Lehn *et al.* used linear ligands containing up to four bipyridine motifs, thus generating cylinders with up to three spatially-separated binding pockets. Although the host-guest behavior of this system was not investigated in detail, the principle of using spatially separated binding pockets

within the same assembly was further explored by others, such as Clever and Crowley (Section 7.4, Figure 63).[91-93]
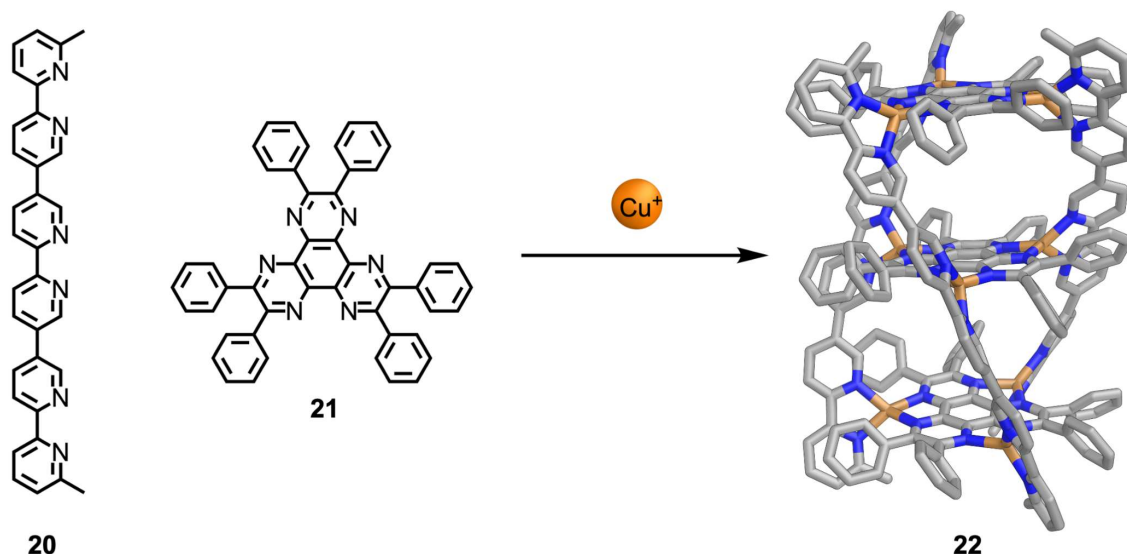
Figure 7. Formation of heteroleptic cylindrical complex **22**, from tris-bipyridine **20** and HAT **21** with two guest-binding compartments.[89,90]

2.2. Ligand Shape Complementarity

Clever *et al.* have reported a multitude of different heteroleptic Pd$^{II}_2$L$_4$ lantern-type structures, based upon their initial work with analogous homoleptic structures, that contain bidentate ligands incorporating pyridine donors with parallel coordination vectors.[94,95] Clever's approach to forming heteroleptic structures exemplifies the use of shape complementarity.[96,97] In the example in Figure 8, bidentate ligand **23** contains isoquinoline donors, and another, **25**, contains pyridine donors, each with non-parallel coordination vectors.[96] Strain is thus incorporated into homoleptic structures **24** and **26**, as the offset coordination vectors cannot close up into a polyhedron by coordinating to square planar palladium(II) without distortion.

When mixed, however, the two ligands come together to form $Pd^{II}_2 23_2 25_2$ heteroleptic architecture **27**, with each ligand *cis* to its complementary partner, thus forming a tilted lantern architecture. The extension of this concept to a wider variety of ligands subsequently enabled the discovery of an unusual self-penetrating heteroleptic cage architecture.[98] Clever and co-workers have reported a range of interpenetrated and heteroleptic systems based on similar principles.[99-103] Severin and co-workers have recently reported the use of similar 'banana-shaped' ligands to create heteroleptic cages based on a virtual combinatorial library involving six separate ligands. This led to the formation of a trigonal-antiprismatic $[Pd^{II}_6 L_6 L'_6](BF_4)_{12}$ structure.[104]
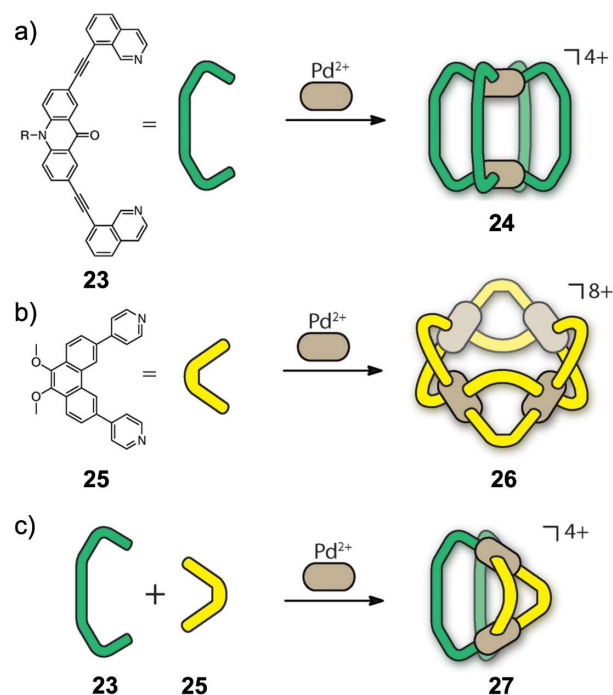
Figure 8. (a) Formation of homoleptic capsule **24**. (b) Formation of homoleptic capsule **26**. (c) Formation of heteroleptic lantern complex **27** driven by ligand shape complementarity between **23** and **25**. R = hexyl. Reproduced with permission from ref 96. Copyright 2016 American Chemical Society.

The Fujita group reported the assembly of a heteroleptic cantellated tetrahedron from ligands **28** and **29** (Figure 9). These ligands have the same angle between coordinating groups, but different lengths.[105] Each ligand forms a $Pd^{II}_{12}L_{24}$ cuboctahedral assembly when combined with Pd^{II} on its own. However, when combined in a 1:1 ratio, the two diastereomers of product **30** shown in Figure 9 form instead. Rather than narcissistic self-sorting, where each homoleptic assembly forms independently, or random mixing, where a collection of different assemblies form with different ratios of the two ligands incorporated, the system instead produces only $Pd^{II}_{12}\mathbf{28}_{12}\mathbf{29}_{12}$ assemblies. Each *cis* pair of ligands coordinating the same Pd^{II} forms part of a smaller $Pd^{II}_3\mathbf{28}_3$ or larger $Pd^{II}_3\mathbf{29}_3$ triangular metallomacrocyle, with four of each of these metallomacrocycles covering the cage surface, sharing edges with $Pd^{II}_4\mathbf{28}_2\mathbf{29}_2$ rectangles. The $Pd^{II}_{12}\mathbf{28}_{12}\mathbf{29}_{12}$ constitution, as opposed to other ratios of **28** to **29**, of **30** thus minimizes strain among these triangles and rectangles.
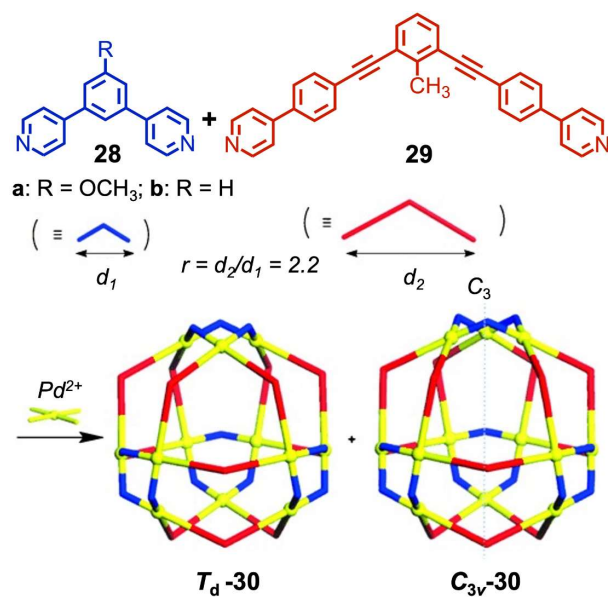
Figure 9. Formation of two diastereomers of a heteroleptic cantellated tetrahedron **30** from two ligands, **28** and **29**. Adapted with permission from ref 105. Copyright 2014 WILEY‐VCH Verlag GmbH & Co. KGaA, Weinheim.

Similar principles were used by Lützen and co-workers to create a dinuclear copper(I) molecular kite from subcomponents that did not assemble into discrete, unstrained structures individually.[106]

2.3. Entropy as a Driving Force for Heteroleptic Assembly

We recently reported a system that undergoes heteroleptic assembly by entropically favoring the mixed architecture (Figure 10).[62] Cube **36** and tetrahedra **34** & **35** are in equilibrium with triangular prisms **37** and **38**, respectively. The triangular prismatic architecture is disfavored enthalpically, but its formation is favored entropically for two reasons. Firstly, the triangular prism has a greater number of conformational microstates: each porphyrin unit adopts a saddled configuration, bowing in or out, in the triangular prism, whereas the porphyrins must lie planar in the cube. Secondly, the combined cavity volumes of two triangular prisms are smaller than those of the cube and tetrahedron combined. Thus, fewer solvent molecules are trapped inside the cavity of the triangular prisms **37** and **38**, relative to tetrahedra (**34** and **35**) and cubes (**36**), leading to a more favorable entropy.
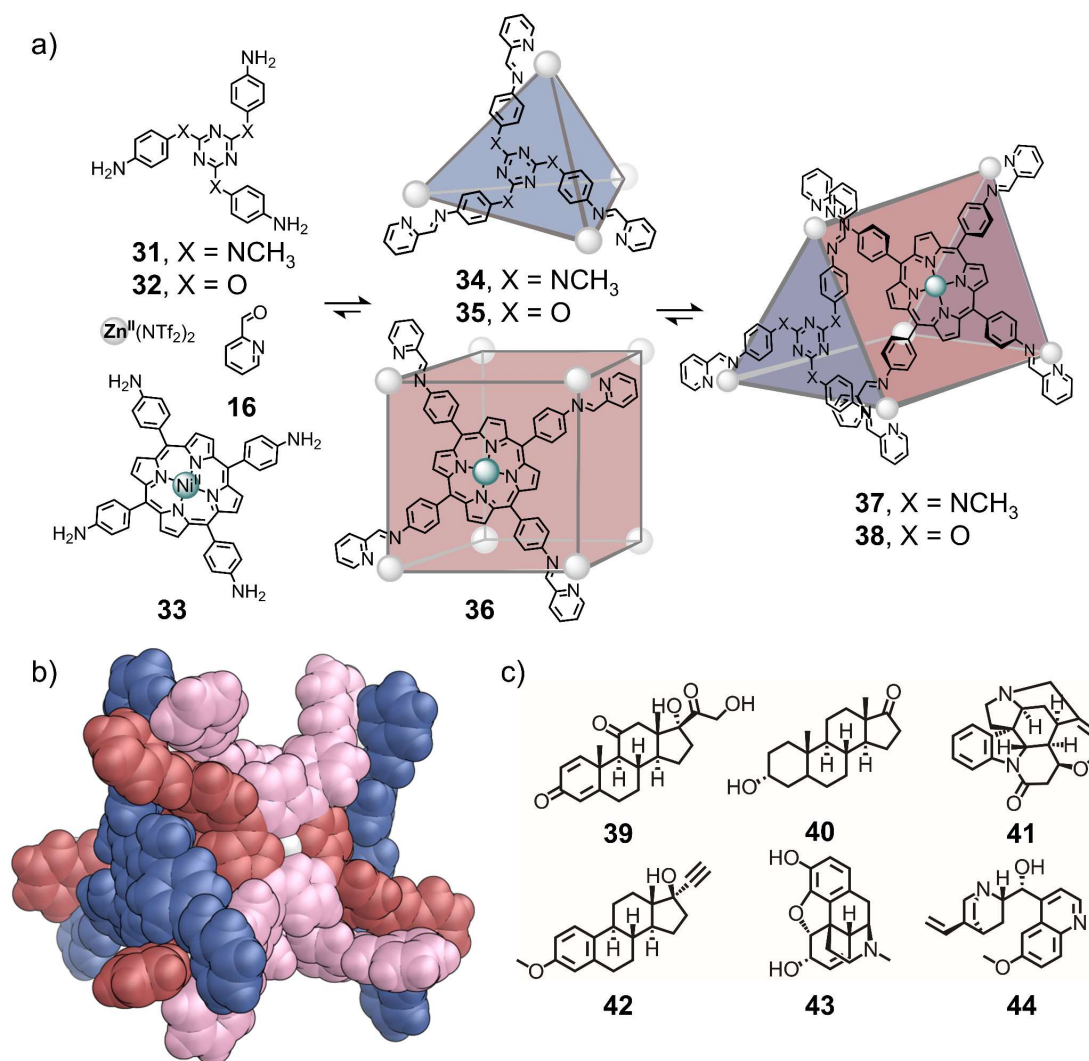
Figure 10. Formation of entropically-favored heteroleptic triangular prismatic complexes able to bind biologically relevant molecules. (a) Assembly of heteroleptic architectures **37** and **38**. (b) Crystal structure of **37**. (c) Pharmaceutical guests bound by the heteroleptic assemblies. Adapted with permission from ref 62. Copyright 2019 American Chemical Society.

Homoleptic structures, such as **34**, **35** and **36**, have higher symmetry and more spherical cavities than corresponding heteroleptic structures **37** and **38**. Such spherical, isotropic cavities are poorly adapted to the binding of more complex, anisotropic, molecules of biological interest. A key advantage of the less-symmetric heteroleptic architectures **37** and

38 is the ability to bind higher-value, more complex substrates (such as **39-44**, Figure 10c), than the more symmetric homoleptic structures.

2.4. Favorable Interactions Between Ligands to Drive Heteroleptic Assembly

Heteroleptic assembly can be favored by engineering additional favorable interactions that are not present in the corresponding homoleptic systems. We reported a system of mixed pyrene- and naphthalenediimide-based pyridyl-imine ligands (Figure 11).[107] Alone, each ligand forms a stable homoleptic structure. However, together subcomponents **45** and **46** form $Fe^{II}_4\mathbf{45}_4\mathbf{46}_2$ elongated structure **47**, with a different connectivity than either of the homoleptic assemblies. Differentially-substituted subcomponent **48**, when combined with **46**, forms the original homoleptic architectures in an example of narcissistic self-sorting. The selective formation of heteroleptic structure **47** is driven by favorable aromatic stacking interactions between electron-rich and electron-deficient aromatic units that exist only in the mixed architecture. This stacking drives the assembly of the mixed architecture even in the presence of a guest which only binds to one of the possible homoleptic species. This system shows the importance of aromatic stacking interactions in metal-organic architectures.

Such stacking interactions were also critical in driving the formation of a recently reported twisted trigonal prismatic architecture.[108] Jung and co-workers have also reported a catenated architecture based on the stacking of electron-deficient and electron-rich aromatic rings.[109] In a similar vein, Yuasa *et al.* demonstrated that favorable inter-ligand charge-transfer interactions can cause a preference for heteroleptic assemblies, over homoleptic alternatives.[110]
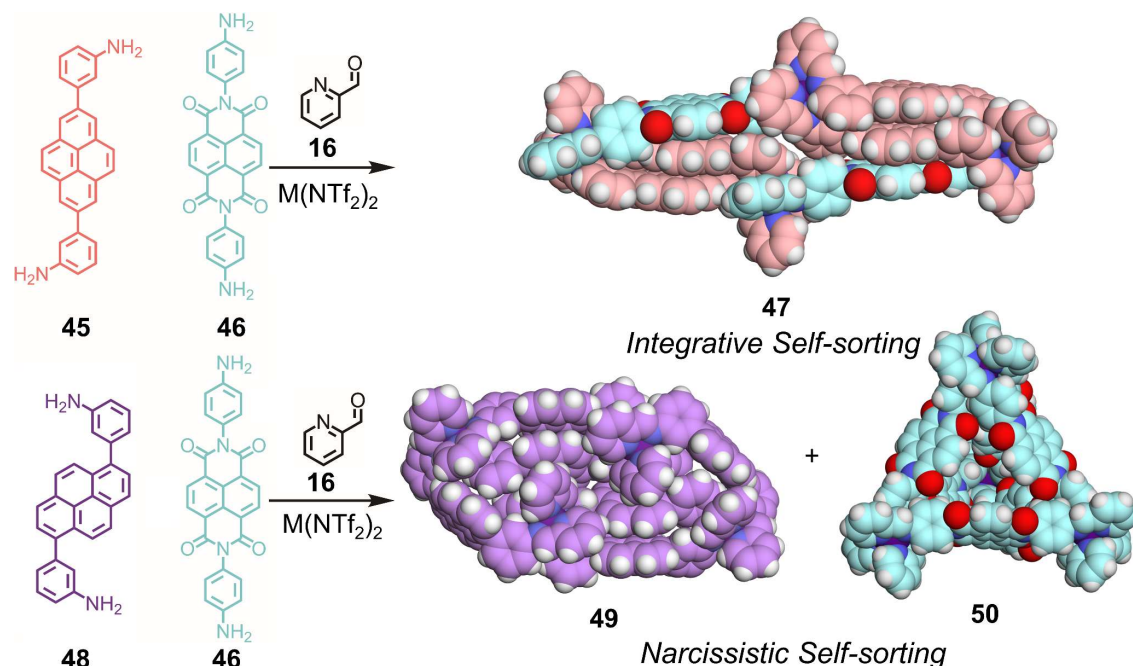
Figure 11. Formation of heteroleptic complex **47**, favored by aromatic stacking interactions, from the interplay of more electron-rich **45** and more electron-poor **46**, and narcissistic self-sorting observed from the combination of **48** and **46** to form homoleptic assemblies **49** and **50**.[107]

Fujita and co-workers developed a heteroleptic $Pt^{II}_6L_2L'_3$ trigonal prism, whose formation is templated by a rigid, flat, aromatic guest, which only binds in the heteroleptic architecture. Guest binding thus drives selective formation of the heteroleptic trigonal prism. After formation, the guest can be removed by extraction with an apolar solvent, leaving the empty trigonal prism.[111] The cavity thus formed can then be used to stabilize the pairing of DNA nucleobases in aqueous solution.[63]

2.5. Complementary Binding Sites

Stang and co-workers have made extensive use of the square-planar geometric preference of palladium(II) and platinum(II) centers to construct metal-organic assemblies.[112] They have obtained heteroleptic assemblies using the concept of complementary binding sites, whereby

each component is unable to self-assemble without a complementary partner. As shown in Figure 12, cuboctahedron **53** can be prepared by the assembly of a three-fold symmetric, planar metalloligand **51** with bidentate pyridine donor **52**. As the metal centers are covalently integrated into one ligand, a second ligand is required for assembly into the nanometer-scale product **53**. This work was subsequently extended to form similar, chiral, adamantanoid cages that incorporate optically active building blocks.[113]
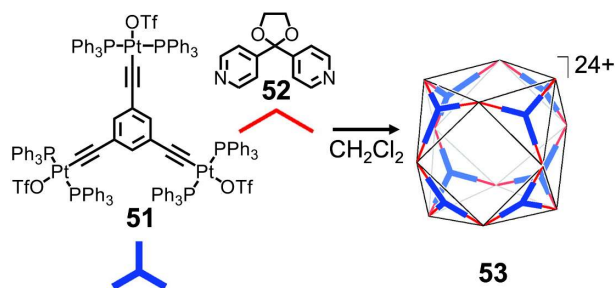
Figure 12. Formation of a heteroleptic cuboctahedron **53** driven by the complementarity of binding sites of the different components. Adapted with permission from ref 1. Copyright 2011 American Chemical Society.

Similar principles have previously been used by Bosnich and co-workers to selectively generate platinum(II)-based heteroleptic rectangles, using terpyridine and mono-pyridine ligands.[114] The Nabeshima and Yam groups have used this concept to create molecular rectangles, and the area of complementary ligand denticity has been recently reviewed.[115-117] The advantages of combining different donor groups in the same system have been further established by Mukherjee and co-workers, who form open 'swings' and 'boats' when using pyridine donors in combination with imidazole donors. These structures can bind C_{60} and catalyze Knoevenagel condensations.[118,119]

Other groups have further developed the concepts described above to form heteroleptic cages with useful properties. For example, the groups of Ribas, Costas and Reek reported the formation of a tetragonal prismatic supramolecular cage from the combination of tetratopic

metalloporphyrin tetracarboxylate **55**, and a macrocycle containing two palladium(II) centers, each coordinated by three nitrogen donors, **54** (Figure 13).[120] In this system, the coordination preferences of Pd^{II} are satisfied by one carboxylate ligand and one macrocyclic ligand, leading to the formation of structure **56**, with $Pd^{II}_8 \mathbf{54}_4 \mathbf{55}_2$ composition.
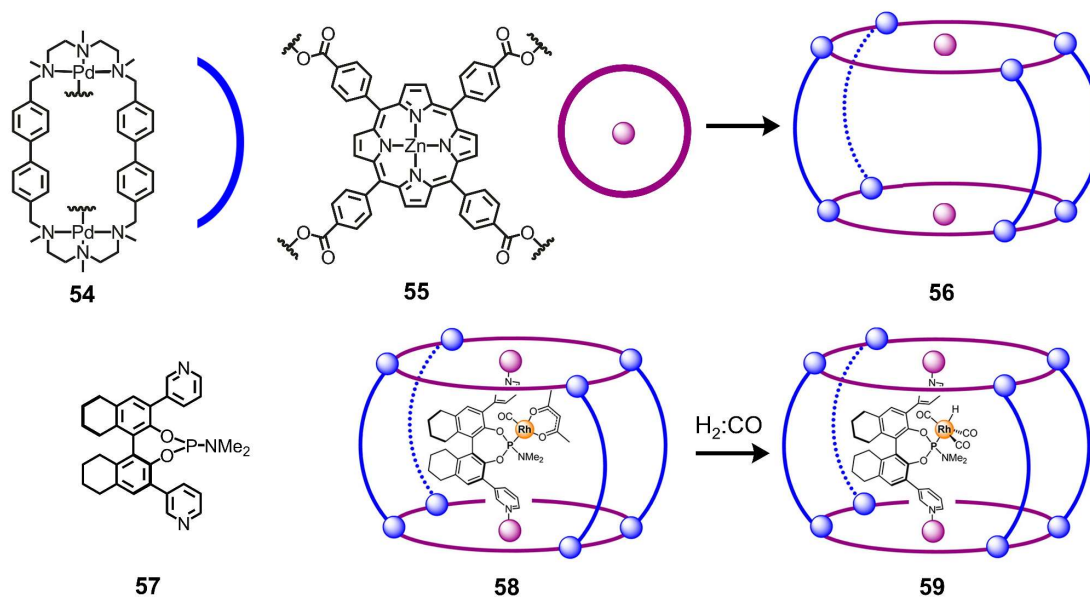
Figure 13. Formation of heteroleptic tetragonal prism **56** driven by the coordination complementarity of ligands **54** and **55**. Cage **56** binds aminophosphite **57**, which then binds rhodium (**58**) to form catalytically-active rhodium complex **59**. Adapted with permission from ref 120. Copyright 2015 American Chemical Society.

This structure encapsulates aminophosphite ligand **57**, which coordinates rhodium (forming **58**). The active supramolecular catalyst thus formed (**59**) operates with a greater degree of chiral induction due to cage control over the second coordination sphere. Similar capsules have been reported and used for the selective extraction and functionalization of fullerenes.[121-123] In collaboration with the von Delius group, the Ribas group has recently reported the formation of a 'matryoshka' Russian doll-type assembly, and its application in the selective formation of a single *trans*-3 fullerene bis-adduct.[124]

Jin and co-workers have reported a system of heteroleptic cages where selective assembly is driven by the interplay between two pairs of distinct chelating sites on a single hydroxamate ligand **60** – a harder *O,O'* site, and a softer *N,N'* site, as shown in Figure 14.[125] Half-sandwich iridium and rhodium metal centers assemble with auxiliary pyridine-based ligands, such as **61**, to form tetragonal and trigonal prisms. The D_2-symmetric diastereomer of cage **62** (Figure 14) binds triflate as guest and template.
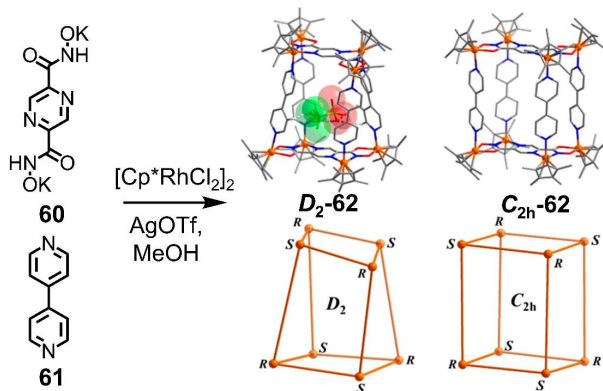
Figure 14. Assembly of molecular prisms of different symmetries based on the hard-soft bis(hydroxamate) donor **60** and 4,4'-bipyridine **61**. Adapted with permission from ref 125. Copyright 2015 American Chemical Society.

The hard/soft character of ligand **60** was also used to form heterometallic macrocycles, with palladium and iridium centers selectively incorporated in the same framework. Within these heterometallic structures, palladium binds the softer nitrogen donors, whereas iridium binds the harder oxygen donors. One of these macrocycles encapsulated tetrathiafulvalene between parallel hydroxamate ligands.[125] The authors have recently reported an extension of this system, where the symmetric dipyridine **61** is replaced by a bridging unit containing one pyridine and one carboxylate donor site, forming a D_2 symmetric heteroleptic species selectively.[126]

We reported a system of Pd[II]-based macrocycles and cages, whose assembly is controlled by the addition of appropriate monotopic pyridine bridging molecules to the assembled Pd[II]-

bound macrocycles. Each Pd[II] is coordinated by three nitrogens from the macrocycle (Figure 15), and one from the bridging ligand.[127] The subcomponents 2,6-diformylpyridine **63** and flexible dianiline **64** assemble around palladium(II) templates to generate metal-organic macrocycles containing either three or four Pd[II] centers, depending on the tri- or tetratopic nature of the pyridine template used. If instead linear, ditopic pyridine template **65** was employed, having a geometry ill-adapted to incorporation within a single macrocycle, three-dimensional capsule **66** was generated. This structure (Figure 15) includes a trimeric macrocycle at each end, with bridging **65** ligands between them. Assembly **66** forms cooperatively, with no structures observed containing fewer than three bridging ligands. Structure **66** encloses a small cavity, which was found to bind tetrafluoroborate selectively.
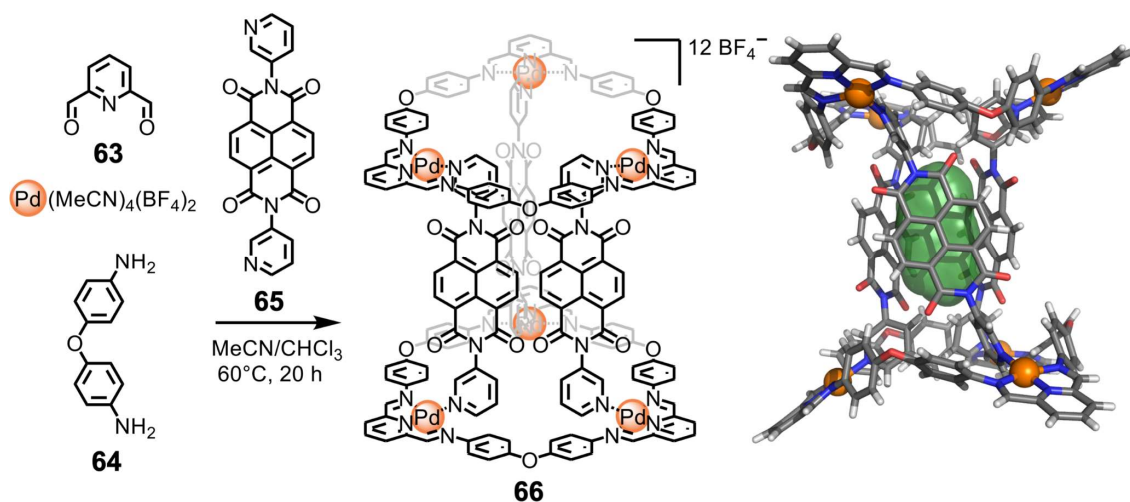
Figure 15. Formation of complex assembly **66** from subcomponents **63** and **64**, Pd[II](MeCN)$_4$(BF$_4$)$_2$, and bipyridine naphthalenediimide **65**. Reproduced with permission from ref 127. Copyright 2019 American Chemical Society.

Similar systems were extended to form truncated tetrahedra and other metal-organic cages by using a tritopic aniline ligand. The dynamic pyridyl-imine bonds formed during self-assembly could be cleanly reduced to form secondary amines, thus disabling the equilibration process and fixing the structures formed.

2.6. Kinetic Traps

Crowley and co-workers reported a novel approach to generating heteroleptic architectures, employing kinetic traps rather than favoring a thermodynamic product (Figure 16).[128] A $Pd^{II}_2L_4$ lantern architecture (**69**), formed from bidentate pyridine-containing ligand (**67**) with parallel coordination vectors (Figure 16), is combined with another ligand (**68**), containing 2-amino-pyridines.

67, R = H, R' = CH$_2$OH

68, R = o-NH$_2$, R' = CH$_2$OH
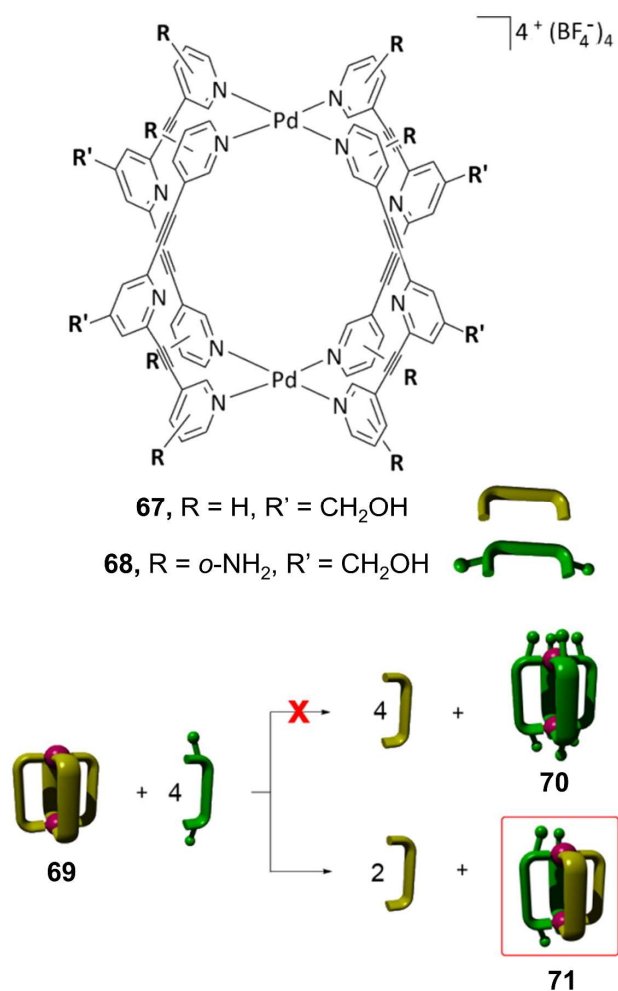
Figure 16. Formation of kinetically-trapped heteroleptic molecular lantern complex **71**, with selective incorporation of pairs of ligands **67** and **68**. Reproduced with permission from ref 128. Copyright 2016 American Chemical Society.

Ligand **68** forms stronger bonds to palladium, so thermodynamics favor its incorporation. When excess ligand **68** is added to $Pd^{II}_2\textbf{67}_4$ lantern **69**, $Pd^{II}_2\textbf{67}_2\textbf{68}_2$ lantern **71** forms selectively, in a *cis* configuration. The selectivity for the *cis* isomer is attributed to hydrogen-bonding between adjacent amino groups. The selective formation of a $Pd^{II}_2\textbf{67}_2\textbf{68}_2$ lantern, rather than complete substitution to form a homoleptic $Pd^{II}_2\textbf{68}_4$ structure, is attributed to the effects of steric repulsion between the 2-amino groups and incoming pyridine ligands in the proposed associative mechanism. This repulsion increases the energetic barrier to ligand exchange, enabling the selective formation of the heteroleptic species. Calculations suggest that the heteroleptic species is a kinetically trapped metastable species rather than the thermodynamic product, with competition experiments supporting this idea. Hydrogen bonding between the pyridine α-CH and adjacent 2-amino-pyridine groups is inferred to reinforce this kinetic stability.

An intriguing use of kinetic control in self-assembly was reported by Lusby, Barran, *et al.*, who used the low lability of cyclometallated platinum corners to create trigonal prismatic assemblies (Figure 17).[129] The identity of the product depends on the sequence of addition, rather than the thermodynamic stability of the product. Starting from a platinum complex with one pyridine, one dimethylsulfoxide, and two phenylato ligands, a bi- or ter-pyridine ligand is then added. This additional ligand displaces weakly-bound dimethylsulfoxide to form an intermediate complex with either two-fold (**72**) or three-fold (**74**) symmetry. In the case of two-fold symmetric intermediate **72**, tritopic pyridine ligand **10** is then added, which forms a new coordination bond *trans* to a phenylato ligand. This process displaces another phenylato ligand, which is then protonated. The phenyl group thus released is left above the three-fold symmetric face of trigonal prism **73**.

If instead 4,4'-bipyridine **61** is added to three-fold-symmetric intermediate **74**, the released phenyl groups of product **75** stack instead above the two-fold symmetric ligand. This isomerism is further manifested in the mass spectrometry data collected, where the weaker coordination bonds *trans* to the phenylato group are observed to rupture preferentially. This approach provides an example of how the sequence of addition can control the outcome of a self-assembly process, and thus provides a novel mode of generating structural complexity.
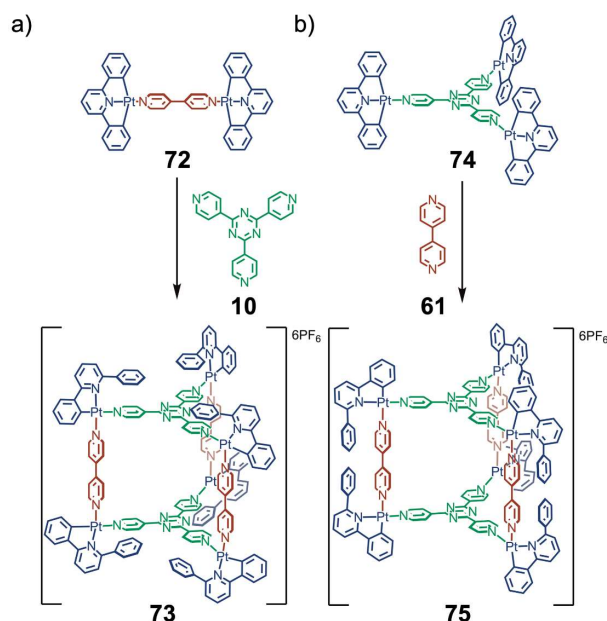
Figure 17. Selective formation of isomeric heteroleptic trigonal prisms **73** and **75** by control over the sequence of addition. (a) Initial addition of ditopic ligand **61**. (b) Initial addition of tritopic ligand **10**.[129]

This section has reviewed different approaches to generating heteroleptic structures, which frequently have novel, lower-symmetry architectures. We have explored how control over both the entropy and enthalpy of formation can be used to bias systems towards thermodynamic heteroleptic assembly. More subtly, we have also seen how fine control of the balance of

kinetics in a system can enable the formation of kinetically-trapped heteroleptic products, without preventing the error-checking vital to the self-assembly of complex architectures.

3. Lower-Symmetry Ligands: Using Reduced-Symmetry Ligands Leads to Reduced-Symmetry Products

The complexity of metal-organic architectures may be increased through the use of components which themselves have more complex structures. This concept has recently been reviewed by Lewis and Crowley.[130] Reduced-symmetry ligands can also lead to an increased number of possible structures. Thus, we also evaluate factors that drive the selective formation of one structure from among multiple possibilities.

3.1. Reduced-Symmetry Ligands

M_2L_4 cages using bis-monodentate ligands and square planar metal centers have been well-studied, and would not be considered "complex" in terms of the scope of this review.[131,132] However, several recent publications have reported the formation of M_2L_4 structures with reduced-symmetry ditopic ligands and a single type of metal ion,[133-137] or two different types of metal ion,[138] leading to greater structural complexity. When M_2L_4 structures assemble from a reduced symmetry ditopic ligand, several isomers are possible (Figure 18). One or more of these isomers is often of lower energy than the others, therefore forming preferentially.
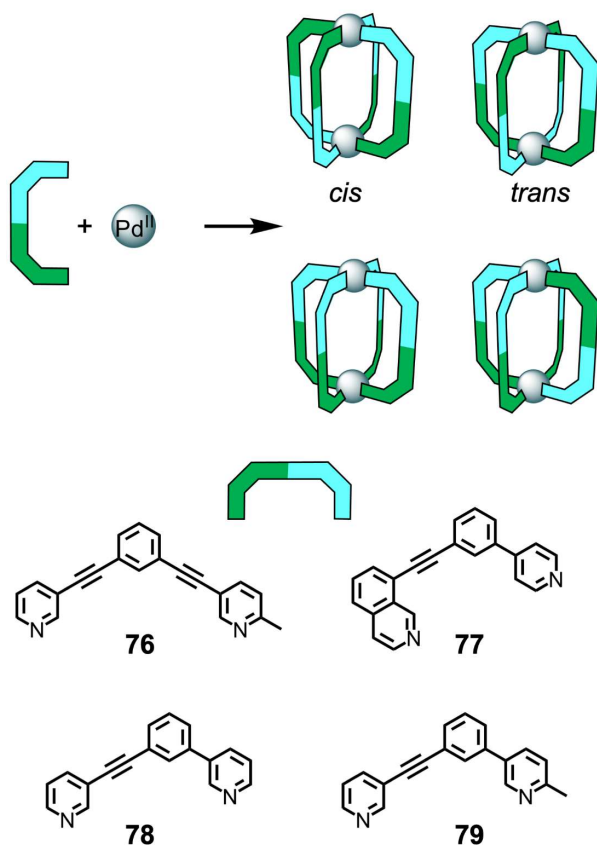
Figure 18. Representations of the four possible isomers of homoleptic $Pd^{II}_2L_4$ cages capable of forming from one of the reduced-symmetry ditopic ligands **76-79**.[133]

Lewis and co-workers showed that the identity of the preferred isomer of a $Pd^{II}_2L_4$ cage can be controlled by changing the identity of the ligand (**76-79**). Hindered ligand **76** produces a C_{2v}-symmetric *trans*-$Pd^{II}_2L_4$ isomer in MeCN, minimizing steric clash, with product identification being supported by DFT calculations.[133] Upon increasing the polarity of the solvent by using DMSO, a mixture of the *trans*-$Pd^{II}_2L_4$ and *cis*-$Pd^{II}_2L_4$ isomers form. This phenomenon is tentatively attributed to selective stabilization by the more polar solvent of the *cis*-$Pd^{II}_2L_4$ isomer, which is predicted by DFT to have a larger dipole moment than the *trans* isomer.

The C_{2h}-symmetric *cis*-Pd_2**77**$_4$ isomer forms selectively in DMSO.[133] This selectivity arises from the presence of different binding sites at each end of the ligand **77**, a pyridine and an

isoquinoline. Within **77**, the planes orthogonal to the coordinate vectors of the nitrogen donor atoms no longer coincide (even when the pyridine and isoquinoline rings are co-planar), thus favoring cis-$Pd^{II}_2\textbf{77}_4$ formation. Subsequent investigations involving ligand **78** indicate that in this case the deviation from co-planarity is not significant enough to yield a single isomer of the $Pd^{II}_2\textbf{78}_4$ complex. However, the greater steric hindrance around the coordination sphere of Pd^{II} bound to **79** results in the formation of a single $Pd^{II}_2\textbf{79}_4$ isomer. Based on DFT calculations, cis stereochemistry was inferred.

Finally, the addition of steric bulk, in this case via the inclusion of methyl groups in **76** or **79**, causes an increase in the helical twist of the structure compared to analogous structures formed by ligands lacking methyl groups. The steric effects of these methyl groups on the conformation of the resulting structure may enable tailoring of the internal cavity space.

The Lewis group has also shown that reduced-symmetry ditopic ligands containing 1,2,3-triazole and isoquinoline binding sites can form a similar $Pd^{II}_2L_4$ cage, as a single cis-$Pd^{II}_2L_4$ isomer.[137] By varying the substituent on the triazole moiety, a series of externally-functionalized cages form. Given the uniformity of the main ligand framework among all of the derivatized ligands, dynamic libraries of mixed-ligand cages are obtained when using mixtures of the different ligands.

Bloch $et\ al.$ recently demonstrated the use of conformational flexibility in producing reduced-symmetry ligands.[139] In their system, a dicarboxylate ligand with a diimine core exists in three different rotational conformations, one of which has lower symmetry. Depending on the crystallization conditions, three distinct cage isomers are isolated from a dynamic library; their structures were determined by single crystal X-ray crystallography. The three cage isomers each contained either two or four ligands in the reduced-symmetry conformation.

Separate studies reported by Yuasa *et al.*[134] and Crowley *et al.*[138] also involve the formation of M_2L_4 structures with unsymmetrical ditopic ligands. Both utilize the differing lability of coordination bonds involving different monodentate donors or metal ions to develop mechanisms for guest capture and release. Yuasa *et al.* alter the stoichiometric ratio of ligand to metal in the reaction mixture to drive the interconversion of a $Pd^{II}_2\textbf{80}_4$ cage, capable of binding anions within its cavity, and a $Pd^{II}\textbf{80}_4$ complex, which does not bind guests (Figure 19). In this mononuclear complex, the imidazole groups of all four ligands are bound to the Pd^{II} center and the four pyridyl donors remain free because imidazole is a stronger donor than pyridine.[134]
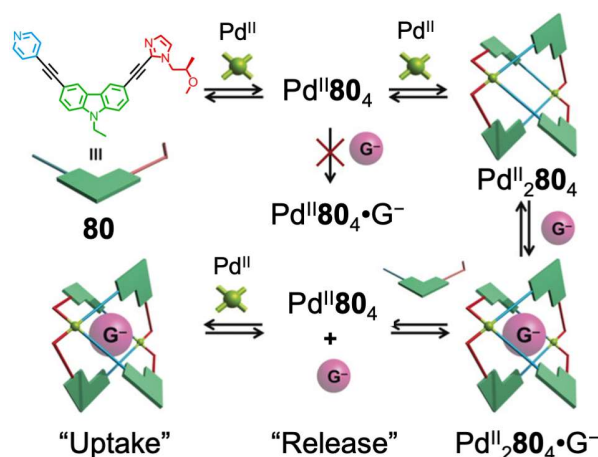
Figure 19. Stepwise self-assembly of a dynamic open $Pd^{II}_2L_4$ coordination cage using unsymmetrical imidazole-pyridine based ditopic ligand **80**. Stoichiometry-controlled structural transformation of this cage allows anion uptake and release. Adapted with permission from ref 134. Copyright 2019 Wiley‑VCH Verlag GmbH & Co. KGaA, Weinheim.

An approach introduced by Crowley *et al.* is based on the design and synthesis of a cage in which the antipodes are Pt^{II}, which forms more inert Pt^{II}-pyridyl bonds, and Pd^{II}, forming more labile Pd^{II}-pyridyl bonds.[138] Following its formation (Figure 20), cage **83** can open and close reversibly. The addition of 4-dimethylaminopyridine (DMAP) selectively sequesters Pd^{II}, forming $Pd^{II}(DMAP)_4$ and opening the cage. Subsequent addition of *p*-toluenesulfonic acid

protonates the DMAP ligands and causes their dissociation from the metal centers, releasing Pd^{II} and reforming $Pd^{II}Pt^{II}L_4$ cage **83**.
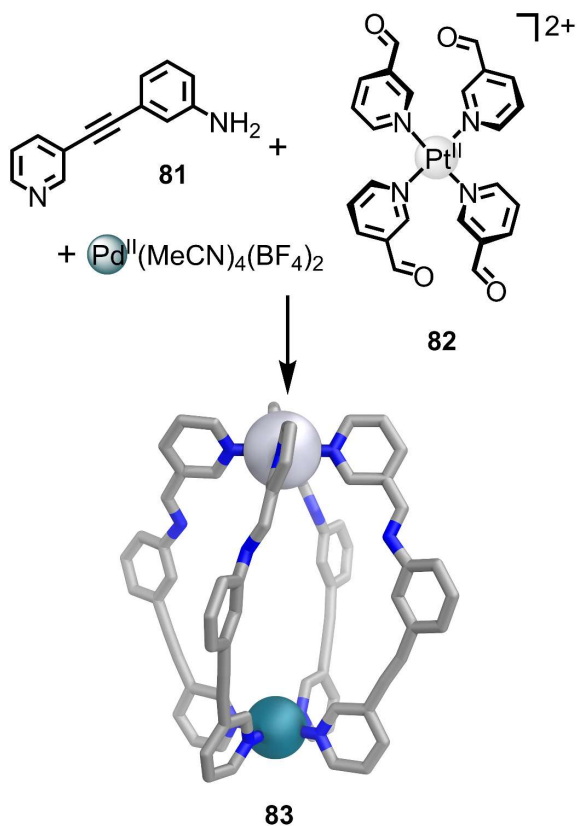
Figure 20. Synthesis of $[Pd^{II}Pt^{II}L_4](BF_4)_4$ cage **83** *via* the combination of preformed Pt^{II}(3-pyridylcarboxyaldehyde)$_4$ complex **82**, 3-[2-(3-pyridinyl)ethynyl]benzenamine **81** and $Pd^{II}(MeCN)_4(BF_4)$.[138]

This stimulus-induced opening and closing of cage **83** also brings about reversible guest uptake and release, illustrating a potential function. Although these structures are relatively simple, they exemplify how functionality can be introduced by using reduced-symmetry ligands. These principles may be combined with other rules, detailed elsewhere in this review, which guide the formation of larger and more complex structures, to yield architectures of greater complexity and functionality.

Hooley and co-workers have reported using a prochiral ligand in the assembly of a desymmetrized $Fe^{II}_4L_6$ architecture (Figure 21).[140] The presence of a prochiral CHOH center in the fluorenone ligand – a motif which they have explored to generate functionalized capsules[141-144] – brought about the selective formation of 'Wizard's Hat' **85**, a distorted tetrahedron. The formation of this unusual architecture is favored by a specific pattern of hydrogen bonding involving the -OH groups at the prochiral carbon atoms of the ligands and a templating perchlorate ion at the base of the assembly. An interesting aspect of this assembly is the presence of three *mer* Fe^{II} centers at the base of the structure, which are rare in self-assembled pyridyl-imine architectures, and often drive the assembly of more complex structures, as discussed in subsequent sections.
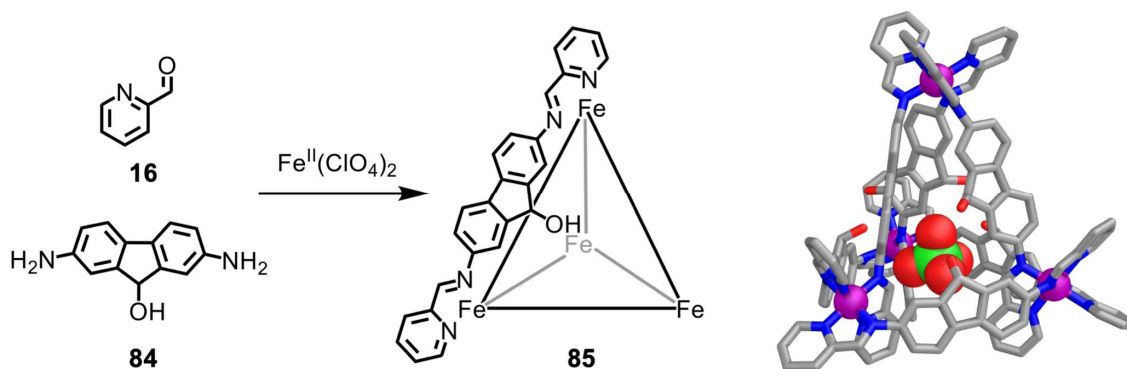
Figure 21. Hooley's 'Wizard's Hat' assembly **85**, stabilized by internal hydrogen bonds, and a templating perchlorate ion. Crystal structure shown on the right.[140]

Along with reduced-symmetry ditopic ligands, tritopic ligands with reduced symmetry can generate complex metal-organic architectures. Su *et al.* demonstrated the use of such tritopic ligands in forming unusual architectures in the preparation of a $Ag^I_6L_6$ tubular structure using an elongated T-shaped ligand.[145]

Hu *et al.* used 5-(pyridin-4-yl)isophthalic acid **87** with *p-tert*-butylthiacalix[4]arene **86** and $Ni^{II}Cl_2$ to form Ni^{II}_{40} coordination cage **88**, with a structure corresponding to the J_{17} Johnson Solid.[146]

As illustrated in Figure 22, the structure of **88**, a gyroelongated square bipyramid, consists of ten Ni$_4$-*p-tert*-butylthiacalix[4]arene shuttlecock-like vertices, and 16 panels of ligand **87**. Four ligands converge at two of the ten vertices, and five ligands converge at each of the other eight, closing the faces of the structure. In order to form the structure, the ligands coordinate to Ni^{II} centers through different donor atoms: through the carboxylate, which can either bridge or chelate Ni^{II}, and through the nitrogen donor of pyridine. The phenoxo oxygen and sulfur atoms of the *p-tert*-butylthiacalix[4]arene units also coordinate Ni^{II}, along with additional **87** units which do not cap the faces of the structure, DMF molecules, chloride ions, and degradation products of DMF in order to satisfy the coordination geometry of Ni^{II}.
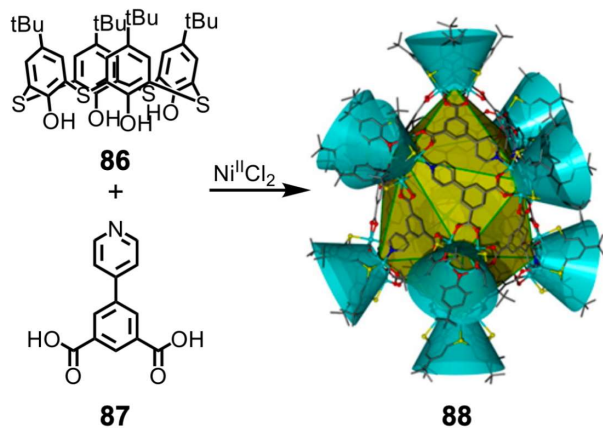
Figure 22. Ni$_{40}$ coordination cage **88** with a structure corresponding to the J$_{17}$ Johnson Solid, formed from *p*-tert-butylthiacalix[4]arene **86**, 5-(pyridin-4-yl)isophthalic acid **87** and Ni^{II}Cl$_2$. Reproduced with permission from ref. 146. Copyright 2016 American Chemical Society.

A tritopic ligand employed by Hong *et al.*, **89**, has three binding sites arrayed asymmetrically along its length (Figure 23). The combination of this reduced symmetry ligand, Ni^{II}(ClO$_4$)$_2$ and pyrazole (Pz) in ethanol yields a Ni$^{II}_9$**89**$_6$Pz$_6$ barrel structure **90**.[147] In **90**, the pyrazole plays two roles, acting as a Lewis base and as an additional donor to satisfy the octahedral coordination sphere of Ni^{II}.
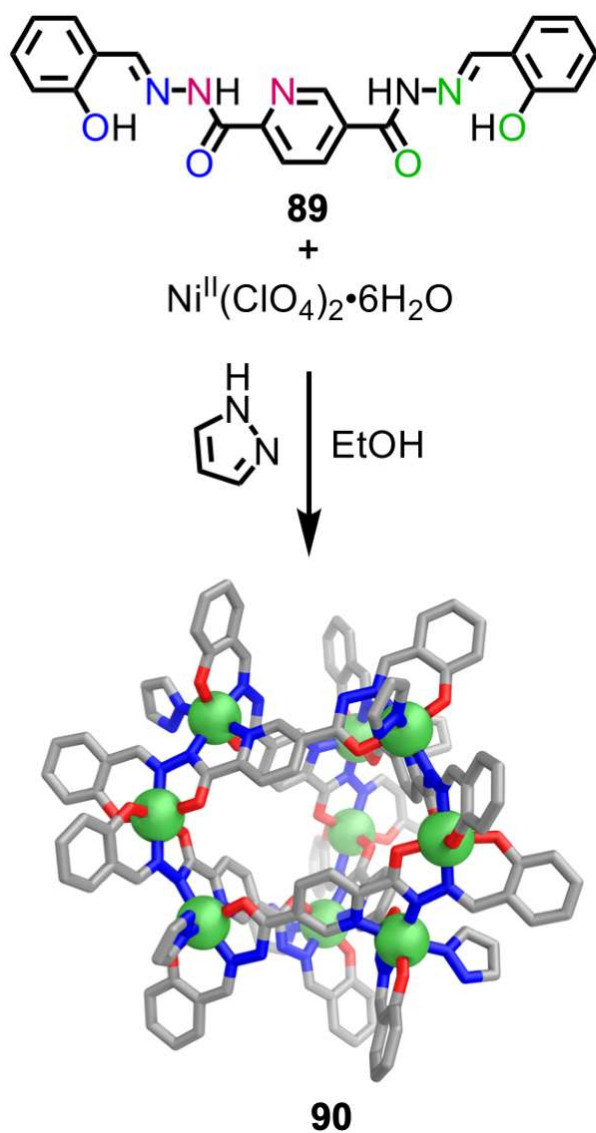
Figure 23. Self-assembly of $Ni^{II}_9\mathbf{89}_6Pz_6$ barrel structure **90**, incorporating asymmetrical tritopic ligand **89**.[147]

Li *et al*. have explored the use of desymmetrized tetratopic ligands resembling trapezoids to form metallosupramolecular architectures. Upon combination of these ligands with 180° dipalladium(II) acceptors, ring-in-ring[148] or 2D Star-of-David[149] structures form.

The reaction of these same ligands with 'naked' palladium(II) ions yields three-dimensional structures. One example is $Pd^{II}_{24}\mathbf{91}_{24}$ sphere-in-sphere architecture **92** (Figure 24), which

forms from ligand **91** and Pd^{II}.[148] The authors drew a contrast between their approach and the one pioneered by Fujita and co-workers.[150] The Fujita approach is based on the orthogonal assembly of two ditopic units into 'independent' $M_{12}L_{24}$ spheres, connected *via* flexible linkers to give the $M_{24}L_{24}$ sphere-in-sphere. In Li's system (Figure 24) precise preorganization of the entire 3D architecture is enforced by the rigid nature of the ligand. Ligand **91** also reacts with a tritopic platinum(II) unit to form a double-layered pentagonal prism.[151]
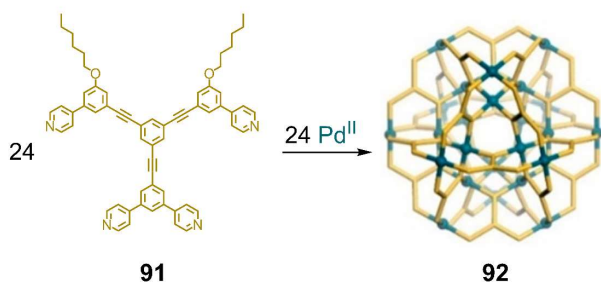
Figure 24. Self-assembly of a Pd$^{II}_{24}$**91**$_{24}$ three-dimensional sphere-in-sphere structure (**92**). Adapted with permission from ref 148. Copyright 2015 American Chemical Society.

Ligand **91** has donor groups arrayed in two distinct ways; Li *et al.* have also designed ligands with four distinct binding sites that form double-layered macrocyclic structures.[152] Their reports exemplify how rationally designing new classes of ligands can allow unique metallosupramolecules with high degrees of complexity to be formed.

3.2. Additional Donor Sites

Another approach to designing ligands capable of forming architectures with greater complexity is the modification of ligands that have previously been used to form metal-organic assemblies, for example by appending additional donor sites. This approach was used to design pentatopic ligands **93** and **94** (Figure 25), which form 3D hexagonal prismatic structures **95** and **96**, consisting of two connected 2D double-rimmed 'Kandinsky circles',

when combined with octahedrally-coordinated cadmium(II) ions.[153] Ligands **93** and **94** are based upon a tetratopic donor previously reported by Li *et al.*,[154] with the fifth terpyridine group appended to allow the two circles to be linked.
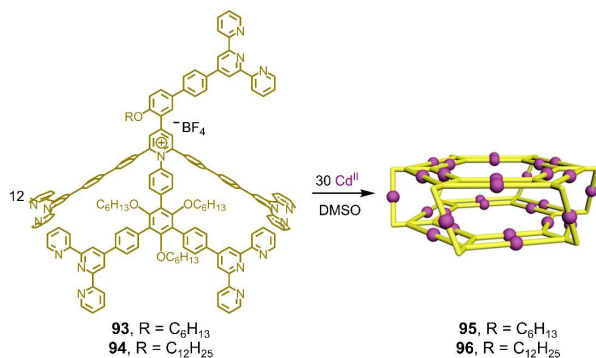
Figure 25. Self-assembly of three-dimensional hexagonal-prismatic structures **95** and **96**, consisting of two connected 2D double-rimmed 'Kandinsky circles', from Cd[II] and ligands **93** and **94**, respectively. Adapted with permission from ref 153. Copyright 2019 American Chemical Society.

As well as providing a method for the formation of 3D structures from known 2D structures, the ligand-modification approach can be used to increase the complexity of an existing 3D structure. Fujita and co-workers employed this approach to form a Pd^{II}_{18}**97**$_{24}$ stellated cuboctahedron **99** using tripyridyl ligand **97**, consisting of a rigid bipyridyl unit with a third pyridyl moiety flexibly tethered to the backbone.[155] As shown in Figure 26, the assembly process occurs in a stepwise fashion. The tripyridyl ligand combines with $Pd^{II}(BF_4)_2$ to yield Pd^{II}_{12}**97**$_{24}$ cuboctahedron **98**, analogous to a previously reported complex that incorporates a rigid bipyridine ligand.[156]
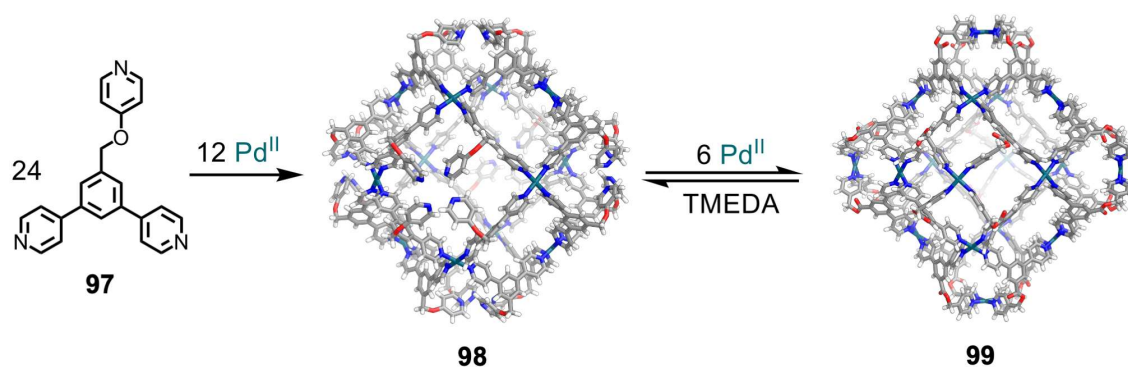
Figure 26. Stepwise assembly of a $Pd^{II}_{18}97_{24}$ stellated cuboctahedron **99** from terpyridine **97** and Pd^{II}.[155]

Initial selective complexation with just one type of pyridine donor to form **98** is perhaps surprising at first sight. The authors suggest that the selectivity observed is due to the high kinetic stability of the cuboctahedral framework. Previous work had shown that ligand exchange on a completed cuboctahedron occurs with a half-life of 20 days.[157] Kinetic trapping of the cuboctahedron thus drives selective assembly.

Subsequent addition of more $Pd^{II}(BF_4)_2$ to intermediate structure **98** resulted in the capping of the square faces by the coordination of four 'free' pyridyl groups to each new palladium(II) center, and consequent stellation of the structure to form **99**. Stellation is reversed by adding *N,N,N',N'*-TMEDA, resulting in the reformation of **98**. The authors note that this reversible opening and closing through stellation may have future applications in guest capture and release.

3.3. Non-Planar Macrocyclic Ligands

As shown in the system in Figure 22, macrocycle-derived subunits can be employed to construct coordination cages.[146,158-161] These components often have greater complexity than simpler small-molecule ligands, while maintaining high symmetry, which increases the

complexity of the resulting metal-organic architectures.[162,163] Furthermore, the use of macrocycle-derived components also may enable combination of the guest binding abilities of the macrocycles with those of the higher-order superstructures that the macrocycles form.[164-167]

Complementing the work of Hu and co-workers, who used *p-tert*-butylthiacalix[4]arene to form the vertices of a metal-organic polyhedron,[146] macrocyclic components have also been employed as the edges and faces of metal-organic cages. Hardie and co-workers reported foundational work in this area, using tritopic cyclotriveratrylene (CTV)-related ligands.[168-170]

The Hardie group's use of CTV-related ligands to provide an array of new structure types culminated in the report of a "Solomon's cube", based upon the topology of a Solomon Link.[171,172] The combination of extended tris-pyridyl cyclotriguaiacylene (CTG) **100** with $Pd^{II}(NO_3)_2$ in DMSO results in $Pd^{II}_4\mathbf{100}_4$ structure **101** shown in Figure 27. While resembling a Solomon link,[171,172] with alternating under and over crossing points of two rings, **101** has additional connections between the rings, linking them.[170] Consequently the structure was described as a "Solomon's cube", with square faces and eight triply-connected vertices.

100   **101**
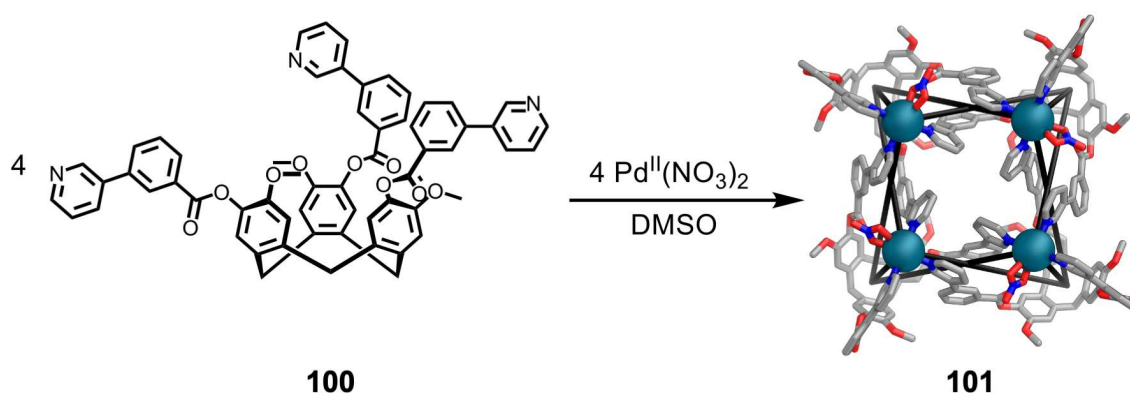
Figure 27. Assembly of $Pd^{II}_4\mathbf{100}_4$ "Solomon's cube" **101**.[170]

Structure **101** may thus be considered in terms of its three stereochemically-distinct subunits: ligand **100**, the Solomon link, and the figure-of-eight motifs lying on each of four sides of the structure. The crystal structure shows two enantiomers, in which all three of these elements concertedly show opposite handedness.

The driving force for the formation of smaller $Pd^{II}_4\textbf{100}_4$ assembly **101**, as opposed to a $Pd^{II}_6\textbf{100}_8$ structure, is likely due to ligand **100** containing *meta*-pyridine-based arms, as opposed to linear *para*-ligand regiochemistry, connected to a rigid macrocyclic core. Further stabilization of this topology may come from inter-ligand π-stacking interactions.

Structure **101** in Figure 27 thus demonstrates the ability of non-planar macrocycle-based ligands to produce more complex structure types than would be observed in analogous cases using planar D_{3h}-symmetric ligands. Interwoven **101** also exemplifies how using novel classes of ligands can lead to serendipitous discoveries.

3.4. Metallosupramolecular Chemistry Meets DNA Nanotechnology

Many of the architectures discussed in this review are assembled using small molecule organic ligands and metal ions. A more exotic example was provided by the metal-nucleic acid cages (Figure 28) of Sleiman *et al.*[173] These structures require stepwise assembly of oligonucleotide strands (**102**). First, triangles (**103**) with corners consisting of two bis-2,9-diphenyl-1,10-phenanthroline ligands (dpp-dpp) form, involving the hybridization of three complementary oligonucleotide strands. Second, by linking two triangles with single strands (**104**), which are then rigidified, trigonal prismatic structures are formed (**105**). Lastly, site-specific metalation, involving the coordination of Cu^I, Ag^I, Au^I, Zn^{II}, Co^{II}, Cd^{II} or Eu^{II} to the dpp-dpp sites, enables the creation of metal-DNA cages (**106**).[173]
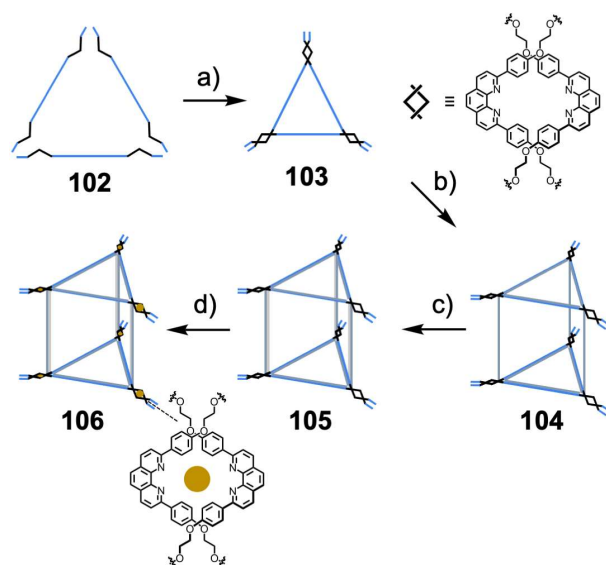
Figure 28. Stepwise assembly of metal-DNA cages from diphenylphenanthroline-containing DNA strands. (a) Hybridization of three complementary oligonucleotide strands. (b) Linking of two triangles with single strands. (c) Rigidification of linking strands. (d) Site-specific metalation.[173]

The Sleiman group also demonstrated that the order of the second and third steps could be swapped: pre-metalation of the triangles followed by single-strand triangle linkage and rigidification results in the same metalated trigonal prismatic structures. Although the flexibility in the order of construction steps indicates that metal-ligand coordination is not required to template the formation of these trigonal-prismatic structures, metalation of the structures increased their resistance to both chemical and thermal denaturation compared to their de-metalated counterparts. Metal coordination was thus demonstrated to enable the formation of robust architectures assembled from strands of DNA, potentially enhancing the range of applications of 3D DNA architectures.[174-178]

Through highlighting some key examples of complex or reduced-symmetry ligands that have led to novel structures, this section has emphasized the roles of both rational design and serendipity. As a general approach, the use of reduced-symmetry and complex ligands often

involves rational design, sometimes with the aid of computational predictions. Post-assembly rationalization has in many cases also played a role, enabling the discovery of new assembly rules, which may then be used for future designs.

4. Ligand Flexibility Drives Structural Complexity

Flexible ligands in many cases assemble into high-symmetry architectures.[179-185] However, flexibility within a ligand can also extend the scope of structure types beyond those having high symmetries. This section summarizes novel structure types generated *via* the incorporation of flexibility into the building blocks used to assemble discrete structures. Ligand flexibility often generates serendipitous results, as ligand degrees of freedom are deployed in unforeseen ways.

4.1. Flexible Ditopic Ligands

Ward and co-workers pioneered the construction of metal-organic architectures with flexible ditopic ligands, focusing on ligands containing two bidentate pyrazolyl-pyridine chelating sites, each attached to a central aromatic group *via* flexible methylene linkages. These ligands were combined in a 3:2 ratio with octahedral metal centers to yield several distinct structure types. Some of these structures have the geometries of Platonic solids, such as tetrahedra,[179-181] and others have lower symmetries and greater complexity.

Several of Ward's M_8L_{12} structures exhibit symmetry reduced from that of a cube.[186,187] For example, as shown in Figure 29a, the combination of **107** with Zn^{II} yields $Zn^{II}_8\mathbf{107}_{12}$ cuboid **108** with S_6 symmetry. An antipodal pair of Zn^{II} centers define the S_6 axis of the structure. These metal centers have *fac* stereochemistry, but opposite handedness.[186] The other six metal centers have *mer* stereochemistry, and are grouped into two sets of three. All metal centers within the same set have the same handedness, opposite to that of the other set. Mass spectrometry data shows the formation of an analogous $M^{II}_8L_{12}$ structure, $Co^{II}\mathbf{107}_{12}$, from Co^{II} and **107**.
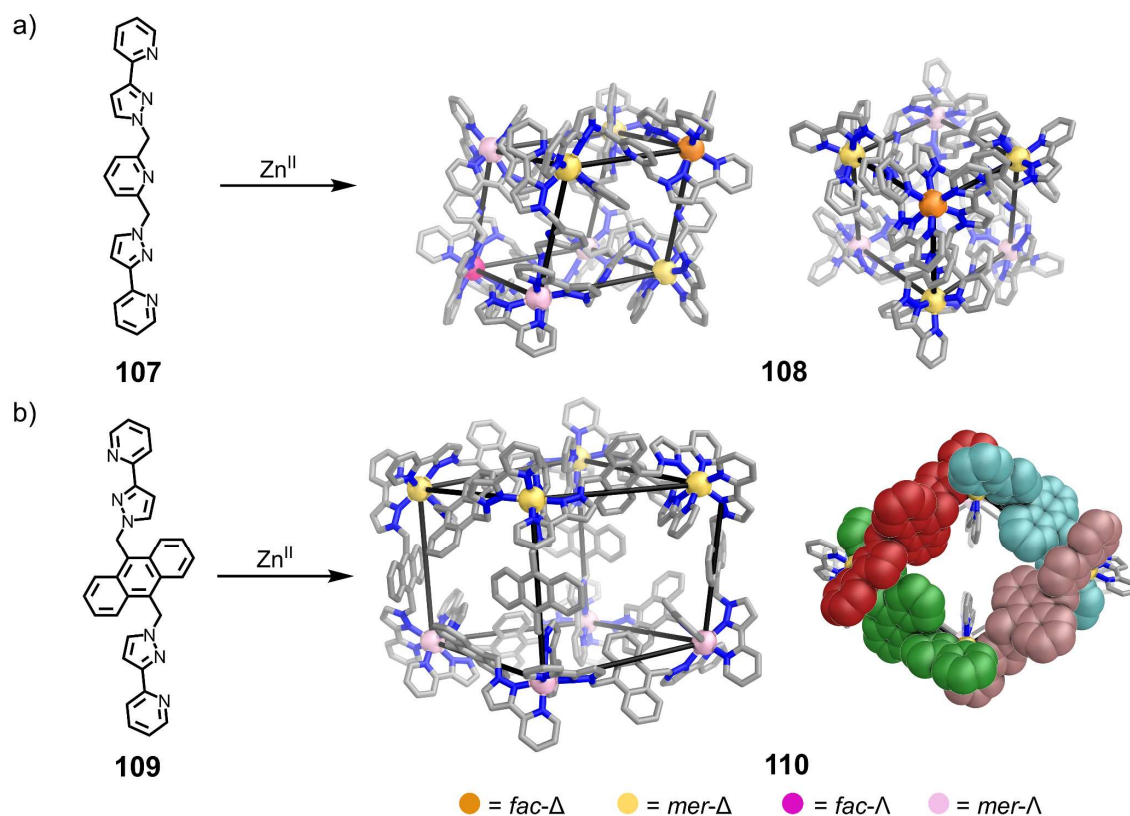
Figure 29. Two distinct $M^{II}_8L_{12}$ structures formed using ditopic pyrazolyl-pyridine ligands and octahedral metal centers.[186,187]

Using anthracene-cored ligand **109**, structure **110** was formed, which has the same $M^{II}_8L_{12}$ composition as **108**, but with significant structural differences. Cuboid **110** consists of two connected $Zn^{II}_4\mathbf{109}_4$ cyclic helical units (Figure 29b).[187] Within each tetrameric unit, the four metal centers are *mer* tris-chelated, and have the same absolute configuration. However, as shown in Figure 29b, the handedness of the four metals centers in one tetrameric unit are opposite to those making up the other tetrameric face. The use of $Cu^{II}(BF_4)_2$ with **109** yields $Cu^{II}_8\mathbf{109}_{12}$, which has a similar structure to **110**.

The diversity of structures formed using such ligands was further demonstrated by the formation of unusual $Ni^{II}_4L_6$ "square" and $M^{II}_6L_9$ (M^{II} = Zn^{II} and Co^{II}) "open book" structures, using **107** and its modified derivatives.[188,189]

Ligand **111** reacts with $Ni^{II}(BF_4)_2$ (3:2 ratio) in $MeOH/CH_2Cl_2$ (Figure 30) to yield a $Ni^{II}_8\textbf{111}_{12}$ structure, which was initially thought to be cubic.[190] However, X-ray crystallography shows that product **112** has an unusual C_{2v}-symmetric cuneane structure, formed by the rearrangement of two edges of a cube (Figure 30b). All eight of its metal centers have *meridional* stereochemistry. Interestingly, seven of the metal centers have the same absolute configuration, with the eighth displaying the opposite handedness.
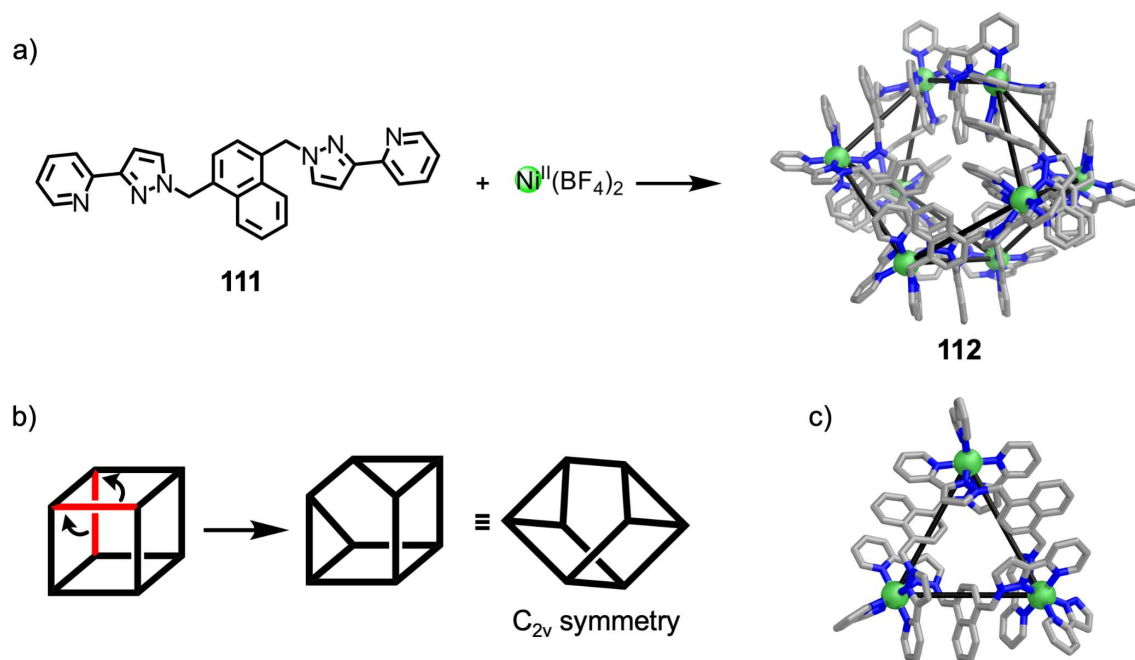
Figure 30. (a) Formation of $Ni^{II}_8\textbf{111}_{12}$ structure **112** with a structure based on a C_{2v}-symmetric 'cuneane' core.[190] (b) The 'cuneane' structure is obtained by the rearrangement of two edges of a cube. (c) View perpendicular to one of the $Ni^{II}_3L_3$ cyclic helical units making up the two triangular faces of **112**.[190]

Each of the two triangular faces of **112** is made up of a $M^{II}_3\textbf{111}_3$ metallomacrocycle (Figure 30c). Such M_3L_3 units have been observed in structures employing similar ditopic ligands.[191–193] The four structure types shown in Figure 31 are built from M_3L_3 subunits, with their different geometries arising from differences in how these subunits are connected to each other.

a)

113

and = Cd^{II} or Zn^{II}

= *mer* configuration
= *fac* configuration

M^{II} = Cd^{II}, **114**
M^{II} = Zn^{II}, **115**

b)

114

c)

113

= Cu^{II}

116

d)

116

e)

113

117

= Cd^{II}, Cu^{II} or Co^{II}

M^{II} = Cd^{II}, **118**
M^{II} = Cu^{II}, **119**
M^{II} = Co^{II}, **120**

f)

118

g)

121

= Cd^{II}, Cu^{II}
or Co^{II}

M^{II} = Cd^{II}, **122**
M^{II} = Cu^{II}, **123**
M^{II} = Co^{II}, **124**

h)

122

48
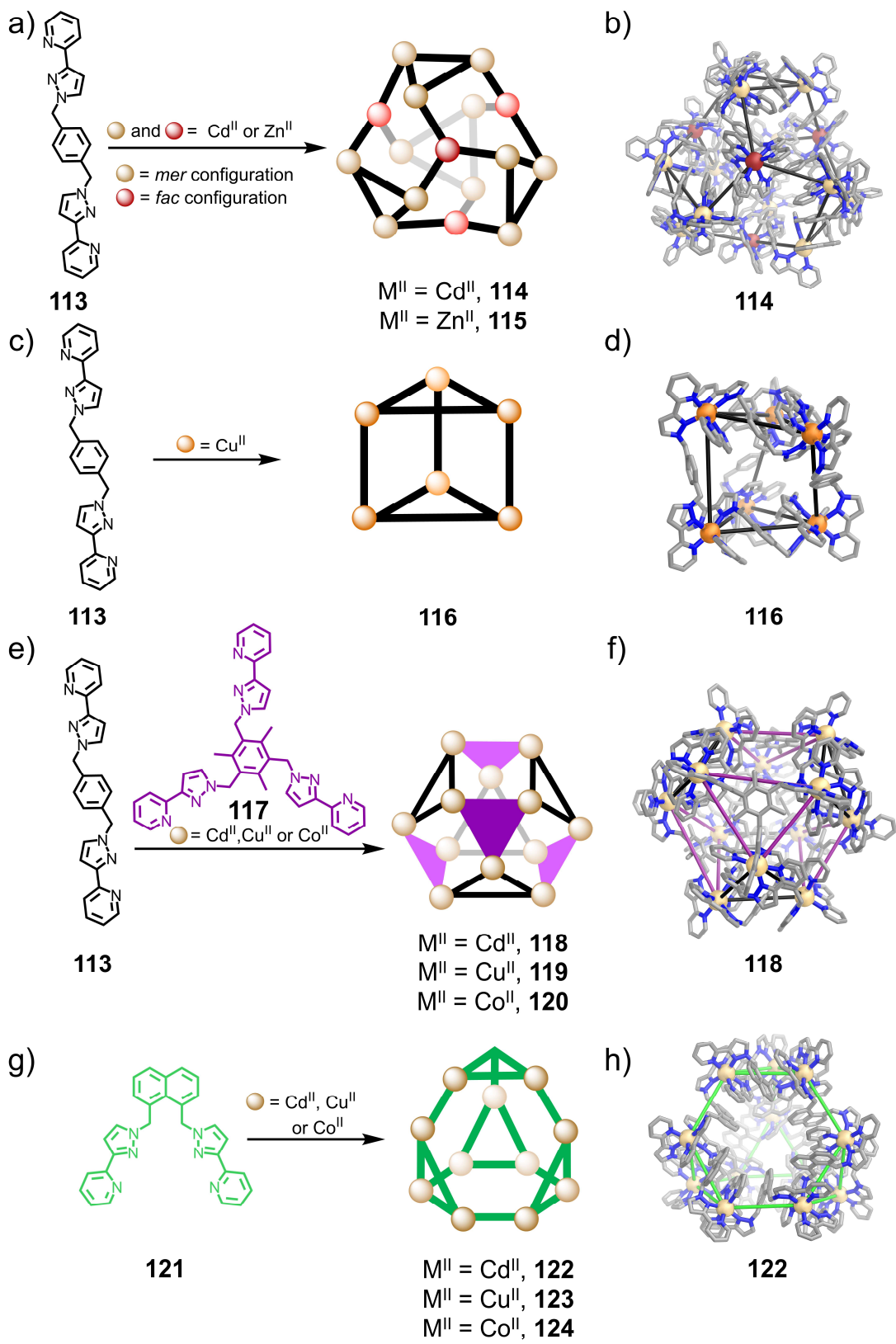
Figure 31. Four different structure types containing M_3L_3 circular helicate units. (a) Schematic view of $M^{II}_{16}\mathbf{113}_{24}$, (b) $Cd^{II}_{16}\mathbf{113}_{24}$,[191] (beige and red spheres correspond to *mer* and *fac* configurations, respectively), c) schematic view of $M^{II}_6\mathbf{113}_9$, d) $Cu^{II}_6\mathbf{113}_9$,[191] e) schematic view of $M^{II}_{12}\mathbf{113}_{12}\mathbf{117}_4$, f) $Cd^{II}_{12}\mathbf{113}_{12}\mathbf{117}_4$,[192] g) schematic view of $M^{II}_{12}\mathbf{121}_{18}$, and h) $Cd^{II}_{12}\mathbf{121}_{18}$.[193]

As shown in Figure 31a, structure **114**, a $Cd^{II}_{16}\mathbf{113}_{24}$ twisted tetracapped truncated tetrahedron, results from the reaction of **113** and Cd^{II} in MeCN; Zn^{II} also forms the analogous structure **115**.[191] Within **114**, four $Cd^{II}_3\mathbf{113}_3$ cyclic helical subunits are linked by $Cd^{II}\mathbf{113}_3$ units, which act as tritopic complex ligands (Figure 31b). The *fac*-configured Cd^{II} centers (red spheres in Figures 31a and b) of the $Cd^{II}\mathbf{113}_3$ units cap each of the four hexagonal faces of a Cd^{II}_{12} distorted truncated tetrahedral core described by the twelve *mer*-configured centers (beige spheres in Figure 31a and b) of the four $Cd^{II}_3\mathbf{113}_3$ units. When ligand **113** reacts with Cu^{II}, the smaller $Cu^{II}_6\mathbf{113}_9$ trigonal prismatic structure **116** forms (Figure 31c). Trigonal prism **116** consists of two $Cu^{II}_3\mathbf{113}_3$ circular helical units bridged by three ligands, with some offset between triangular faces leading to distortion towards a trigonal anti-prismatic structure (Figure 31d).

The reaction of $Ni^{II}(BF_4)_2$ with **113** produces a $Ni^{II}_8\mathbf{113}_{12}$ cubic cage, which does not contain trinuclear helicate units. The observation of different structures with the same ligand but different metal ions was attributed to variations in ionic radii and stereoelectronic preferences of the metal centers.[191] Furthermore, reaction of the same ligand (**113**) together with flexible tris-bidentate ligand **117** and Cd^{II}, Cu^{II} or Co^{II} in a 3:1:3 ratio yielded a $[M^{II}_{12}\mathbf{117}_4\mathbf{113}_{12}]$ cage with approximately cuboctahedral geometry (Figure 31e).[192] Of its eight triangular faces, four are capped by **117** and the remaining four each consist of a $M^{II}_3\mathbf{113}_3$ circular helical subunit, similar to those found in the other structures.

The fourth structure type, shown in Figure 31g, is an $M^{II}_{12}\mathbf{121}_{18}$ truncated tetrahedral cage framework with idealized *T* symmetry. This structure results from the reaction of **121**, which

has a napthyl central linking group, with Cu^{II}, Co^{II} or Cd^{II}.[193,194] These structures consist of four $M_3\textbf{121}_3$ circular helical motifs which are connected directly by six bridging ligands.

A common thread linking the different geometries shown in Figure 31 is the presence of linked $M^{II}_3L_3$ circular helicate subunits, where the three metal centers have *meridional* tris-chelate geometry. Another important feature of these four structure types is the prevalence of inter-ligand aromatic stacking interactions, often between electron-rich central aromatic moieties on one ligand and electron-deficient pyrazolyl-pyridine units of another.[191-193] This elegant work by the Ward group has thus established the utility of relatively simple, flexible, ligands in the construction of assemblies with structures beyond the Platonic solid, whose geometries are controlled by subtle variations in reaction conditions and ligand structure.

^{1}H NMR spectroscopy and mass spectrometry show that the $Cd^{II}_{16}\textbf{113}_{24}$ structure **114** described above is initially present in solution, but the structure rearranges to give a smaller $Cd^{II}_6\textbf{113}_9$ trigonal prism over weeks in solution.[191] Replacing the 1,4-phenyl moiety of **113** with the 1,4-naphthyl of ligand **111** results in a $Cd^{II}_{16}\textbf{111}_{24}$ tetracapped truncated tetrahedron (in contrast to the cuneane structure observed for **111** with Ni^{II}, shown in Figure 30a), which does not rearrange in solution. The additional inter-ligand π-stacking provided by the naphthyl spacer was inferred to stabilize the tetracapped truncated tetrahedron in solution.[195]

In contrast, the reaction of **111** with Cu^{II} does not selectively yield any species analogous to those shown in Figures 30 and 31. Instead, crystals of an unusual $Cu^{II}_{12}\textbf{111}_{15}$ structure form in low yield, consisting of two $Cu^{II}_3\textbf{111}_3$ units linked by an equatorial belt of six Cu^{II} ions, each with a coordination number of 4 or 5.[195]

Utilizing ligand **111** also allowed Ward *et al.* to analyze the $Cd^{II}\textbf{111}_{12}\textbf{117}_4$ analog of the structures shown in Figures 31e and 31f in solution. $Cd^{II}\textbf{111}_{12}\textbf{117}_4$ was shown to exist as three different diastereomers in solution, with T, C_3 or S_4 symmetry.[196] The difference between the

diastereomers arises from the different relative helical handedness of the four $Cd^{II}_3L_3$ circular helical units in the structure.

Kwong *et al.* reported the formation of D_3-symmetric $M^{II}_{12}L_{18}$ hexagonal prismatic architectures following the reaction of 2-formylpyridine **16**, *m*-xylylenediamine **125** and $Mn^{II}(ClO_4)_2$ or $Cd^{II}(ClO_4)_2$ in acetonitrile (Figure 32).[197] The crystal structure of **126** reveals two M_6L_6 hexagons, having chair conformations, made up of alternating Λ- and Δ-configured metal centers. Bridging ligands connect metal centers with a Λ configuration on one ring with those with a Δ configuration on the other, resulting in *mer*-Λ and *fac*-Δ configured metal centers within prism **126**. Other metal-organic structures beyond the Platonic solid constructed using similarly flexible ditopic ligands include a $Hg^{II}_4Cl_8L_4$ S_4-symmetric coordination nanotube[198] and a $[Dy^{III}_8L_8(\mu_2\text{-}CH_3OH)_4]^{8+}$ dual triple-stranded helicate.[199]
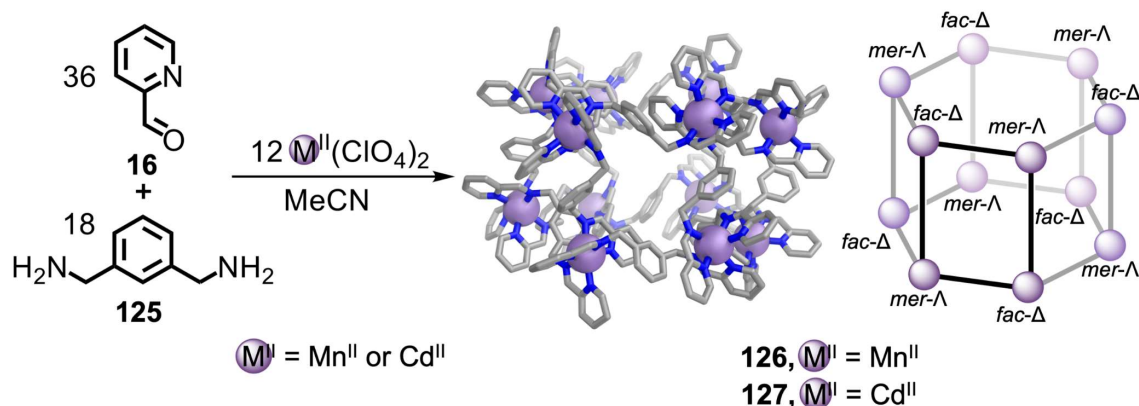
Figure 32. Subcomponent self-assembly of D_3-symmetric, $M^{II}_{12}L_{18}$ hexagonal prismatic structures **126** and **127**.[197]

Mirkin and co-workers have developed the 'weak-link approach' to forming reduced-symmetry structures with complex functions.[200] Figure 33 shows a dimeric capsule produced using this approach, incorporating resorcin[4]arene and calix[4]arene subunits linked by platinum(II) centers.[201] In the absence of chloride, 'weak-link' thioethers coordinate to platinum(II) binding sites. Upon the addition of chloride ions these thioethers are selectively displaced, causing

expansion of the cavity. The addition of silver(I) tetrafluoroborate reverses this expansion by abstracting chloride from the platinum(II) centers and regenerating the closed state of the capsule. In the thioether-coordinated form **131**, estradiol **133** is bound selectively. In the chloride-coordinated form **130**, two molecules of dextromethorphan•HCl (**132**) bind instead. Sequential addition of chloride to **131** and silver(I) tetrafluoroborate to **130** brings about reversible binding and release of dextromethorphan, showcasing the ability to reversibly generate cavities with different sizes and shapes, and thus control guest binding.
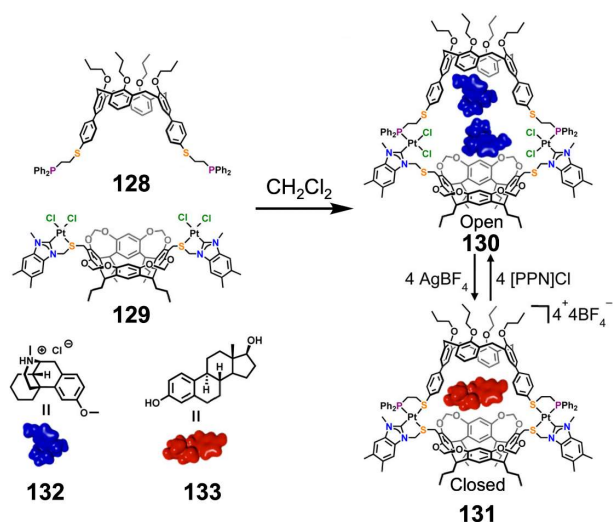
Figure 33. Controlled guest release and uptake using a 'weak-link' approach, using ligands **128** and **129**. [PPN]Cl = bis(triphenylphosphine)iminium chloride. Adapted with permission from ref 201 Copyright 2017 American Chemical Society.

4.2. Flexible Tritopic Ligands

The combination of flexible *tris*-formylpyridine subcomponent **134** with $Cd^{II}(OTf)_2$ and *p*-toluidine **135** yields a mixture of three products (Figure 34).[202] Two of these are *T*-symmetric $Cd^{II}_4L_4$ tetrahedra (**137** and **138**). In **137**, the central methyl groups of the ligands point inside the cavity (*endo*), whereas in **138** these methyl groups point outward (*exo*). The third, minor,

product is $Cd^{II}_8L_8$ tetragonal antiprism **139** with D_4 point symmetry. The eight metal centers defining the vertices of the structure have the same handedness, each with a *meridional* arrangement of ligands.
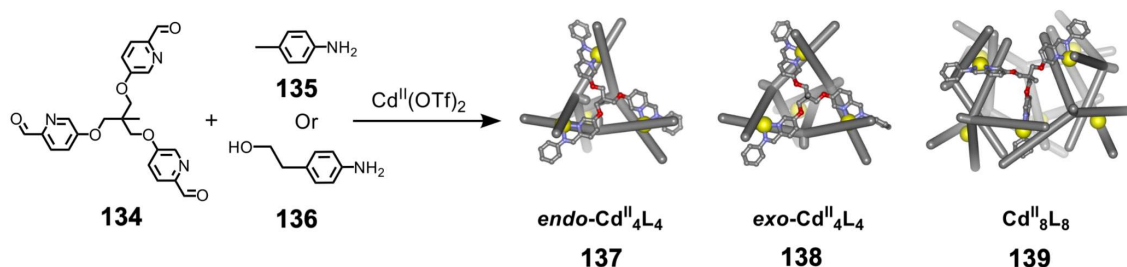
Figure 34. Conditions-dependent subcomponent self-assembly of three discrete products: tetrahedra **137** and **138**, and $Cd^{II}_8L_8$ tetragonal antiprism **139** with D_4 point symmetry. Adapted with permission from ref 202. Copyright 2016 American Chemical Society.

The relative amount of the $Cd^{II}_8L_8$ antiprismatic structure **139** grows with increasing concentration, by reducing the entropic penalty of forming a larger $Cd^{II}_8L_8$ species instead of the smaller $Cd^{II}_4L_4$ complexes. Even more effective at driving the formation of the $Cd^{II}_8L_8$ structure is the use of 2-(4-aminophenyl)ethanol **136** as a subcomponent in the place of *p*-toluidine (**135**), and the use of a 1:3 CH_2Cl_2:MeCN solvent mixture. We hypothesized that these conditions allow the formation of stabilizing hydrogen bonding interactions between the hydroxy groups of the aniline residues in the $Cd^{II}_8L_8$ antiprismatic structure. In this example, the analysis of a serendipitous result enabled the rational development of design principles for the optimized preparation of a complex architecture, illustrating the synergy between serendipity and rational design.

Hong *et al.* used a tris(pyridine) ligand, which had a similar flexible core to **134**, for the construction of open $Ag^I_6L_4$ cages upon reaction with Ag^IBF_4. These cages undergo further assembly to produce higher-order polycatenanes and polycages, depending on the reaction conditions.[203]

4.3. Flexible Tetratopic Ligands

In Sections 7.2 and 7.3 (below) we explore how barrel-like and other complex architectures have been constructed using tetratopic ligands that are elongated along one axis, or curved. Expanding upon this approach, Duan *et al.* used tetratopic ligands with flexible linkers separating two bis-tridentate units to prepare structure types that include trigonal prismatic barrels, cube-like structures and bicoronal trigonal prisms.[204-207] Assembly **141** (Figure 35a) is a $Ce_8\textbf{140}_6$ cuboidal architecture with pseudo-S_4 symmetry, forming from $Ce^{III}(NO_3)_3$, KOH and ligand **140**.[205] The crystal structure of **141** shows that four of its ligands have their long axes aligned, with their central methylene groups bent towards the inside of the cage, and the ligands at the top and bottom of the structure each have their methylene groups bent outside of the cage.
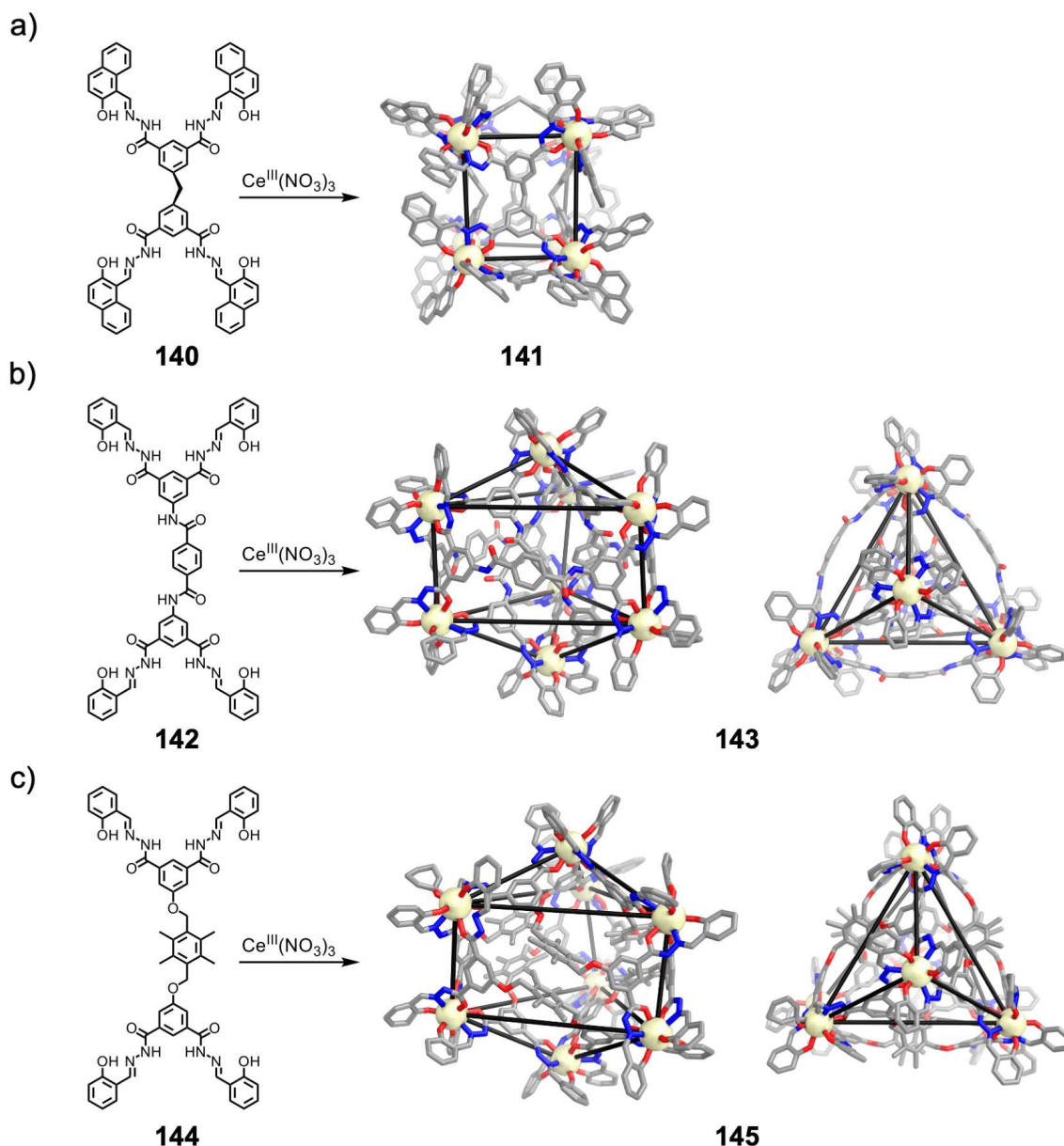
Figure 35. With Ce^{III}, tetratopic ligand **140** forms (a) cube-like **141**, (b) **142** forms **143** and (c) **144** forms **145**; both **143** and **145** are bicoronal trigonal prisms.[205-207]

However, such a pseudo-cubic structure type does not form when the similar ligands **142** and **144** (Figure 35) are used, forming instead the Ce$_8$L$_6$ complexes **143** and **145**, respectively. Assembly **143** consists of a Ce$_6$**142**$_3$ trigonal prismatic framework, with two additional metal centers and three ligands forming a helical pillar within the prism. Two of the tridentate moieties of each ligand of the helical pillar bind to the apical cerium centers, and the other two

tridentate sites chelate two of the metal centers making up the prismatic framework (Figure 35b).[206] In contrast, **145** has a cage-like structure, with the flexible ligand twisting so that the four cerium centers binding to the same ligand are not coplanar.[207] Furthermore, stacking interactions between the benzyl groups on neighboring ligands are inferred to stabilize the unusual structure of **145**.[207]

Sun and co-workers have also reported the use of flexible tetratopic ligands in the synthesis of unusual 'conjoined twin-cages'.[208,209] They were further able to control which species formed, either a $Pd^{II}_{12}L_6$ cage with three mechanically coupled cavities, or two helically isomeric $Pd^{II}_6L_3$ cages, by the judicious choice of assembly conditions.[208]

4.4. Flexible Ligands Containing More than One Type of Coordinating Motif

This section considers flexible ligands that bind metal centers using more than one type of donor atom or binding moiety incorporated into the same ligand. Octanuclear helicate **147** (Figure 36), with a cavity large enough to bind amino acids enantioselectively, exemplifies this approach.[210] The combination of $Zn^{II}Cl_2$ and chiral salen-based ligand **146** produces **147**, which consists of two bowl-like Zn^{II}_2**146**$_2$ dimers, linked by four equatorial zinc centers. Within the dimer, the 5-coordinate zinc centers are each chelated by the N_2O_2 pockets of the ligands, and the two metal centers are linked by two phenalato oxygen atoms. The two pendant pyridyl groups of each ligand remain free to coordinate to additional Zn^{II} ions, whose tetrahedral geometries are satisfied by coordination of two chloride ions, resulting in the formation of the Zn^{II}_8**146**$_4Cl_8$ structure **147**.
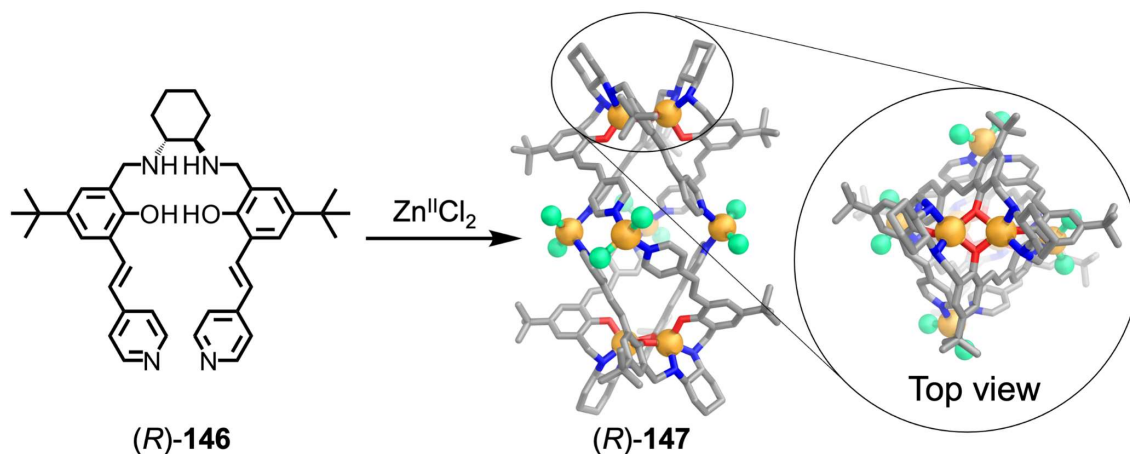
Figure 36. Assembly of octanuclear helicate **147**, consisting of two bowl-like $Zn^{II}_2146_2$ dimers, linked by four equatorial $Zn^{II}Cl_2$ units.[210]

The use of enantiopure ligand **146** is essential for the formation of cage-like helicate **147**. The use of racemic **146** results in the formation of dimeric units containing ligands with opposite handedness, which causes the four peripheral pyridyl groups to point towards different faces of the Zn^{II}_2 core, precluding helicate formation.

Li *et al.* reported cobalt-imidazolate cage **152**, which assembles by combining 2-methyl-4-formylimidazole **148**, *m*-xylylenediamine **125** and Co^{II}.[211] The twelve ligands form *in situ*, combining with twelve OH^- ions, four water molecules, four octahedral Co^{III} centers, four tetrahedral Co^{II} ions and twelve distorted square-pyramidal Co^{II} centers to form a *T*-symmetric tetartoid structure (Figure 37a). Furthermore, the addition of (*D*)- or (*L*)-menthol during self-assembly yields enantiopure *ΔΔΔΔ*-**152** or *ΛΛΛΛ*-**152**, respectively. The imidazolyl 2-methyl substituent was an effective steric structure-directing feature. This methyl group points inside the pentagonal face of the structure, whereas it could not fit within the smaller window of a cube.
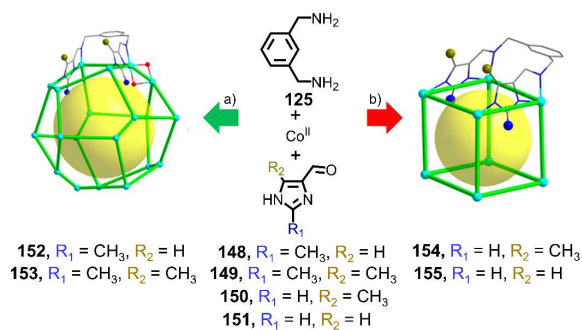
Figure 37. Subcomponent self-assembly of metal imidazolate (a) tetartoids and (b) cubes. The geometry of the assembled structure is governed by the steric properties of substituent R_1. Adapted with permission from ref 211. Copyright 2017 American Chemical Society.

In contrast, when 5-methyl-4-formylimidazole (**150**) or 4-formylimidazole (**151**) combine with Co^{II} and *m*-xylylenediamine, cubic cages **154** and **155** (Figure 37b) form, with the 5-methyl groups pointing away from the faces of the structure in **154**.[212] Thus, the substituents in the 5-position of the imidazolyl ring do not exert steric control over the structure formed, in contrast with 2-substituents. This work, together with Kwong's (Figure 32),[197] highlights the role that flexible subcomponents play in directing self-assembly. The same simple diamine subcomponent formed complexes with very different structures depending on the steric properties of other subcomponents within the system.

Li recently reported the use of a different flexible bis-imidazole ligand **156** (Figure 38) to form bicapped square antiprismatic structure **157** upon reaction with Cu^{II} under solvothermal conditions (Figure 38).[213] Single-crystal X-ray diffraction shows formation of $Cu^{II}_{10}\mathbf{156}_8$ cages that have two types of Cu^{II} centers. Eight equatorial Cu^{II} ions have a distorted square pyramidal geometry, with tetradentate chelation of one ligand and monodentate binding of a second. The two axial Cu^{II} centers are each bound by four imidazolate donors, with additional coordination of anions and water molecules to complete their coordination spheres.
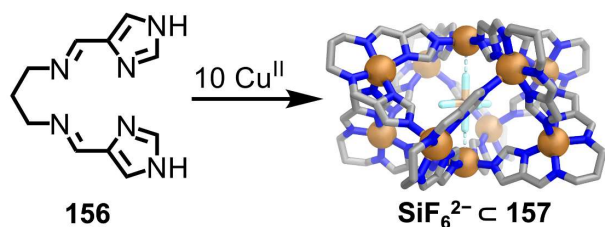
Figure 38. Self-assembly of adaptable $Cu^{II}_{10}\mathbf{156}_8$ bicapped square antiprism **157**.[213]

Bicapped square antiprismatic structure **157** can expand or compress vertically to accommodate different anions in its cavity, due to its flexible ligands. Among the anions encapsulated (SiF_6^{2-}, ClO_4^-, Br^- and Cl^-), SiF_6^{2-} gives the largest cavity volume, and Cl^- the smallest. Cage compression is triggered through anion exchange, for example, by the addition of KCl to a cage binding ClO_4^- internally. Li *et al.* also employed ligand **156** to form a mixed-valence Cu^{II}/Cu^I metallocycle.[214] Upon combination of this metallocycle with triethylenediamine in a 2:3 ratio, a trigonal prismatic structure forms.[215] This trigonal prism undergoes a structural transformation to form **157** upon oxidation of Cu^I to Cu^{II}.

4.5. Ligand Flexibility Arising from Substituent Positioning

An alternative way to introduce flexibility into ligands, without incorporating alkyl or other flexible linkers, is to vary the position of substitution of aryl rings or change the metal-binding moieties so as to provide multiple conformers capable of binding metal ions in different ways.

For example, tri- and tetra-topic ligands have been used that employ 3-pyridyl binding sites or imidazoles, in place of conformationally-locked 4-pyridyl binding sites. When binding to *cis*-protected square planar metal centers, such tritopic ligands can form M_6L_4 open cages (**159**)[216] or bowl-like[217] structures. Mukherjee *et al.* reported $Pd^{II}_6\mathbf{158}_4$ open cage **159**, which forms from tritopic ligand **158** with imidazole donor groups (Figure 39), and can catalyze Knoevenagel condensations and Diels-Alder reactions within its hydrophobic cavity in water.[216] Recently

Klajn and co-workers adopted this cage for the investigation of photoswitching in confined environments.[218-221]
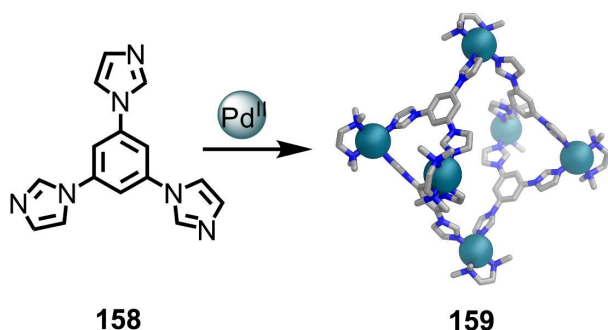
Figure 39. Self-assembly of open $Pd^{II}_6 158_4$ cage **159**.[216]

Analogous tetratopic ligands have been shown to form M_6L_3 trifacial[222,223] and M_8L_4 tetrafacial[64,224] barrels, structurally similar to those formed using the elongated tetratopic ligands discussed in Section 7.2. A similar type of ligand flexibility was employed by Schröder and co-workers to form a Cd_{66} nanosphere with idealized T symmetry. Its dual-shell structure consists of a sphere of 66 Cd^{II} centers, bridged by μ^3-hydroxide, μ^3-oxo, and μ^5-NO_3^- anions, enclosed by 12 DMF ligands and 20 tritopic organic capping ligands.[225]

4.6. Flexible Pseudolinear Polypyridyl Ligands

Fujita and co-workers have demonstrated that, in addition to inducing the formation of nanotubes from relatively rigid polypyridyl ligands through guest templation (Section 7.4, below), nanotubular structures are also obtained using more flexible ligands. The combination of $Pd^{II}(en)(NO_3)_2$ with ligand **160** (Figure 40) and a rod-like guest template results in the formation of $Pd^{II}_6 160$, an end-capped tube (**162**).[226] The flexible nature of the benzene-tetracarboxylate-containing core of the ligand allows it to fold and form structure **162** containing only one folded ligand. Selective guest binding within this tube was observed, whereby a biphenylcarboxylate guest bound unidirectionally, with the biphenyl group

ensconced in the hydrophobic pocket of the tube, and the hydrophilic carboxylate exposed to the solvent.
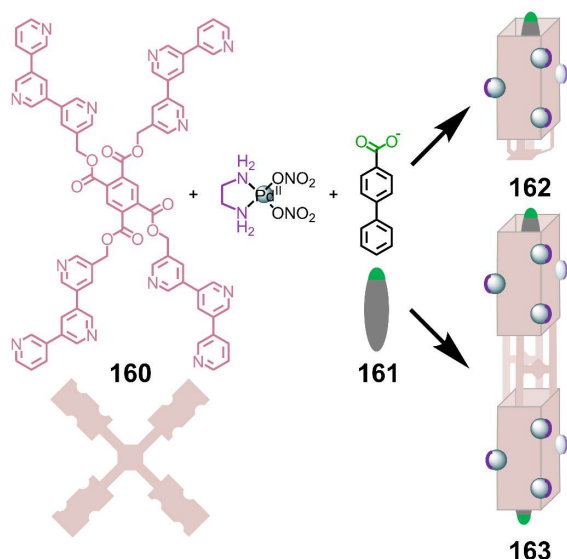
Figure 40. Flexible ligand **160** forms $Pd^{II}_6\mathbf{160}$ and $Pd^{II}_{12}\mathbf{160}_2$ nanotubes **162** and **163**.[226]

At higher concentrations the longer $Pd^{II}_{12}\mathbf{160}_2$ tube **163** forms as a minor species and was isolated *via* crystallization. X-ray crystallography reveals a doubly open-ended tube 3 nm in length, with two template molecules residing inside the cavity.

Similarly, Chand *et al.* showed that a flexible pseudo-linear tripyridine ligand forms a $Pd^{II}_3L_4$ double-decker cage. Upon reducing the metal:ligand ratio from 3:4 to 1:2, the ligand reconfigures into a U-shaped conformation in which the two terminal pyridines bind to the same Pd^{II} center to form a $Pd^{II}L_2$ spiro-type complex. The central pyridine donors of each ligand remain uncoordinated.[227] Interconversion between the two structure types occurred following alteration of the metal:ligand ratio of the reaction mixture.

A consistent theme for this section is that the structures formed from flexible ligands can be difficult to reliably predict, meaning results are often serendipitous. However, as elsewhere, rules and hypotheses derived from these initial observations can enable the design of related

structures and components, to selectively form a desired structure, which may have initially been observed to form as one component of a mixture. The adaptability exhibited by some structures formed using flexible ligands is more rarely observed for structures formed with more rigid ligands. The reconfiguration of these more flexible structures can lead to new functions, often related to guest binding.

5. Complexity Derived from Solvent, Anions and Templates

Changes in the environments where metal-organic cages form can alter the structure formed. The course of self-assembly may be reconfigured by changing the solvent, adding a guest, or manipulating external conditions such as temperature and concentration. Although the effects of environment on structure may be challenging to predict beforehand, they may be rationalized, and the resulting knowledge again used to infer self-assembly rules. In this section we review techniques used to generate complex architectures from simple subcomponents by the modulation of external conditions and by guest addition.

5.1. Solvent- and Concentration-Dependent Complexity

One of the most straightforward methods to direct the assembly of complex architectures is to vary the solvent used. We reported a system where tetrahedral metal-organic cage **165** forms in water, but where a mixture of methanol and water leads to the selective formation of pentagonal antiprism **166** instead (Figure 41).[228] By tuning the temperature in addition to the solvent, either architecture can be prepared exclusively, with lower temperatures favoring the pentagonal antiprism. This process involves a switch from *facial* (*fac*) coordination stereochemistry around the metal centers in the tetrahedral cage to all *meridional* (*mer*) metal centers in the pentagonal antiprism, where the lower-symmetry *mer* coordinative linkages give rise to increased structural complexity.[229-232] Antiprism **166** is kinetically stable to changes in solvent, requiring heating for a week to convert to the thermodynamically preferred tetrahedron **165** following solvent exchange. The pentagonal antiprism is, however, responsive to the addition of a competing aniline – addition of 4-methoxyaniline to a mixture of pentagonal antiprism **166** and tetrahedron **165** brings about the selective disassembly of **166**. Severin and co-workers were able to trigger the rearrangement of an octanuclear prismatic cage, which forms in chloroform, to a tetranuclear complex, by exchanging the

chloroform solvent for dichloromethane.[233] This work illustrates how even quite subtle changes in solvent can trigger substantial transformations in assembly structure, especially when the structures have specific binding interactions with that solvent.
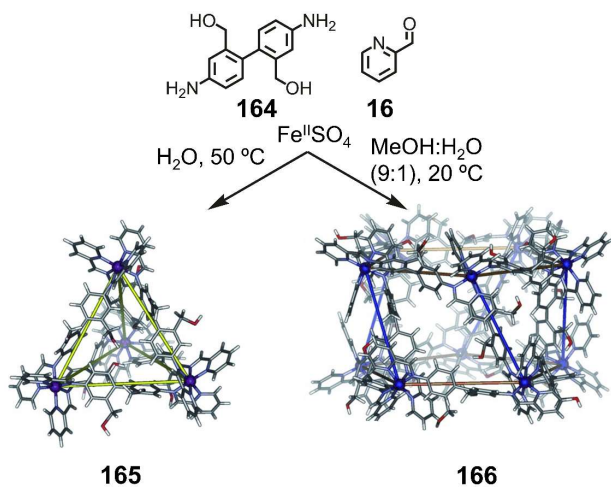
Figure 41. Formation of a self-assembled tetrahedron (**165**) and pentagonal antiprism (**166**), controlled by solvent polarity. Adapted with permission from ref 228. Copyright 2013 WILEY‐VCH Verlag GmbH & Co. KGaA, Weinheim.

Newkome, Wesdemiotis *et al.* reported an assembly process where at higher concentrations ligand **167** assembles with Cd[II] to produce bis-rhombohedral structure **168**, whereas at lower concentrations the simpler tetrahedron **169** is favored (Figure 42).[234] The use of tris-terpyridine ligands with Cd[II] provided the delicate balance of lability and stability required for these structures to form. At higher concentrations, the bis-rhombohedral architecture forms exclusively, whereas the tetrahedron is the exclusive product at lower concentrations. To confirm the structure of the tetrahedron, which cannot be isolated due to rapid equilibration back to the bis-rhombohedral architecture, a ruthenium(II)-containing metalloligand, essentially consisting of two units of **167** connected by the coordination of one (blue) terpyridine unit on each **167** to a kinetically inert ruthenium(II) center, was employed. The formation of a similar tetrahedral architecture confirmed the structural assignment of **169**. The

authors subsequently reported a system whereby the predominant product among three architectures – a cuboctahedron, an octahedron, and a triangular sandwich complex – depended upon the concentration.[235] These systems provide a way to generate and switch between complex architectures selectively in solution through manipulating concentration.
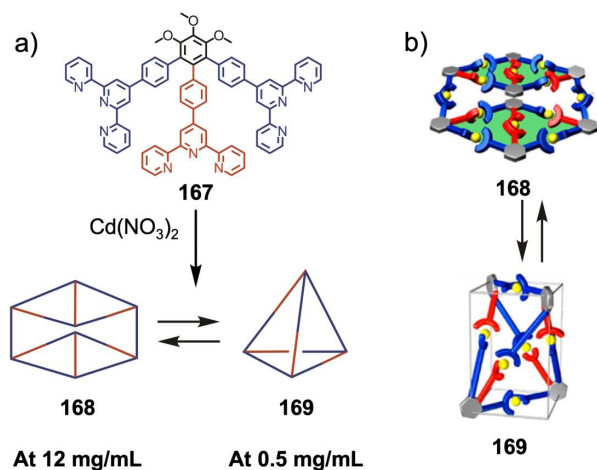
Figure 42. (a) Formation and switching between bis-rhombohedral complex **168** and tetrahedron **169** in a concentration-dependent process. (b) Schematic view. Adapted with permission from ref 234. Copyright 2014 American Chemical Society.

Shionoya and co-workers reported that tritopic ligand **170** forms bowl-like structure **171** and pseudo-tetrahedron **172** (Figure 43).[236] Conversion between **171** and **172** is governed by different stimuli. Changes in solvent, metal-ligand stoichiometry, guest addition, or pH leads to the formation of one architecture over the other. For example, increasing the proportion of water in the acetonitrile solvent leads to selective formation of capsule **172** from bowl **171**, and addition of further zinc triflate to a solution of **172** produces **171**.

Shionoya's group reported the use of a similar ligand with four-fold symmetry in combination with zinc triflate and a mixed solvent system to generate an unusual D_3-symmetric enneahedron.[237] We have also made use of solvent effects in a system where a tetrahedron interconverted with dimeric and trimeric stacked structures based upon different chemical

stimuli.[238] Analogous stacked structures had previously been generated from a more rigid, achiral subcomponent, where interconversion between double and triple stacks was controlled by subcomponent substitution.[239]
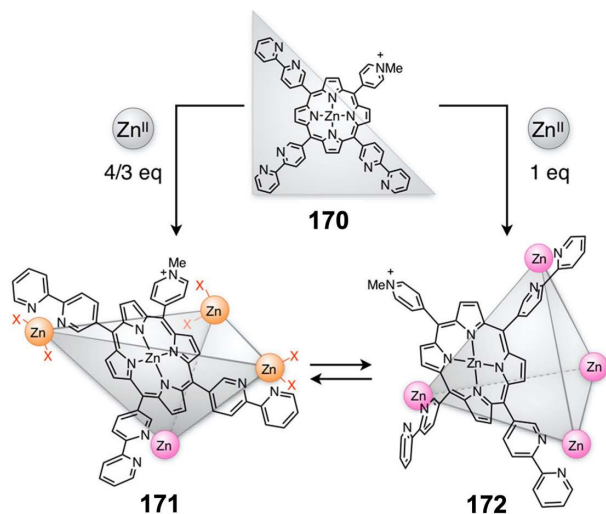
Figure 43. Formation of bowl **171** or pseudo-tetrahedron **172** from tris(bipyridyl)porphyrin **170**. Reproduced with permission from ref 236. Copyright 2020 American Chemical Society.

5.2. Temperature Dependent Assembly

Hiraoka and co-workers reported the intriguing system of Figure 44, where two similar building blocks sort with a selectivity that varies as a function of temperature.[240] Although these capsules are purely organic (Figure 44), held together by van der Waals forces, cation-π interactions, and the hydrophobic effect, their novel mechanism of sorting warrants inclusion in this review. The authors use gear-shaped amphiphilic molecules **173** and **174**, with hexaphenylbenzene cores, which self-assemble to form hexameric cubic architectures. These two hexaphenylbenzenes differ in the presence (**173**), or absence (**174**), of methyl groups in three positions (Figure 44). These additional methyl groups have a significant effect on the thermal stability of the formed hexameric architectures, with assembly **175**, composed of

trimethylated **173**, dissociating at 130 °C, whereas assembly **181**, formed from non-methylated **174**, dissociates at 65 °C. When both **173** and **174** were mixed and the mixture allowed to equilibrate at room temperature in water, a statistical distribution of capsules **175-181** formed, containing both panels, due to the structural similarities between them. The authors then heat the scrambled system above the disassembly temperature of **181**. This leads to survival of only **175** at 100 °C. The authors then quench the system by rapid cooling, trapping it in a metastable state consisting of only the two homogenous capsules **175** and **181**. These capsules then reequilibrate, taking 2 days at 25 °C to reach the equilibrium state of a statistical distribution. This process is further controlled by binding guests in the cavities of these self-assembled architectures. This work provides a unique example of control over the statistical distribution of a system of capsules using temperature-quenching techniques analogous to those used in metallurgy.
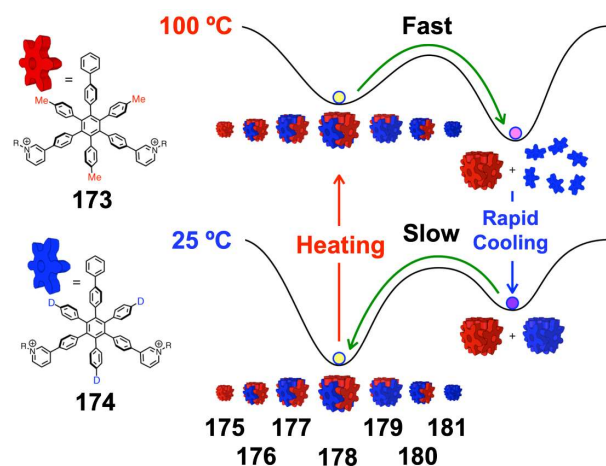
Figure 44. Temperature dependent self-sorting and scrambling behavior driven by quenching equilibria. R = CH_3. Reproduced with permission from ref 240. Copyright 2019, The Authors.

5.3. Guest-Templated Assembly

Fujita and co-workers prepared self-assembled heteroleptic trigonal prism **184** (Figure 45), the assembly of which requires the presence of certain π-extended guest molecules.[241] When no guest was present, oligomeric species and homoleptic octahedral [(ethylenediamine)Pd^{II}]$_6$**10**$_4$ predominated. Selective formation of heteroleptic **184** is driven by aromatic stacking interactions between electron poor-cage panels (**10**) and coronene (**183**), but also by the steric bulk of the linear bipyridine 'strut' **182**, which disfavors the coordination of two linear bipyridine ligands to a single palladium center. When the bipyridine struts are extended, allowing formation of larger trigonal prisms, three guest molecules stack selectively within the capsule cavity. Both capsules, containing two or three guests, were shown by UV/Vis spectroscopy to exhibit charge-transfer character.
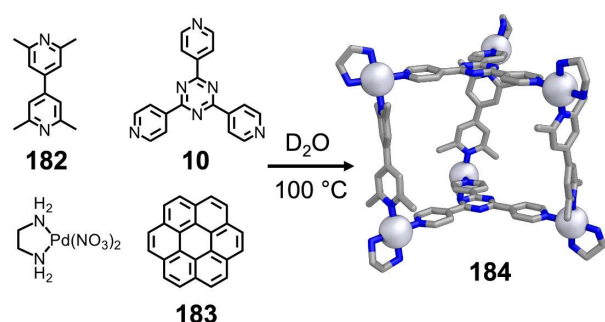
Figure 45. Self-assembly of ditopic **182** and tritopic **10** with (ethylenediamine)Pd^{II}(NO$_3$)$_2$ to form guest-templated trigonal prism **184**. The two bound coronene (**183**) guests not shown for clarity.[241]

The Fujita group has also reported systems of capsules formed from Pd^{II} with *cis*-chelating bidentate ligands, and pyridine or pyrimidine donor ligands, where guest binding triggers structural transformations. In one example, a trigonal bipyramidal cage transforms into an octahedral architecture on guest binding.[242] In another, an octahedral Pd^{II}$_{20}$L$_8$ structure transforms to an open Pd^{II}$_8$L$_4$ bowl shaped structure.[243] Further to this, Fujita and Hiraoka were able to control the specific constitutional isomer formed of a Pd$_3$L$_2$ complex, from a reduced-symmetry tripyridyl ligand, by judicious choice of guest molecules. Addition of a flat guest

molecule (1,3,5-benzenetricarboxylic acid) favoured the formation of a capsule with a relatively flat cavity, whereas the addition of a spherical guest ($CBrCl_3$) resulted in the formation of an isomer with a more spherical cavity, providing an early example of guest control of isomer formation.[244] We reported the transformation of a tetrahedral $Fe^{II}_4L_6$ cage, with porphyrin-panel edges, upon the addition of C_{60} or C_{70}. After addition of fullerene to the system, a $Fe^{II}_3L_4$ cone-like architecture forms. Selective transmetallation of a single iron(II) vertex for copper(I) was favored, resulting in the formation of a heterometallic $Cu^IFe^{II}_2L_4$ structure, exploiting the coordinative unsaturation of iron(II) at a single position.[245] Our group also reported the formation of a cuboctahedron that shows cooperative binding of a pair of C_{60} molecules. The binding of these guests triggers a rearrangement of the original O-symmetric structure to an S_6-symmetric analog, which optimizes fullerene binding.[246]

Müller and Möller reported the formation of a trigonal bipyramidal capsule, which incorporated its template. Sodium 5,5-ethylbarbiturate was added to a three-fold symmetric guanidinium-based ligand that chelated three Pd^{II} centers, leading to the formation of a trigonal bipyramidal architecture containing 33 distinct building blocks.[247] While investigating the endohedral functionalization of metal-organic polyhedra *via* the coordination of organophosphonates to polyoxovanadate units at the vertices of the cages, Fang *et al.* observed the formation of a barrel-like structure, instead of a tetrahedral structure that would ordinarily be expected to form.[248] The observed preference for the barrel-like structure is attributed to steric effects, as the interior cavity of the tetrahedron would be too small to accommodate the sterically bulky organophosphonate groups. Donnelly, Abrahams, Paterson, and co-workers have likewise reported the guest-induced formation of coordination nanotubes able to bind small molecules such as CO_2, CS_2 and acetonitrile.[249]

The Yoshizawa group reported a modification of their anthracene-paneled M_2L_4 lantern architectures, whereby guest binding drives the formation of heteroleptic structures (Figure 46).[250] They use two pyridine-based bidentate ligands of different lengths, **185** and **186**. Each

ligand independently assembles to form an M_2L_4 lantern architecture, with spherical internal cavities capable of binding aromatic guests. When the two cages are mixed together, a complex mixture of hetero- and homo-leptic architectures forms. However, when C_{60} is added to this mixture, a single heteroleptic host-guest species is seen, with the composition $Pd^{II}_2\textbf{185}_2\textbf{186}_2 \subset (C_{60})$. Computational models suggested that the *cis* isomer of this architecture is favored over the *trans* isomer. The observed preference for the heteroleptic architecture is attributed to the optimization of aromatic stacking interactions between guest and host.

This guest-driven host-rearrangement concept might be employed to selectively generate a range of architectures tailored to specific guest-binding tasks. In this approach, the cavity of the host is already filled, thus precluding its use for the binding of guests with lower affinity than the template, or necessitating the optimization of template removal. Yoshizawa and co-workers have recently reported the use of a guest template to drive a system of equilibrating atropisomeric cages towards a single isomer in a similar system.[251]
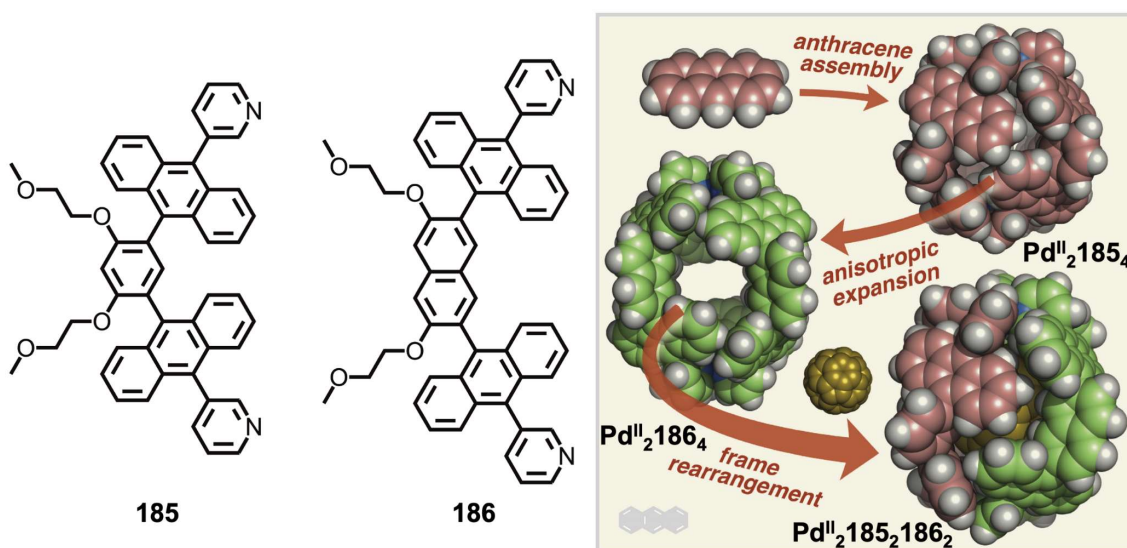
Figure 46. The formation of a heteroleptic lantern driven by guest encapsulation. Reproduced with permission from ref 250. Copyright 2015 WILEY‑VCH Verlag GmbH & Co. KGaA, Weinheim.

5.4. Anion-Templated Assembly

We reported a system of complex architectures based on anion binding and subcomponent self-assembly (Figure 47).[252] Diformylbipyridine subcomponent **187** combines with *p*-toluidine (**135**) and cobalt(II) triflimide to generate an initial mixture of architectures. The addition of a triflate template leads to the assembly of a $Co^{II}_4L_6$ tetrahedron. However, when lithium perchlorate or potassium hexafluorophosphate are added to either the dynamic library or the tetrahedral architecture, clean conversion to pentagonal prism **188** (Figure 47) is observed upon heating.
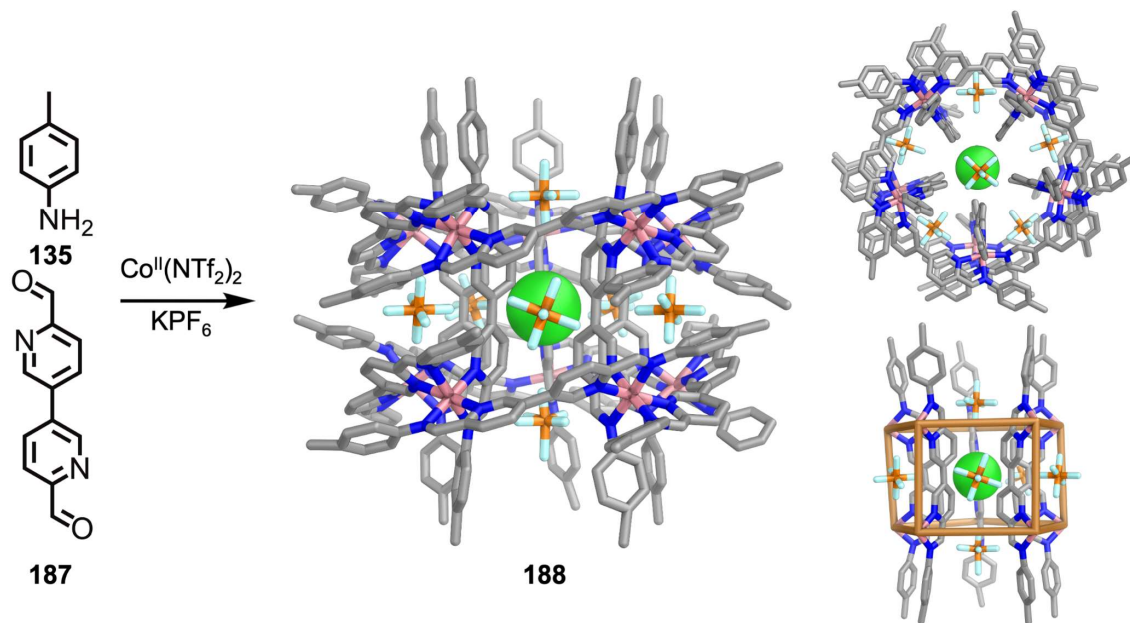
Figure 47. Formation of anion-templated pentagonal prism **188**.[252]

$Co^{II}_{10}L_{15}$ architecture **188** consists of two parallel $Co^{II}_5L_5$ pentagonal rings connected by five bridging ligands, creating a barrel-like structure. This structure is templated by five perchlorate or hexafluorophosphate anions in binding pockets between pairs of bridging ligands. Forming a pentagonal prism in place of the initial tetrahedral structure is favored for reasons that include the maximization of stacking interactions, and a better size-match of perchlorate or hexafluorophosphate with the smaller cavities found in the pentagonal prism.

The formation of pentagonal prism **188** also generates a central binding pocket, surrounded by ten internally-facing pyridine CH groups. This pocket is occupied by a chloride ion, scavenged during synthesis, which is so strongly bound that it cannot be removed by addition of silver(I), in analogous fashion to other self-assembled systems found to bind strongly to halides.[253-255] This system thus provides an unusual way to generate a secondary anion binding site by the addition of an initial anionic stimulus. Further work explored different architectures formed by subcomponent self-assembly using this same dialdehyde **187**.[256-259]

Chifotides and Dunbar have reported the use of anion-π interactions to control the formation of tetrameric or pentameric helicates, depending on the identity of the anion used.[260] The choice of anion during self-assembly likewise dictates the identity of the product formed in the work of Pan, Xu *et al.*, where the formation of either a $Pd^{II}_2L_4$ or a $Pd^{II}_3L_6$ capsule is driven by the addition of nitrate (favoring $Pd^{II}_2L_4$) or triflate/tetrafluoroborate (favoring $Pd^{II}_3L_6$). This selectivity is driven by differential guest binding within each capsule.[261] Lützen and co-workers also reported the formation of a chiral $Pd^{II}_4L_8$ flexible architecture, whose formation is dependent on templation by tetrafluoroborate.[262]

6. Multimetallics: Heterometallic and Cluster-Containing Architectures

Complexity may be enhanced through the development of heterometallic self-assembled systems, which employ the differing coordination preferences of more than one metal. The development of systems that take advantage of the coordinational flexibility and unusual geometries of metal clusters can also lead to the formation of novel architectures. Either the kinetics or the thermodynamics of self-assembly may be employed to direct the outcome of a multi-step process, as described in the examples below.

6.1. Ligand Coordination Preference

An early example of heterometallic supramolecular assemblies was provided by Raymond and Wong, who used ligand **189** that contains both hard and soft donors (Figure 48) to selectively bind two different metal ions.[263,264] The catechol group of ligand **189** binds to hard metal centers such as Ti^{IV} and Sn^{IV}, and the phosphine to softer metal centers, such as Pd^{II}. A stepwise process was initially employed, first installing the catechol-binding metal, as insoluble polymers were observed when phosphine coordination was attempted first. However, under optimized conditions Ti^{IV}- and Sn^{IV}-containing mesocates are generated in a single step *via* selective self-assembly. Similar principles using other ligand designs have been used by the groups of Wang,[265] Duan,[266,267] Brechin,[268] and Youngs[269] to generate other trigonal bipyramidal assemblies.
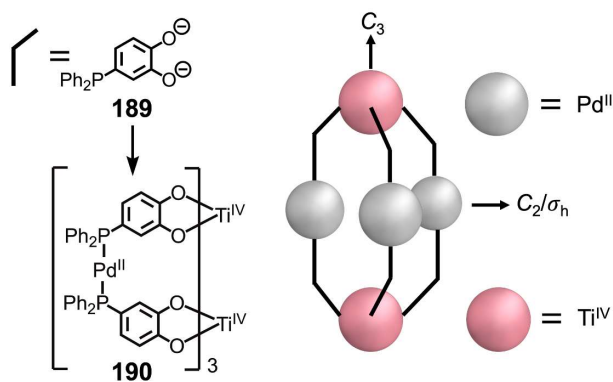
Figure 48. Heterobimetallic $Ti^{IV}_2Pd^{II}_3\mathbf{189}_3$ mesocate **190**, formed using ligands that contain both hard and soft donors.[263,264]

Expanding upon the principles developed by Raymond and Wong,[263,264] Lützen *et al.* reported a system incorporating both Fe^{II}, which is selectively bound by pyridyl imines, and Pd^{II}, which binds selectively to monotopic pyridine donors, to form a system capable of complex-to-complex switching, with a concomitant spin-state transition (Figure 49).[270] Selective binding is driven by both intrinsic ligand preference (avoidance of steric clash at palladium centers ligated by pyridyl imines) and by the pre-assembly of Fe^{II} metalloligand **193** using chelating tris(2-aminoethyl)amine (**192**). This chelating ligand enforces *fac* hexadentate coordination on the assembly. Subsequent addition of $[(dppp)Pd^{II}(OTf)_2]$ (where dppp = 1,3-bis(diphenyl-phosphino)propane) causes selective assembly of trigonal bipyramid **194**, where two palladium coordination sites are occupied by the bidentate phosphine ligand. When $[Pd^{II}(MeCN)_4](BF_4)_2$ is instead employed, cubic architecture **195** is generated, having a structure analogous to one that we prepared using a pre-assembled platinum complex metalloligand.[271] When a less sterically-hindered aldehyde subcomponent is added, the more hindered subcomponent **191** is displaced and the iron(II) transitions from a high-spin state to a low-spin state.
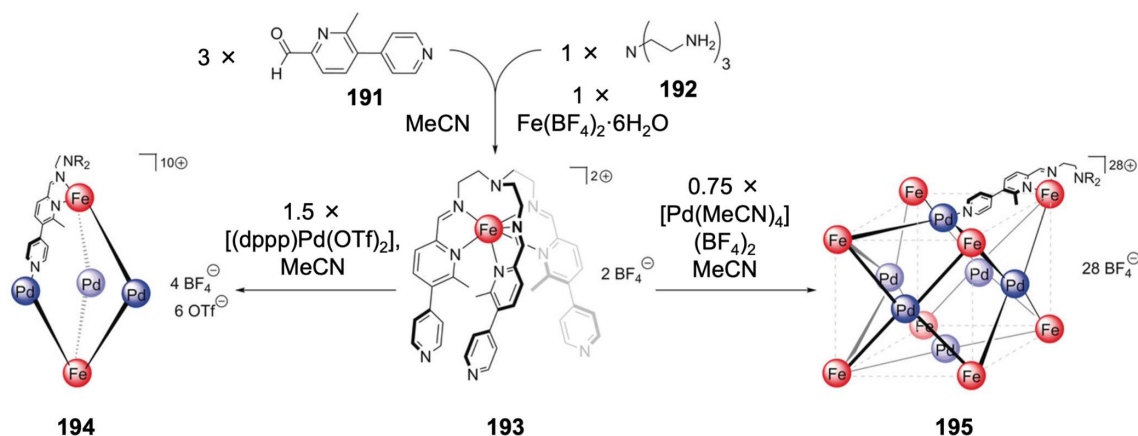
Figure 49. The self-assembly of subcomponents **191** and **192** with Fe^{II} to produce metalloligand **193**, which then forms bimetallic trigonal bipyramidal (**194**) and cubic (**195**) architectures. Reproduced with permission from ref 270. Copyright 2020 WILEY‐VCH Verlag GmbH & Co. KGaA, Weinheim.

Crowley and co-workers reported a nona-nuclear heterometallic Pd$^{II}_3$Pt$^{II}_6$ donut-shaped cage, where the use of two different metal binding sites on each ligand – bidentate triazole-pyridine, versus monodentate pyridine – enables heterometallic assembly. The architecture catalyzes the light-mediated hetero-Diels-Alder reaction of anthracene with singlet oxygen.[272]

6.2. Combining Kinetically Inert and Labile Metal Ions

The use of a mixture of kinetically inert and labile coordination centers has been explored extensively by the Ward group (Figure 50).[273-276] Their stepwise approach involves the initial formation of a coordination complex between three pyrazolyl-pyridine ligands and kinetically inert Ru^{II} or Os^{II}. This complex is formed as a statistical mixture of *fac* and *mer* isomers, and the minor *fac* isomer is then isolated, exploiting the inertness of these metals.[277] This fac Ru**113**$_3$ complex is represented in red in Figure 50. One coordinating site on each ligand is occupied by the Ru^{II}, leaving the other free for coordination to a coordinationally labile metal center. Subsequent addition of labile Co^{II}, Cd^{II} or Ag^{I} then results in self-assembly with efficient

error checking, as the structures undergo coordinative reconfiguration about the labile metal ion.
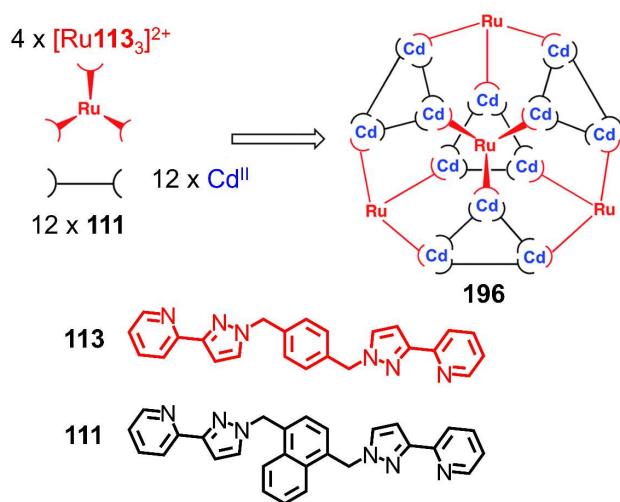
Figure 50. Formation of $Ru^{II}_4Cd^{II}_{12}111_{12}113_{12}$ twisted tetracapped truncated tetrahedral assembly **196**, containing both kinetically inert and labile coordination centers and two distinct ligands. Reproduced with permission from ref. 276. Copyright 2016 The Royal Society of Chemistry.

The Ward group were able to further develop this system to install two types of ligands selectively into a heterometallic architecture (Figure 50), to form $Ru^{II}_4Cd^{II}_{12}111_{12}113_{12}$ twisted tetra-capped truncated tetrahedral array **196**.[276] The design of this structure builds upon the homometallic $M_{16}L_{24}$ structures previously reported by the same group, depicted in Figure 31a.[191]

The Jin group have also reported a series of heterometallic capsules that combine kinetically inert metals, such as rhodium and iridium, with kinetically labile metals, such as silver and zinc.[278]

6.3. Multimetallic Vertices

Dicopper 'paddlewheel' vertices have been used to generate an array of molecular capsules.[279,280] An elegant example generated a 'capsule-within-a-capsule', **198**, using dicopper paddlewheel complexes as nodes (Figure 51) and was reported by Schmitt and co-workers.[281] Extended tri-*meta*-benzoic acid ligand **197**, once deprotonated, reacts with $Cu^{II}(NO_3)_2$ to form **198**. X-ray crystallography reveals a complex octahedron-within-cuboctahedron architecture, with the inner assembly fully linked to the outer. The architecture, which can be made soluble by post-assembly modification with alkylpyridine donors, can absorb 7-amino-4-methylcoumarin from solution.
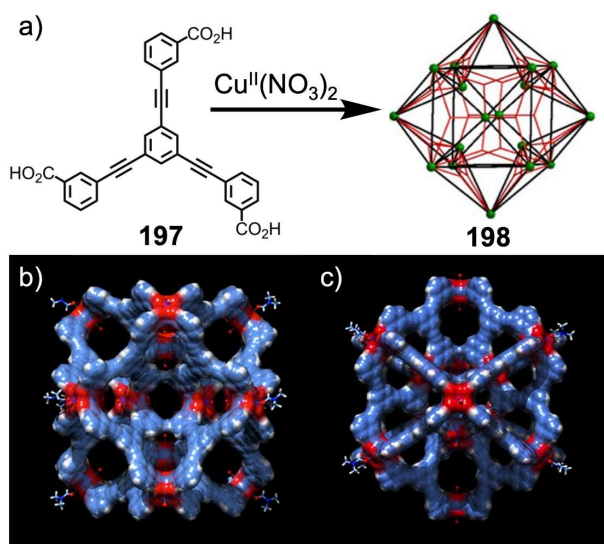
Figure 51. (a) Formation of 'capsule-within-a-capsule' **198**, (b)+(c) composed of an octahedron nested within a cuboctahedron, shown from two perspectives. Adapted with permission from ref. 281. Copyright 2017 Springer Nature.

The potential of using coordinationally-flexible bimetallic clusters was recently highlighted by our group, in the assembly of a trigonal prismatic cage that incorporates disilver vertices

(Figure 52).[282] The non-converging coordination vectors of 2-formyl-1,8-napthyridine **200** combined with the flexible coordination sphere of silver(I) leads to the formation of disilver vertices. The geometry of tris(4-aminophenyl)amine **199** and an appropriate anionic template (Figure 52b) generates a $Ag^I_{12}L_6$ trigonal prism, **201**.

Crystallographic analysis of **201** shows that two anions are bound within its cavity, held in proximity by the surrounding metal-organic architecture. Two HSO_4^- anions bind in close proximity, stabilized by additional hydrogen bonding interactions, as seen in the cyanostars of Flood and colleagues.[283] Linear, covalently-linked dianions also serve as competent templates for the trigonal prism. Even highly-oxidizing species such as peroxodisulfate, which is known to oxidize Ag^I to Ag^{II},[284] can be used, demonstrating the power of self-assembly to alter the properties of structural subunits.[2,35,62,285] Silver clusters have also been used to generate a Ag_{180} nanocage 2.5 nm in diameter, based on silver 'trigons' – three silver ions in a triangular arrangement.[286]
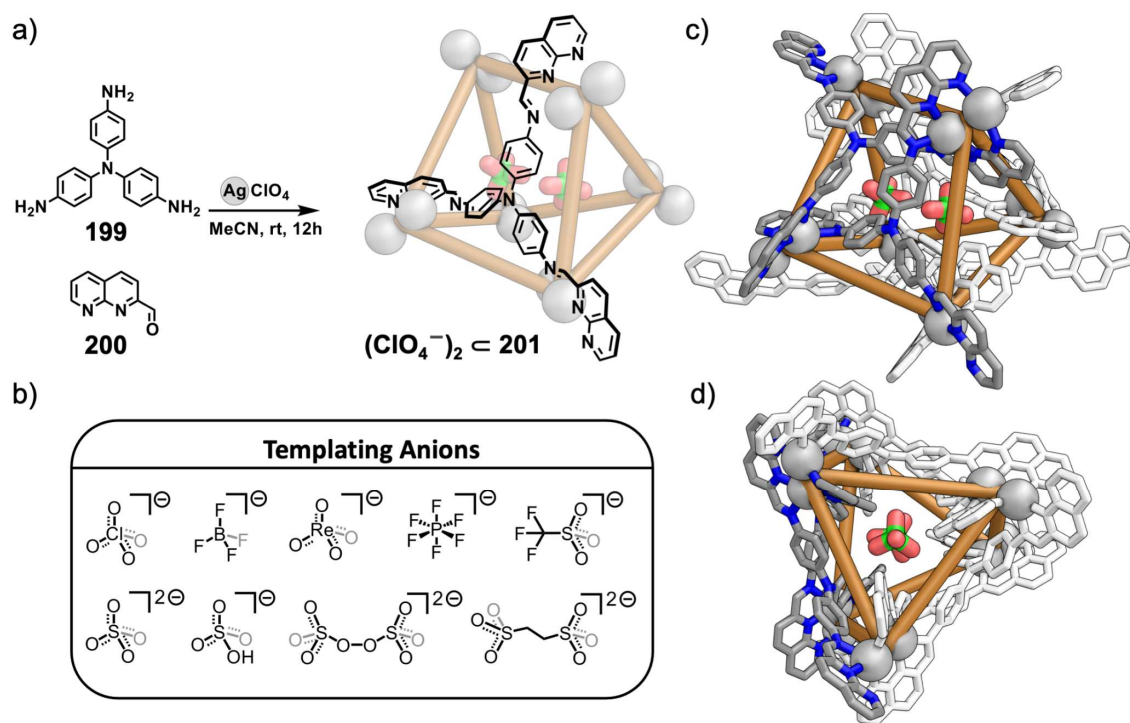
Figure 52. (a) Formation of trigonal prism **201** from silver(I) and subcomponents **199** and **200**, which binds (b) pairs of anions, or dianions, driven by the coordinational flexibility of silver(I) and anion templation. Two views of the crystal structure of **201** are shown in (c) and (d). Reproduced with permission from ref. 282. Copyright 2019 American Chemical Society.

We further extended this concept to incorporate not just bimetallic corners, but also Ag^I_4 and Ag^I_6 clusters as integral structure-directing motifs, using the ditopic subcomponent **202**.[287] As shown in Figure 53b, **202** and **203** initially form mixtures of tetrahedra and three-stranded helicates (**204**–**207**). The mixture of **204** and **206** then proceeds to generate six-stranded helicates **208** and **209** in the presence of suitable anionic templates (Figure 53c,d), while analogous structures do not form from subcomponent **203**. Key to the formation of these unusual structures is the judicious choice of anion. Whereas the addition of other anions to the equilibrating mixture of **204** and **206** does not effect structural transformation, addition of iodide, bromide or sulfate triggers rearrangement to a six-stranded helicate that resembles a sheaf of wheat. Its elongated structure is confirmed by X-ray crystallography and by solution NMR spectroscopy. This work provides an unusual example of the mutual stabilization between metal clusters and a self-assembled architecture, with anions playing a central role in structuring the metal cluster, and so the superstructure, thus formed.[287]
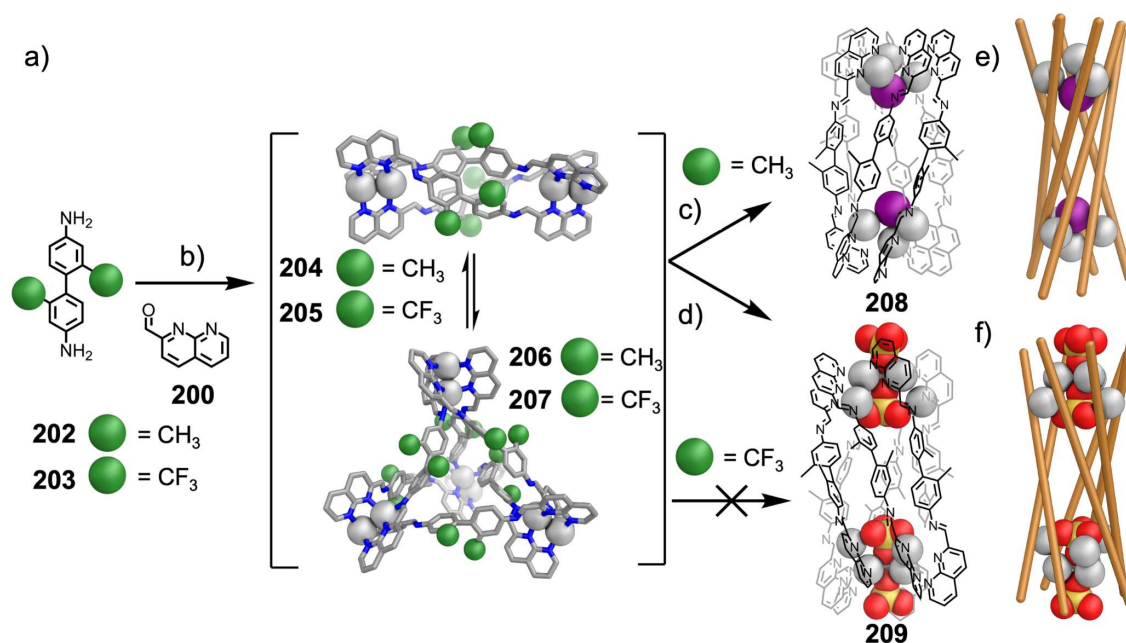
Figure 53. (a) Synthesis of six-stranded helicates **208** and **209**, formed during self-assembly from dianiline **202**, but not from dianiline **203**, capped by Ag_4 or Ag_6 clusters. (b) $AgNTf_2$, MeCN; (c) Tetrabutylammonium iodide; (d) tetramethylammonium sulfate. Structures of **204** and **206** are MM3 models, and those of **208** and **209** are based on crystallographic data. Simplified representation of six-stranded helicate e) **208** and f) **209**. Adapted from ref. 287.

Other metal clusters have been used as capsule vertices,[288] including polyoxometalate-derived caps,[289] which formed a capsule with an unusual 'near-miss Johnson' geometry, tungsten-copper synthons, which enabled the formation of distorted octahedral structures,[290] tripalladium vertices ligated by tetrazole linkers,[291] and trizirconium clusters, which formed the corners of a chiral coordination cage capable of performing sequential asymmetric reactions.[292] Manganese has also been employed to generate cages related to truncated tetrahedra.[293]

6.4. Organometallic Macrocyclic Tubes

Tubular assemblies may be generated by linking macrocyclic ligands with a band of metal centers, as exemplified by the work of Pöthig and Altmann (Figure 54), representing an alternate form of structure-directing metal cluster.[294] The reaction of macrocycle **210**, containing four imidazolylidene and two pyrazolate rings, with silver(I), then gold(I) ions leads to the formation of extended tube **211**. The cavity of **211** binds the linear guest 1,8-diaminooctane in organic and aqueous solutions. Architecture **211** exemplifies a novel approach to metal-driven self-assembly, where the metal ions define a central ring, rather than vertices. Such architectures have been used to form mechanically interlocked organometallic [2]rotaxanes.[295] Shionoya and co-workers have previously reported an Ag_3L_2 structure, where two ligand discs are linked by a ring of three silver ions, in a conceptually related example, but using solid disc shaped ligands rather than macrocycles.[296]
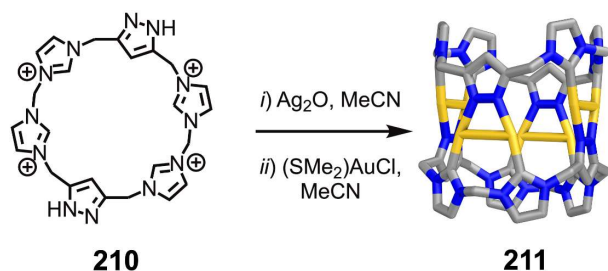
Figure 54. Formation of organometallic macrocyclic tubular structure **211**.[294]

Hetero- and multi-metallic self-assembled structures have not been used as extensively as other techniques to generate complex architectures, but there is clearly great potential in this approach. A focus of future work will be utilizing the properties of the multiple metal ions to achieve tasks that cannot be achieved by a single ion. The use of metal clusters with coordinational flexibility as vertices likewise shows promise in the generation of complex architectures from simple ligands.

7. Geometric, Steric, and Subtle Noncovalent Effects

Geometric constraints can shape the self-assembly of high-symmetry structures. Key examples from the Fujita group have shown that even slight alterations of bend angles (θ, Figure 55), or flexibility, of dipyridyl ligands can result in the formation of polyhedra with dramatically different sizes (Figure 55).[297,298] The selective formation of tetrahedra or cubes also depends upon the relative orientations of the coordination vectors in bis-bidentate ligands.[28] Similar geometric principles have been shown to drive the formation of more complex, lower-symmetry architectures, and to enable discrimination between different structures of high complexity. This section will highlight instructive examples of geometric control, along with cases demonstrating the impact of subtle steric effects and noncovalent interactions on the outcome of self-assembly processes.
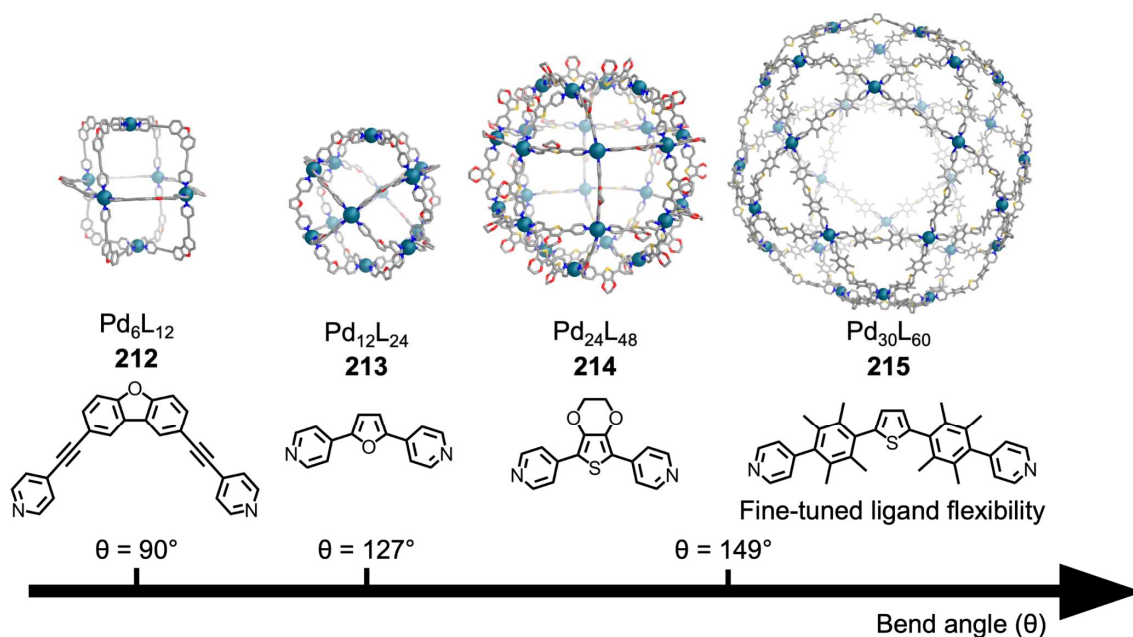
Figure 55. Family of spherical, polyhedral structures that Fujita *et al*. constructed by varying the bend angle, or flexibility, of ditopic, "banana-shaped" bipyridines.[31,156,297,298]

7.1. Bend-angle Dependence of Ditopic Struts

Key work by Fujita and others has demonstrated that myriad metal-organic structure types with the general formula $M^{II}_nL_{2n}$ are formed through the self-assembly of bis(pyridyl) ligands having different bend angles with square planar Pd^{II} and Pt^{II} cations. These products are symmetrical polyhedra (Figure 55), including $Pd^{II}_6L_{12}$ octahedron **212**,[31] $Pd^{II}_{12}L_{24}$ cuboctahedron **213**,[156] $Pd^{II}_{24}L_{48}$ rhombicuboctahedron **214**,[297,299] and $Pd^{II}_{30}L_{60}$ icosidodecahedron **215**.[298] Higher-order structures are observed when ligands have a larger bend angle.[300,301] However, other dipyridyl ligands have been shown to form architectures that deviate from these Platonic and Archimedean ideals.

Fujita *et al.* demonstrated that dipyridyl ligand **216** (Figure 56), having a bend angle of 60°, assembles with $Pd^{II}(NO_3)_2$ in DMSO to give Pd^{II}_4**216**$_8$ box **217**.[302] In contrast, carrying out the reaction in CD_3CN results in the formation of smaller Pd_3**216**$_6$ tube **218**. The selective formation of **217** requires the presence of both DMSO and nitrate, with a mixture of **217** and **218** observed when $Pd^{II}(OTf)_2$ in DMSO is used. Finally, the ratio of **217** to **218** tracks the DMSO:MeCN ratio of the solvent mixture. Using similar principles, the Yoshizawa group obtained a $Pd^{II}_2L_4$ polyaromatic capsule, structurally contracted in comparison to a previously reported capsule using a similar ligand.[303]
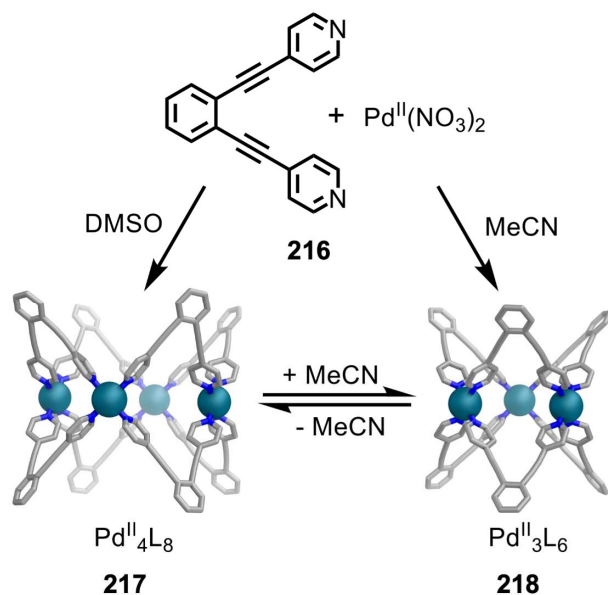
Figure 56. Solvent-dependent self-assembly of ditopic ligand **216**, having a 60° bend angle, and $Pd^{II}(NO_3)_2$ into $Pd^{II}_4L_8$ (**217**) and $Pd^{II}_3L_6$ (**218**) box-shaped structures.[302]

In targeting the next-largest structure in the series of regular $Pd^{II}_nL_{2n}$ assemblies shown in Figure 55 – a $Pd^{II}_{60}L_{120}$ rhombicosidodecahedron – by widening the bend angle of the ditopic ligand, Fujita *et al*. instead formed an unexpected new architecture. Selenophene-centered ligand **219** (Figure 57) exhibits a bend angle (θ) of 152°, a modest increase upon the 149° of the thiophene-centered ligands previously reported to assemble into $Pd^{II}_{24}L_{48}$ **214** and $Pd^{II}_{30}L_{60}$ **215** (Figure 55).[297-299] The assembly of **219** and Pd^{II} in DMSO instead yields structure **220**, with a $Pd^{II}_{30}\mathbf{219}_{60}$ formula, the same composition as icosidodecahedral structure **215**.[304]

a)

$\theta = 152°$

219

220
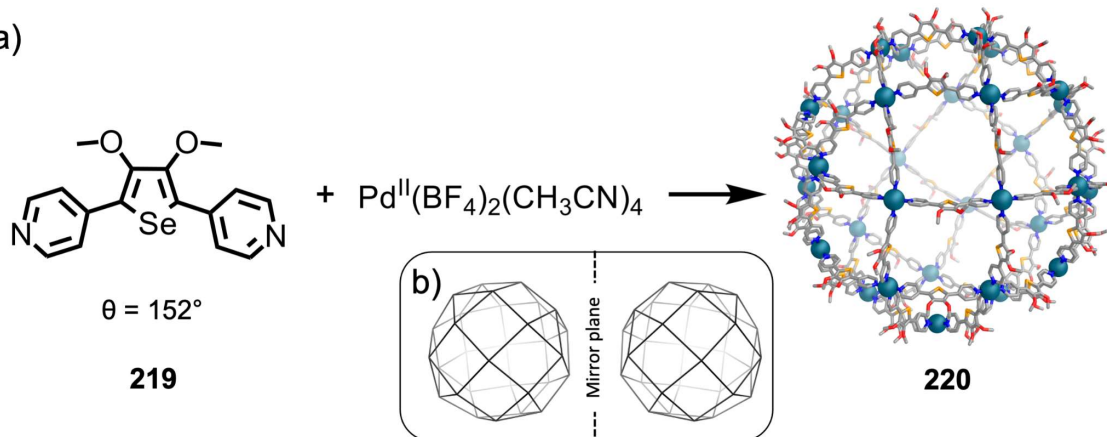
Figure 57. (a) Formation of metal-organic architecture **220**, corresponding to a chiral tetravalent Goldberg polyhedron. (b) Schematic representations of the two enantiomers of **220**.[304]

Refinement of X-ray crystallographic data through the extension of techniques originally developed for protein crystallography revealed that the surface of structure **220** is tiled by 8 triangles and 24 squares. Fujita's team developed a mathematical description of this new class of structures, which they named tetravalent Goldberg polyhedra. According to their nomenclature, **220** is a *tet*-G(2,1) polyhedron, with the numbers in parentheses describing the relative orientations and spacings of the triangles among its squares. In **220**, a given triangle is located two steps horizontally and one step vertically away from its nearest neighbor. Structure **220** is chiral, existing as a pair of enantiomers (Figure 57b). Using graph theory, the authors predicted that $Pd^{II}_{48}L_{96}$, *tet*-G(2,2), structures would be the next largest members of their new series. Meticulous modelling predicted that a ditopic ligand with a bend angle of 152° should favor the formation of such a $Pd^{II}_{48}L_{96}$ architecture, suggesting that the initially observed $Pd^{II}_{30}\mathbf{219}_{60}$ structure is a kinetically trapped species.

Through optimization of the conditions of self-assembly, and screening many crystals, the Fujita group was once more able to use their novel crystallographic methods to identify a $Pd^{II}_{48}\mathbf{219}_{96}$ structure with the geometry of a larger *tet*-G(2,2) polyhedron. This remarkable structure demonstrates the power of using the analysis of serendipitous results in the targeting and discovery of new structures. Such structures are among the largest synthetic assemblies known, rivaled only by those incorporating biomolecular building blocks. For example, the Heddle group have used the metal-driven assembly of protein subunits to produce large assemblies with unusual structures, such as the snub cube.[305]

Newkome *et al.* demonstrated the role that geometric constraints can play in the assembly of heteroleptic structures. They report that mixing hexatopic ligands **221** and **222** with Cd^{II} in a

1:3:12 ratio results in the formation of the $Cd^{II}_{48}\mathbf{221}_4\,\mathbf{222}_{12}$ truncated tetrahedral structure **223** with a molecular weight of approximately 70,000 Da (Figure 58).[306] Each of the individual bent **222** ligands acts to connect two hexagonal **221** units, four of which make up the faces of the truncated tetrahedron. The rigidity of bent **222** enables the selective formation of the desired structure, which does not form when a more flexible alkyl linker is used as the spacer between the two tris-terpyridine units. Instead, double-decker hexagons are formed.[307]
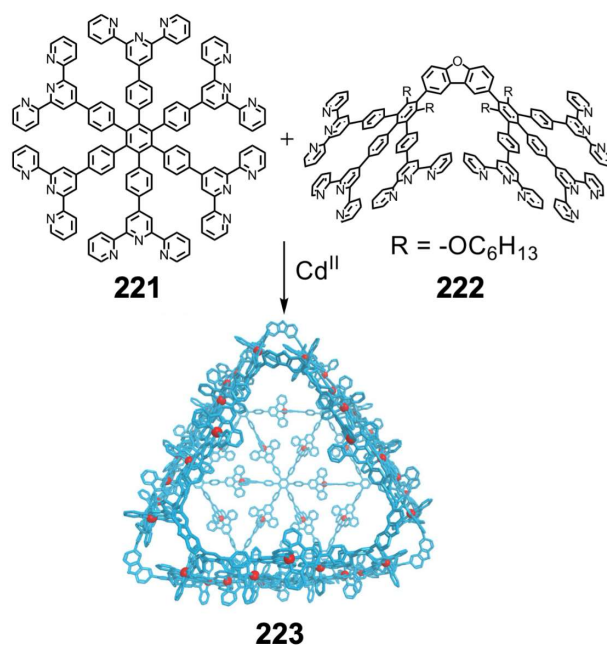
Figure 58. Self-assembly of a heteroleptic truncated tetrahedron **223** (energy minimized structure from molecular modelling) from ligands **221** and **222** together with Cd^{II}. Adapted with permission from ref. 306. Copyright 2020 American Chemical Society.

7.2. Stretching Ligands – Elongated Tetratopic Ligands

Metal-organic cages with a high degree of enclosure are often targeted, as well-enclosed cavities tend to exhibit superior guest binding properties. However, other classes of supramolecular host, such as cucurbiturils[308] and pillarenes,[309] have open-ended structures and have been used in applications where this openness is useful. Control of the degree of

enclosure can also affect guest binding kinetics,[310,311] which is a vital parameter in designing functional systems. As a result, metal-organic architectures with open-ended box-, barrel-, and tube-like structures have been investigated.

The combination of elongated tetratopic pyridyl-based ligands and *cis*-protected square planar metal centers has been shown to yield a variety of trigonal,[312-314] tetragonal,[315-318] pentagonal[319] and hexagonal[320] barrel-like structures (**224-227**, Figure 59).[321,322] Intriguingly, recent reports have demonstrated that ligands of this class can also form structures with gyrobifastigium,[323-325] triangular-orthobicupola[326,327] and square orthobicupola[319] geometries (**228-230**), in some cases selectively, and in others as a minor product. Thus, while the combination of elongated tetra-pyridyl ligands with *cis*-protected square planar metal centers can yield different structures (Figure 59), control over the thermodynamics of the system is required to ensure a single product is formed.
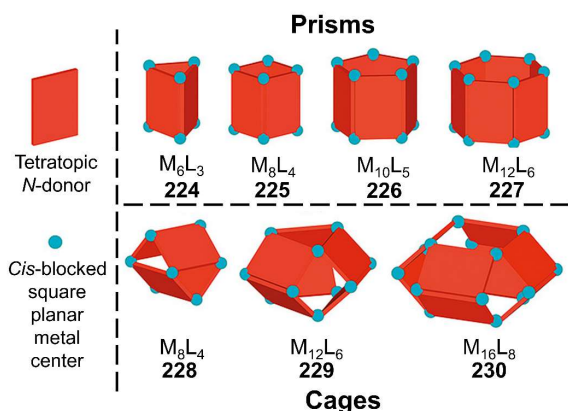
Figure 59. Geometries that can be formed by the combination of elongated tetratopic *N*-donor ligands and *cis*-protected square planar metal centers in a 1:2 ratio. Reproduced with permission from ref 325. Copyright 2019 WILEY‐VCH Verlag GmbH & Co. KGaA, Weinheim.

Recent work by Severin and co-workers sought to uncover the design principles responsible for the assembly of several different structures, particularly taking into account geometric

considerations.[319] When the authors postulated that the ligands were fully rigid, geometric analysis predicted that larger, often pentagonal, barrels would form. However, tetragonal or trigonal prismatic barrels are observed in practice. The formation of these entropically-favored smaller assemblies is thus attributed to the conformational flexibility of the ligands, which enables them to deviate from planarity, and also to flexibility arising from the potential for a slight misalignment between the coordinate vectors of the ligand and the metal−ligand bonds.

Severin's group also discovered that ligands containing bulky cores can form structures with gyrobifastigium-like (**228**, Figure 59) geometries.[323] This geometry allows greater distance between bulky ligand cores, thereby reducing steric clash as compared to barrel-like geometries. Further geometric analysis indicated that the gyrobifastigium emerges only in a certain window of ligand length-to-width ratios. Further elongation of the ligand precludes gyrobifastigium formation, favoring instead the formation of larger barrel-like assemblies, which also reduce steric clash between ligand cores.[319]

Factors beyond simple geometric considerations were also revealed to be important in determining which among the many architectures shown in Figure 59 might predominate. For example, favorable inter-ligand noncovalent interactions can influence the preferred geometry of the structures formed.[325] Although analysis of geometric considerations does not yet provide a definitive guide to selectively obtaining each of the seven structure types of Figure 59, these principles may be used to guide the targeting of other structure types, using ligands with bulky metal(II) clathrochelate cores.[319]

Mukherjee *et al.* further demonstrated the utility of this class of structures using a water-soluble tetra-facial barrel **232**, selectively formed *via* the combination of tetrapyridyl ligand **231** and *cis*-Pd[II](en)(NO$_3$)$_2$ in a 1:2 ratio (Figure 60). This barrel acts as a carrier for curcumin.[315] Complexation within the cavity increases the water solubility of curcumin, and also protects it from photodegradation in aqueous solution when exposed to either daylight or UV. The

authors attribute the photostabilizing property of the metal-organic barrel to the aromatic panels of the structure absorbing most of the incident photons, reducing the number absorbed by the curcumin guest. Curcumin has been shown to have pharmacological activity,[328] but two factors limiting its potential use in therapeutics are its tendency to undergo photodegradation[329] and its low bioavailability arising from poor aqueous solubility,[330] both of which may be alleviated by supramolecular carrier **232**. The Mukherjee group also reported a urea-functionalized trigonal prism, which was capable of catalyzing Diels-Alder reactions in aqueous media, further demonstrating the potential application of water soluble, open cages.[331]
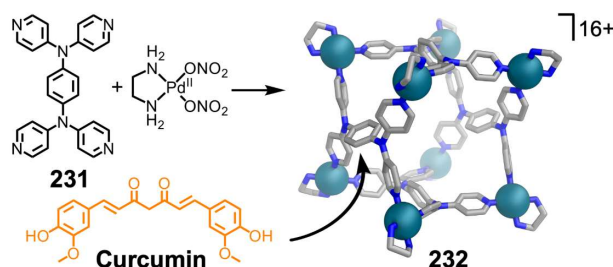
Figure 60. The formation of water-soluble tetrafacial barrel **232** from tetrapyridine **231** and cis-Pd^{II}(en)(NO$_3$)$_2$. Barrel **232** increases the water solubility and photostability of curcumin.[315]

Utilizing the principles discussed above, along with those illustrated in Figure 3, Zhang and co-workers constructed heteroleptic tetragonal barrel-shaped metallacages, which were emissive in both solution and the solid-state.[332]

We reported the formation of a series of tubular M$^I_8$L$_4$ structures (**235**) via subcomponent self-assembly (Figure 61), with narrower cavities than the other structures discussed above. They are obtained from the reactions of elongated tetra-anilines (**233a-c**), a 2-formylpyridine (**16**, **234a** or **234b**), and Ag^I or Cu^I.[333,334] The tube-like hosts exist in two possible diastereomeric forms, either D_2/D_{2d}-**235** or D_4-**235**. Equilibria between diastereomers depend upon ligand length, substituents, the identity of the metal ion, the counteranion, and the temperature.[334]

Furthermore, the linear cavities of the D_4-symmetric isomers of these structures bind and stabilize unusual, linear, cyanide-based guest species, such as **236**, illustrating an advantage to the formation of elongated cavities.
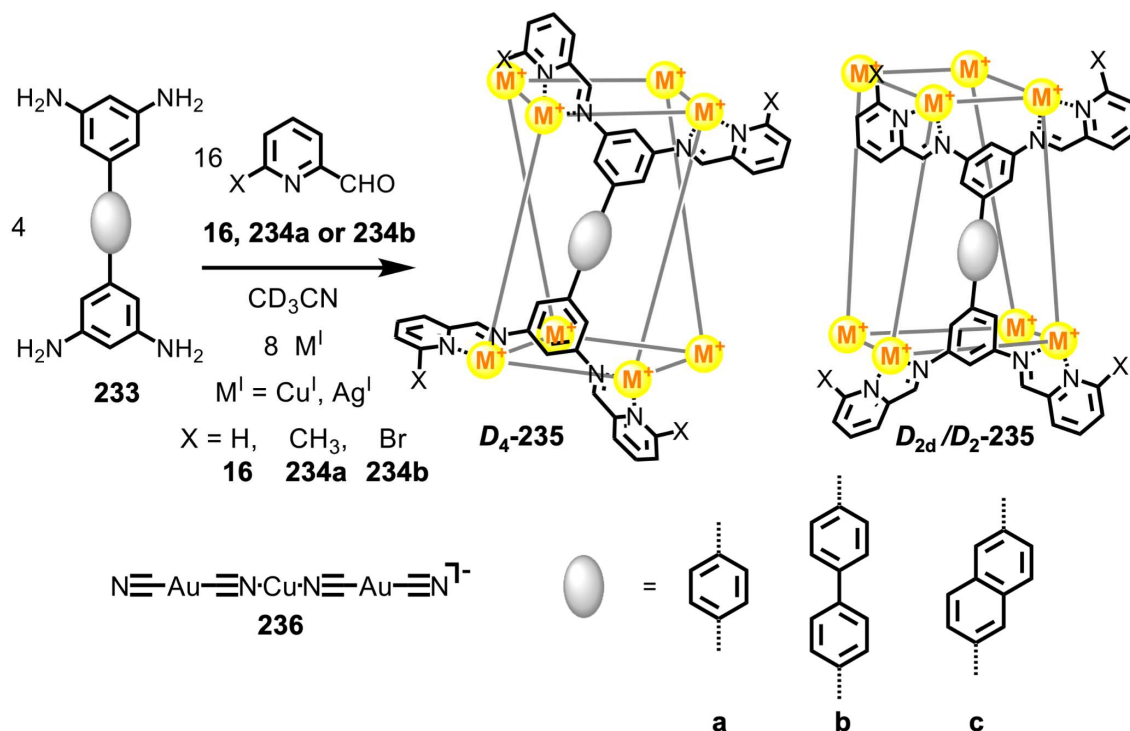
Figure 61. Subcomponent self-assembly of $M^I_8L_4$ tube-like structures (**235**) with narrow cavities capable of binding linear cyanoaurate guest complexes (**236**). Adapted with permission from ref 334. Copyright 2014 American Chemical Society.

7.3. Curved vs. Planar Ligands

Much of Section 7.1 focused upon architectures produced from bent, ditopic ligands and their analogs. Using similar reasoning, curvature can be introduced into ligands with higher topicities. When they are planar or nearly planar, such ligands have been employed as panels in the formation of diverse architectures, with both high and low symmetries.[1,66,335] The

deviation of a ligand from planarity can favor the formation of metal-organic complexes with greater complexity and lower symmetry.

Salle *et al*. have used tetra-pyridyl ligands based on π-extended tetrathiafulvalenes (exTTF) to construct M_4L_2[336] and M_6L_3[337] ring-like structures, as well as a larger $M_{12}L_6$[338] species. The combination of curved tetratopic ligand **237** with Ag^IBF_4 in mixed $CHCl_3/CH_3NO_2$ forms $Ag^I_{12}\textbf{237}_6$ architecture **238** (Figure 62).[338] Although an X-ray crystal structure was not obtained for **238**, solution studies and molecular modelling enabled its assignment as shown in Figure 62. The modeled structure has a ligand curvature of 87°, close to the 86° value observed for the free ligand. An analogous structure forms by the assembly of ligand **237** with *trans*-$Pd^{II}Cl_2(MeCN)_2$ in DMSO.[338]
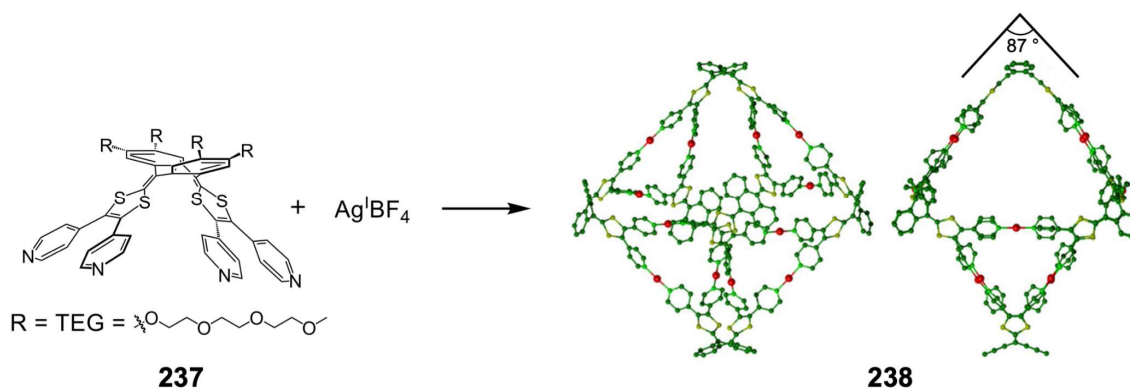
Figure 62. Proposed structure of **238**, assembled from ligand **237** and Ag^IBF_4. Reproduced with permission from ref. 338. Copyright 2018 Wiley ‑ VCH Verlag GmbH & Co. KGaA, Weinheim.

An additional feature of electron-rich ligand **237** is its ability to undergo two-electron oxidation. The conformational change of the ligand core that accompanies this oxidation was exploited to drive the redox-controlled disassembly and re-assembly of a M_4L_2 coordination cage. This redox-governed process was coupled with guest binding to provide a means of guest release and re-capture.[339] $Ag^I_{12}\textbf{237}_6$ structure **238** rearranges from the discrete cage into a three-

dimensional supramolecular polymer when the ligand units oxidize to a dicationic state. In contrast, the $Pd^{II}_{12}\mathbf{237}_6$ cage remains intact upon oxidation.[338]

7.4. Linear Polytopic Ligands

The development of structures that can bind more than one guest is of great interest in the context of new coordination cage applications.[57] This goal may be achieved through the design and synthesis of metallosupramolecular structures that contain multiple linked cavities with a high degree of enclosure, and which are therefore expected to exhibit guest binding. Crowley and co-workers expanded on design principles for the formation of simpler $Pd^{II}_2L_4$ structures to design pseudo-linear polypyridyl ligands that form multi-cavity structures.[93] These architectures contain similar cavities linked end-to-end.

As shown in Figure 63, combining hexapyridyl ligand **239** and Pd^{II} leads to the formation of triple-cavity cage **240**. A higher temperature is required than is typically needed for the formation of $Pd^{II}_2L_4$ complexes, in order for the error-correcting disassembly of misassembled intermediate structures to occur during the formation of multi-cavity structures. To illustrate the potential use of such cages, the authors demonstrated the segregated binding of two distinct types of guests within the two different cavity types, terminal and central, within **240**. Cisplatin is encapsulated in the terminal cavities, whereas triflate is bound in the central cavity, as well as externally at each end of the structure.[93]

239, R = $O(CH_2)_2O(CH_2)_2OCH_3$
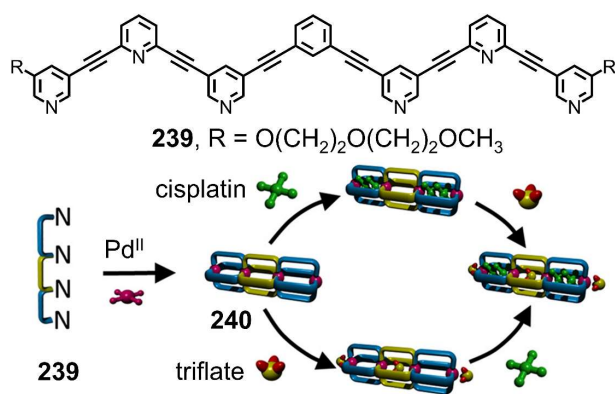
Figure 63. The self-assembly of ligand **239** with Pd^{II} into triple-cavity cage **240**, which is capable of binding two different types of guest molecule within two distinct types of internal cavity. Reproduced with permission from ref. 93. Copyright 2017 American Chemical Society.

Clever *et al.* formed double- and triple-cavity cages by expanding upon these principles. A topologically-interpenetrated dimeric species forms from the double-cavity cage upon addition of chloride or bromide ions.[340] Each of the five segregated interior cavities of the structure can bind chloride or bromide.

Yoshizawa *et al.* reported the assembly of W-shaped tripyridine ligand **241** with Pd^{II} to form Pd^{II}_3**241**$_4$ double capsule **242**.[341] When structure **242** is heated with C_{60}, the central Pd^{II} is ejected, resulting in the formation of Pd^{II}_2**241**$_4$•$(C_{60})_2$ "molecular peanut" **243** (Figure 64), with extensive stabilization from aromatic stacking interactions between the anthracene panels of the host and the fullerene guests outweighing the energetic cost associated with a loss of coordinative saturation of the central pyridine. Capsule **242** also binds simultaneously different guests, diamantane and phenanthrene, with the preference for heterotopic encapsulation of these guests to form **242**•(diamantane)(phenanthrene)$_2$ (**244**) attributed to cooperative changes in the volume of each of the two cavities that occur upon guest binding. The same group has since shown that similar peanut-shaped polyaromatic shells form under much milder conditions when the central pyridine ring is replaced by a phenyl ring, which allows the stepwise encapsulation of two C_{60} molecules.[342]
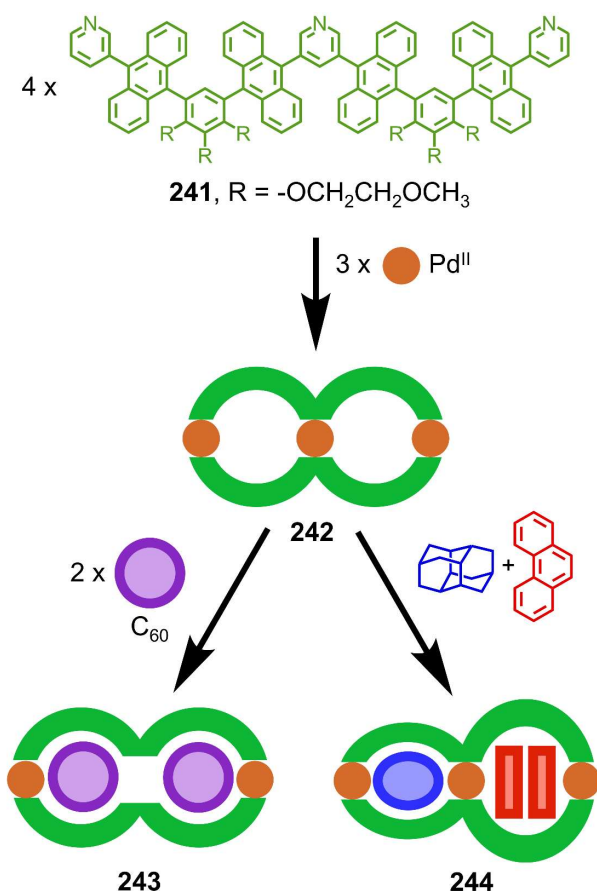
Figure 64. Molecular double capsule (**242**) which can form "molecular peanut" **243** upon ejection of the central Pd^{II} ion and encapsulation of two C_{60} molecules, or heterotopic diamantane-phenanthrene$_2$ complex **244**.[341]

Chand and co-workers have reported that ligands **245**-**247** form the conjoined cages **248**-**250** (Figure 65), further developing the concepts introduced above. Instead of the different cavities having similar sizes and shapes, ligands were rationally designed to form architectures consisting of laterally or linearly conjoined $Pd^{II}_2L_4$ and $Pd^{II}_3L_6$ units (Figure 65).[343] Structures **248**-**250**, which were all confirmed by X-ray crystallography, assemble from one or more of the carefully designed ligands **245**-**247** and Pd^{II} in DMSO. In the cases of **248** and **249**, integrative self-sorting results in the selective formation of heteroleptic structures. The different types of cavities bind different guests. Small anions, such as NO_3^- and Cl^-, bind within the smaller cavity, and their presence is required to template the formation of structures **248**-**250**.

Crystallography also showed that multiple DMSO molecules reside in the larger, trigonal, cavity.
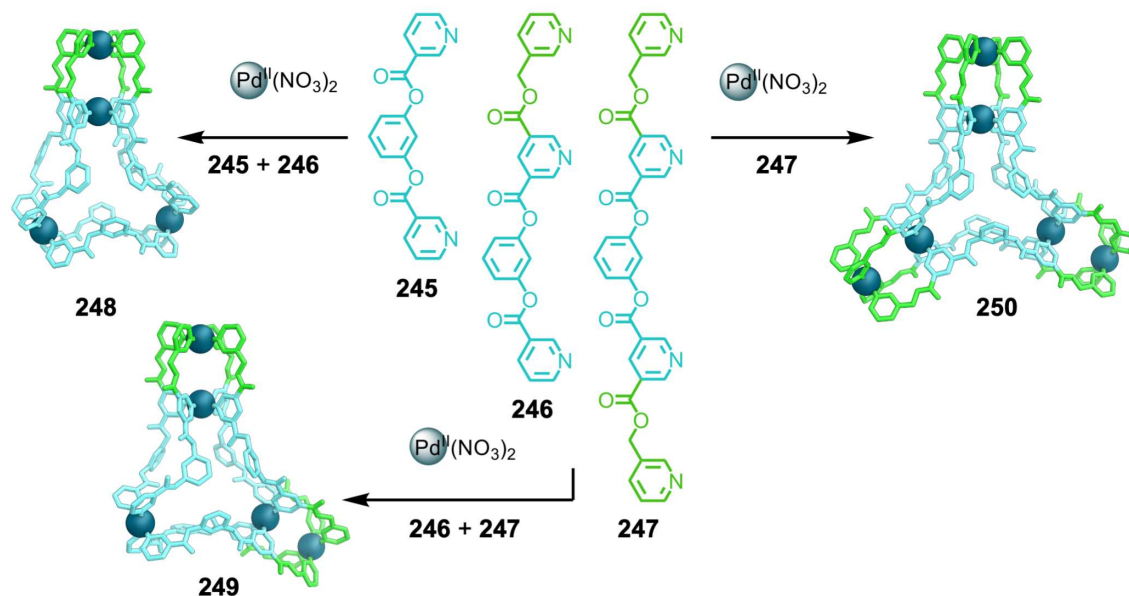
Figure 65. Conjoined cages (**248-250**), consisting of laterally or linearly conjoined $Pd^{II}_2L_4$ and $Pd^{II}_3L_6$ units; heteroleptic **248** and **249** form selectively *via* the integrative self-sorting of mixtures of the corresponding ligands.[343]

Fujita *et al*. have reported the use of linear polypyridyl ligands in the formation of a series of nanotubular architectures. The combination of ligand **251** (Figure 66a) with *cis*-protected Pd^{II} and a template, such as 4,4'-biphenyl dicarboxylate, leads to the formation of $Pd^{II}_6L_4$ **252**; elongated **253** (Figure 66b) and **255** (Figure 66c) lead correspondingly to $Pd^{II}_8L_4$ **254** and $Pd^{II}_{10}L_4$ **256**. A suitable template is essential to generate well-defined, discrete assemblies.[344] The $Pd^{II}_6\mathbf{251}_4$ and $Pd^{II}_{10}\mathbf{255}_4$ nanotubes, **252** and **256**, respectively, exist as single isomers. However, the $Pd^{II}_8\mathbf{253}_4$ structure forms as a mixture of isomers, having C_{2h} (**254**) and D_{2h} symmetries.[345]
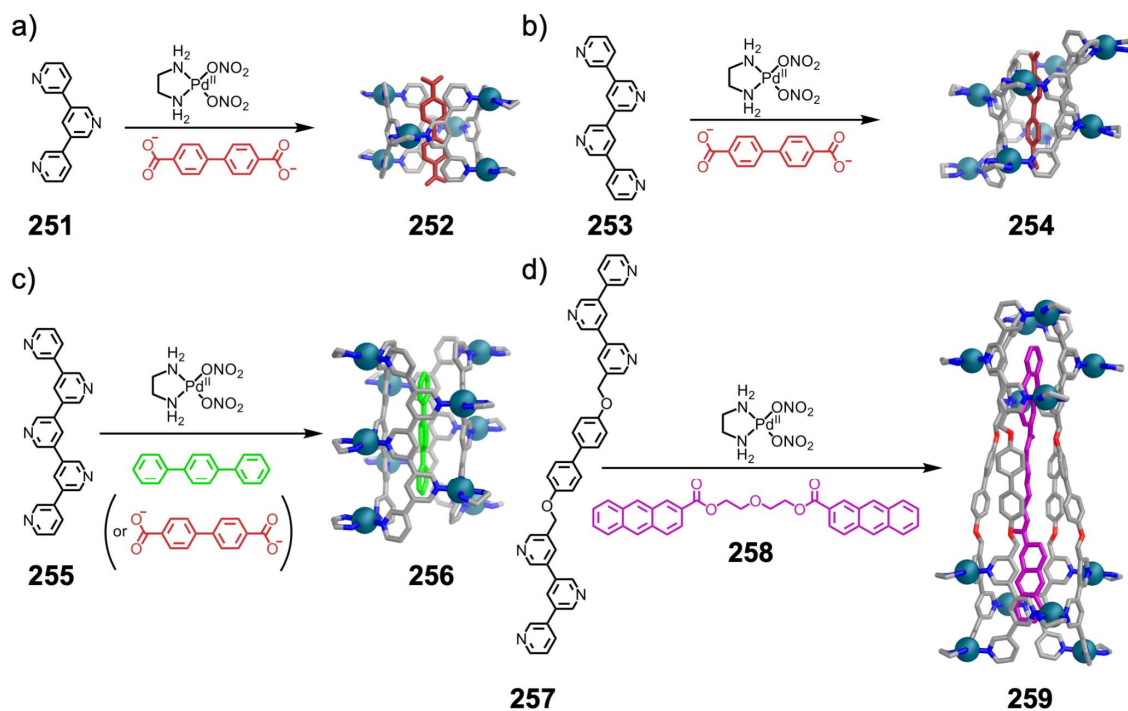
Figure 66. (a) Pd$^{II}_6$**251**$_4$ (**252**), (b) Pd$^{II}_8$**253**$_4$ (**254**), (c) Pd$^{II}_{10}$**255**$_4$ (**256**), (d) Pd$^{II}_{12}$**257**$_4$ (**259**) nanotubes, prepared through the assembly of the given ligand with *cis* protected Pd^{II} centers and a rod-like template.[344-346]

Later work showed that elongation of these tube-like structures through extension of the ligand with additional pyridine rings was not possible, due to poor solubility.[346] This problem was circumvented by the design of hexapyridine ligand **257** (Figure 66d) in which two terpyridine units are separated by a spacer. Importantly, the biphenyl spacer, as opposed to an alkyl moiety, ensured that the ligand remained linear instead of folding into a U-shaped conformation. Combination of **257** with *cis*-protected Pd^{II} and the specially designed template molecule **258** allowed the construction of 3.5 nm nanotube **259**.

7.5. Pyrimidine vs Pyridine

The combination of pyridine donors with *cis*-protected square planar metal centers has yielded many new coordination cages, some of which are described in this review. Pyrimidine donors are also able to coordinate to M^{II} centers, acting as a 120° μ^2 bridging ligand.

Triangular hexadentate 1,3,5-tris(3,5-pyrimidyl)benzene **260** is designed to form structures in which the metal centers lie upon the edges of polyhedra, as opposed to their vertices.[347] The combination of **260** with $Pd^{II}(en)(NO_3)_2$ in aqueous solution yields enclosed $Pd^{II}_{18}\textbf{260}_6$ hexahedron **261** with a trigonal bipyramidal structure, consisting of six edge-sharing triangular panels with two metal centers on each edge (Figure 67a).
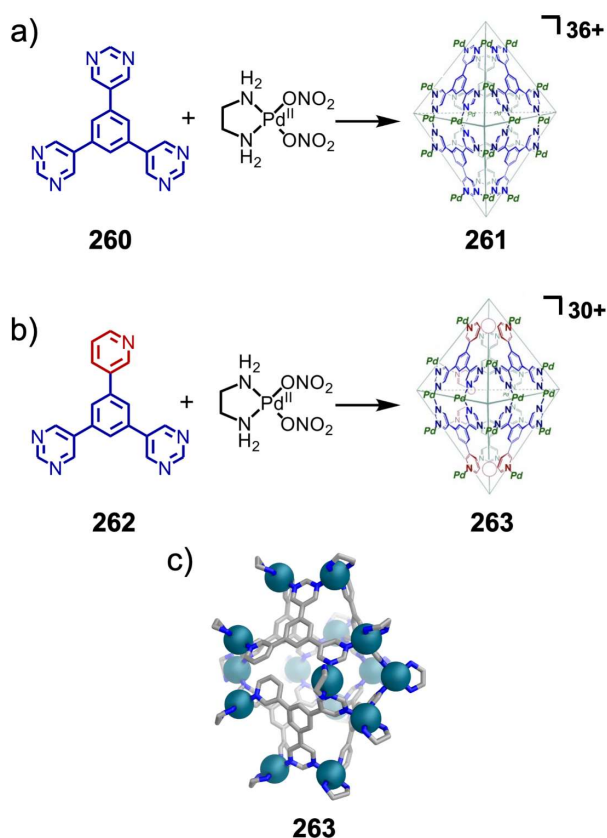
Figure 67. The preparation of (a) $Pd^{II}_{18}\textbf{260}_6$ (**261**) and (b) $Pd^{II}_{15}\textbf{262}_6$ (**263**) hexahedral architectures from ligands **260** and **262**, respectively, and $Pd^{II}(en)(NO_3)_2$. Adapted with

Subsequent work produced the similar $Pd^{II}_{15}262_6$ hexahedron **263** (Figure 67b) from modified ligand **262**, in which one pyrimidine is replaced with a 3-pyridyl moiety.[348] Although **261** and **263** are of similar shape and size, the presence of open clefts at the apical non-binding sites in **263** is hypothesized to allow easier access of guest molecules into the cavity for binding, in contrast to the more enclosed **261**.

Architectures **261** and **263** demonstrate how the geometric constraints of a ligand can result in the formation of novel structures. Subsequent alterations can then be made, allowing for a desired structure type to be maintained, but with altered properties. Further replacement of the pyrimidine sites of **262** with 3-pyridyl moieties yields different architectures, of both higher and lower symmetries, including a tetrahedron and "open cones", depending on the conditions used.[349]

Mukherjee *et al.* have also used ligands containing pyrimidine moieties to prepare complex architectures. The combination of 1,4-di(pyrimidin-5-yl)benzene or 4,4'-di(pyrimidin-5-yl)-1,1'-biphenyl with *cis*-[(dch)Pt^{II}(NO$_3$)$_2$] (where dch is 1,2-diaminocyclohexane) in water results in the formation of Pt$^{II}_8$L$_4$ nanotubes with lengths of up to 22.0 Å.[350] Assembly of hexadentate ligand **264** (Figure 68) with Pd^{II} in a 1:1 ratio produces structure **265**.[351] Crystallography indicates that **265** is a discrete $Pd^{II}_{24}264_{24}$ complex, wherein only four of the nitrogen atoms on each ligand bind to Pd^{II}, leaving two nitrogen atoms on each ligand (highlighted in purple in Figure 68) uncoordinated. The authors describe this structure as a 'pregnant molecular nanoball', consisting of a Pd$^{II}_{12}$ 'baby-ball' within a larger Pd$^{II}_{12}$ 'mother-ball'. Interestingly, the 'mother-ball' stabilizes the internal, smaller, structure, as an analogous Pd$^{II}_{12}$L$_{24}$ cuboctahedral nanosphere does not form from the reaction between pyrimidine and Pd^{II}.
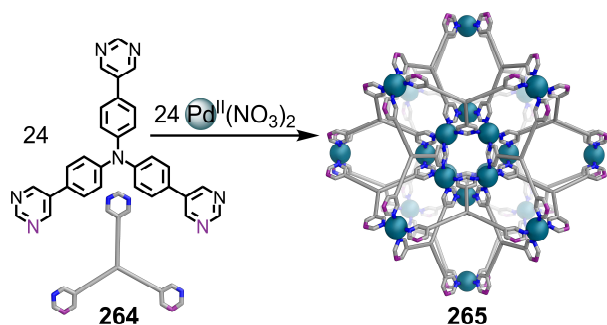
Figure 68. $Pd^{II}{}_{24}\mathbf{264}_{24}$ 'pregnant molecular nanoball' (**265**). *N*-Donor atoms highlighted in purple remain uncoordinated in the observed product structure.[351]

7.6. Flexible Coordination Geometry of Metal Building Blocks

Many of the examples in previous sections utilize metal ions with rigid coordination spheres, for example many structures contain Pd^{II} or first row transition metal ions in the +2 oxidation state, adopting exclusively square planar and pseudo-octahedral coordination geometries, respectively. Ions of the f-block metals can more readily adopt a wider range of coordination numbers, and geometries, which can result in the formation of complex metal-organic architectures.

Jeong *et al.* utilized the coordinative flexibility of lanthanum to assemble the complex $[La^{III}{}_{18}\mathbf{266}_{24}(CO_3)_2(H_2O)_{32}]^{2+}$ structure **267** (Figure 69), which the authors refer to as Lanthanitin, owing to its similarity to the structure of ferritin.[352] Crystals of both (*S*)- and (*R*)-Lanthanitin are obtained from mixtures of $La^{III}Cl_3$ and the rigid, bent ligand **266** having either (*S*,*S*) or (*R*,*R*) stereochemistry. Within **267**, La^{III} ions have different coordination numbers; a mixture of eight and ten coordinate La^{III} is observed.
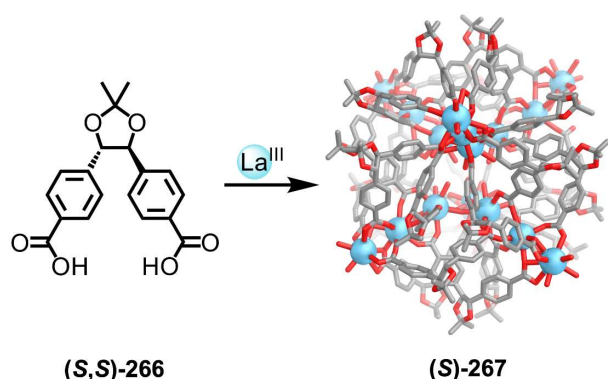
Figure 69. $[La_{18}266_{24}(CO_3)_2(H_2O)_{32}]^{2+}$, 'Lanthanitin'.[352]

Duan and co-workers used a different f-block ion, cerium(IV), to construct a $Ce^{IV}_4L_6$ basket-like tetragon, using ditopic ligands consisting of two tridentate binding sites connected by a carbazole-based core.[353] Four Ce^{IV} centers define the four corners of a square, and are bridged by four edge-defining ligands. The final two ligands each also bind to two of the four cerium ions and define the bottom of the basket.

Raymond and co-workers exploited the variable coordination geometry of lanthanum to form a $La^{III}_8L_8$ structure with a square anti-prismatic geometry.[354] Within the structure, all lanthanum centers are nine-coordinate; however, two different coordination geometries are observed — distorted monocapped square antiprismatic and distorted tricapped trigonal prismatic. Similarly, Kawai *et al.* recently reported an octanuclear circular helicate with a D_4-symmetric square anti-prismatic geometry, which exhibited circularly polarized luminescence (CPL) activity.[355]

7.7. Noncovalent Interactions and Steric Effects

The importance of steric control and favorable noncovalent interactions in driving the selective formation of particular structures has been alluded to in previous sections. In this section we

will present a few key examples in which these, often subtle, effects exert a decisive influence on the self-assembly process.

Saalfrank *et al.* reported an early example whereby steric effects determine self-assembly outcomes.[356] The combination of rigid, three-fold symmetric, tris-bidentate, pyrazolone-based ligand **268** with gallium(III) acetylacetonate in DMSO resulted in the serendipitous formation of $Ga^{III}_6268_6$ distorted trigonal antiprismatic cylinder **269**, having D_3 symmetry and all six gallium centers of the same handedness (Figure 70). Although this structure represents an initially surprising deviation from the expected M_4L_4 tetrahedral assembly, molecular modeling indicates that the shorter metal-metal distance in a putative M_4L_4 tetrahedron would cause an increase in unfavorable steric clashes. Further work by the same group utilized molecular modelling to clarify the steric preference for the formation a $Fe^{III}_4L_4$ structure in the case of one ligand, versus a $Fe^{III}_6L_6$ trigonal antiprism with a different ligand, on the basis of favorable aromatic stacking interactions in the trigonal antiprism.[357]

268   **269**
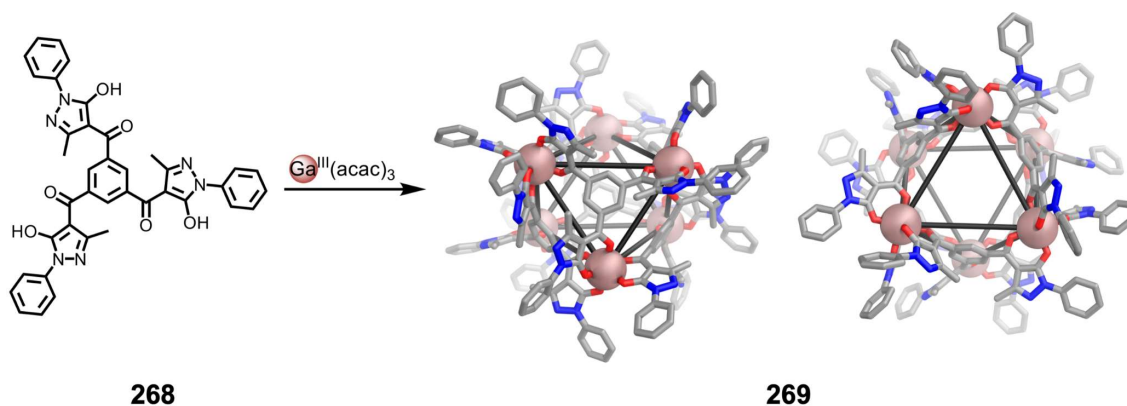
Figure 70. $Ga^{III}_6L_6$ distorted trigonal antiprism **269** assembles from rigid, three-fold symmetric, tris-bidentate ligand **268** and gallium(III) in DMSO.[356]

Clever and co-workers described the assembly of $Pd^{II}_2270_3$ bowl **271** (Figure 71), based on a $Pd^{II}_2L_4$ cage framework lacking a fourth ligand.[358] The formation of **271** is driven by the steric demands of its ligands. In the case of ligand **270**, steric clash between hydrogen atoms near

the coordinating nitrogen of the quinoline is alleviated in a $Pd^{II}_2\mathbf{270}_3$ structure, stabilizing **271** with respect to a $Pd^{II}_2\mathbf{270}_4$ structure. Upon prolonged heating of a solution of the $Pd^{II}_2\mathbf{270}_3$ structure, partial conversion to the $Pd^{II}_2\mathbf{270}_4$ structure was observed. However, this conversion could be prevented by the binding of C_{60} in the open cavity of the bowl.
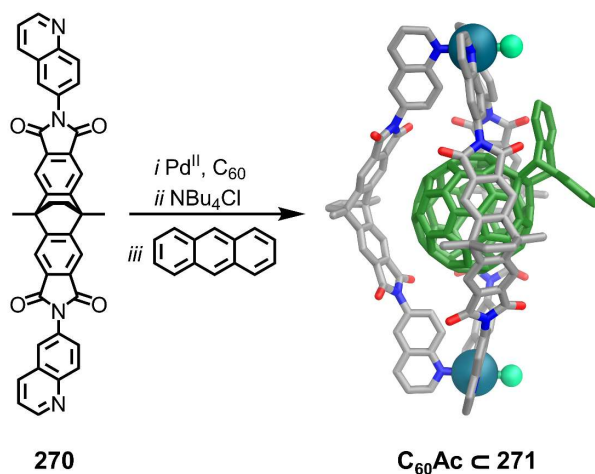
Figure 71. $Pd^{II}_2L_3$ bowl **271** is formed, rather than a $Pd^{II}_2\mathbf{270}_4$ cage, due to the steric demands of quinoline-based ligand **270**. Bowl **271** acts as a supramolecular protecting group, enabling the selective formation of a C_{60}-anthracene monoadduct ($C_{60}Ac$).[358]

Bowl **271** can also act as a supramolecular protecting group. When a solution of $[C_{60}\subset Pd^{II}_2\mathbf{270}_3Cl_2]^{2+}$ is treated with 10 equivalents of anthracene, the C_{60}-anthracene monoadduct ($C_{60}Ac$) is selectively formed, without undergoing further reaction with anthracene. As shown in Figure 71, the bowl-like cavity of **271** encloses most of the surface of the C_{60} guest, leaving only a small region available for reaction with anthracene. Finally, a pill-shaped dimer can be formed by bridging the bowls of two equivalents of **271** with a sterically undemanding terephthalate unit,[358] utilizing similar principles to those outlined in Section 2.1. The example described above (Figure 71) demonstrates that introducing steric bulk close to the coordinating sites of ligands can increase their propensity to form more complex structures.

Mukherjee and co-workers reported the reaction of 1,1'-bis(diphenylphosphino)ferrocene platinum(II) with 5,10,15,20-tetrakis(4-pyridyl)porphyrin **272** ligands to form open hexagonal box **273** (Figure 72), as opposed to a more symmetric cubic architecture.[359] The bulky ferrocene-derived diphosphine ligand disfavors cube formation, and allows formation of hexagonal box **273**, with an internal cavity of 43,550 $Å^3$. The formation of **273** depends on the introduction of steric bulk in peripheral coordinating ligands, rather than directly affecting ligand-metal binding. This unusual self-assembled architecture senses the presence of zinc(II), with distinct changes in UV/vis absorbance bands observed in methanol solution, caused by metalation of the porphyrins.
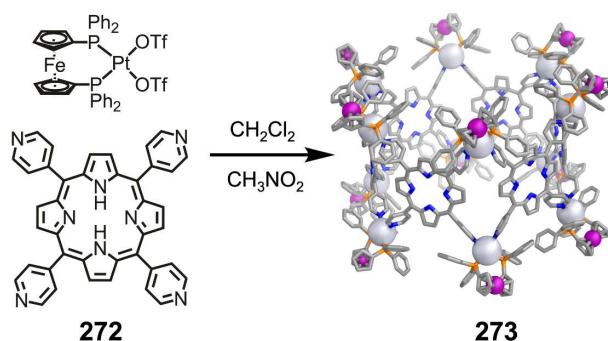
Figure 72. Formation of multimetallic porphyrin-based open hexagonal box **273** from tetrapyridylporphyrin **272**.[359]

Liu and co-workers have built metal-organic architectures with complex structures using Eu[III]. The ditopic ligands **274**, **276**, and **278**, each with two pyridine-2,6-dicarboxamide tridentate chelating sites connected by a 1,1'-bi-2-naphthol derived core, produce architectures **275**, **277** and **279**, respectively (Figure 73).[360] The key difference between the three ligands is the amount of steric bulk in proximity to the tridentate binding sites. All Eu[III] centers within the three structures are nine-coordinate. In **275**, each of the six Eu[III] centers are chelated by three pyridine-2,6-dicarboxamide moieties resulting in a structure with a twisted triangular prismatic geometry (Figure 73a).

a)

274 $\xrightarrow{\text{Eu}^{\text{III}}(\text{OTf})_3}$ **275**

b)

276 $\xrightarrow{\text{Eu}^{\text{III}}(\text{OTf})_3}$ **277**

c)

278 $\xrightarrow{\text{Eu}^{\text{III}}(\text{OTf})_3}$ **279**

○ - Eu^{III} chelated by three pyridine-2,6-dicarboxamide moieties

● - Eu^{III} coordinated by two pyridine-2,6-dicarboxamide moieties and three water molecules
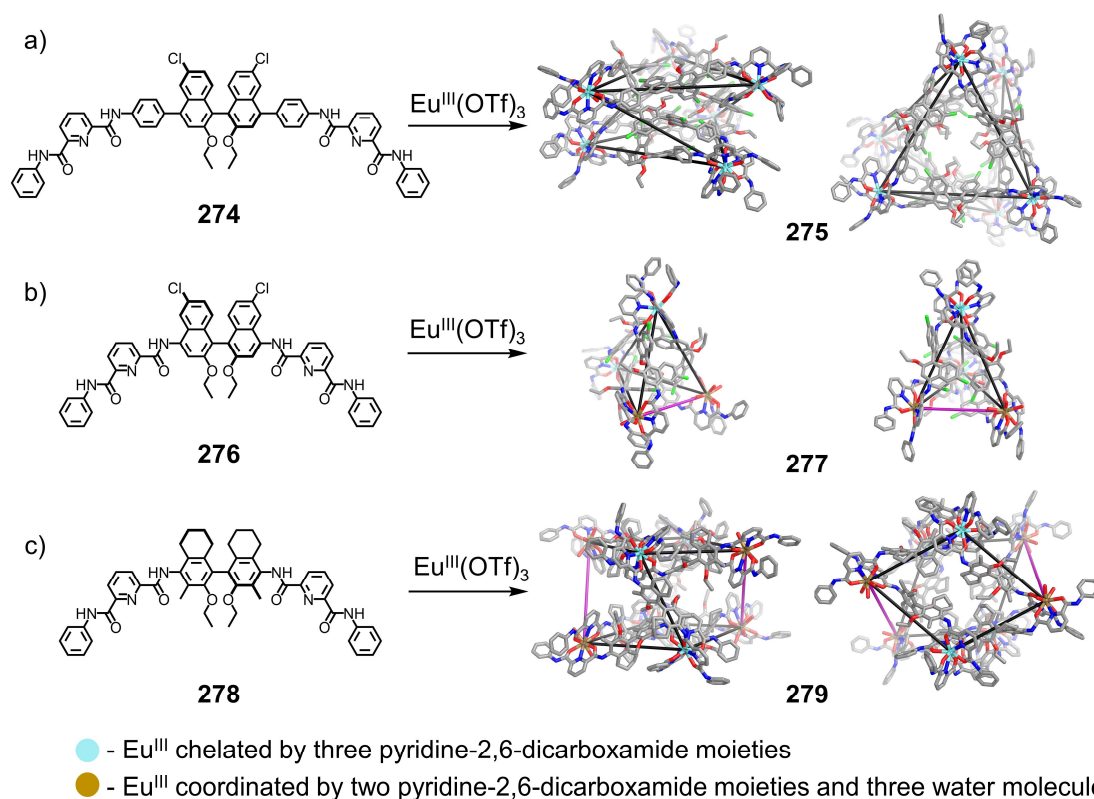
Figure 73. The assembly of ligands **274**, **276** and **278** with Eu^{III} formed (a) twisted triangular prism **275**, (b) "defective" tetrahedron **277**, with one missing edge, and (c) "defective" hexahedron **279**, with two edges missing. The "missing" edges in the structures are indicated with purple struts.[360]

Due to the increased steric hindrance near the binding sites in ligands **276** and **278**, however, structures **277** and **279** contain Eu^{III} centers which are chelated by only two pyridine-2,6-dicarboxamide units, with the remaining coordination sites on Eu^{III} occupied by water ligands. The result is the formation of "defective" cages **277** and **279** (Figure 73b,c). $Eu^{III}_4\textbf{276}_5(H_2O)_6(OTf)_{12}$ architecture **277** has a structure approximating a distorted tetrahedron with one missing edge (Figure 73b). In contrast, $Eu^{III}_8\textbf{278}_{10}(H_2O)_{12}(OTf_2)_{24}$ structure **279** resembles a hexahedral cage in which two edges are missing (Figure 73c).

We also utilized steric effects and noncovalent interactions to drive the formation of barrel-like prismatic structures instead of simple tetrahedra.[229] By enforcing *mer*-selectivity at the metal centers, on the basis of reduced steric crowding and increased inter-ligand aromatic stacking interactions, M_8L_{12}, $M_{10}L_{15}$ and $M_{12}L_6$ prismatic barrel structures could be formed using fluorinated ligands. We hypothesize that the presence of favorable edge-to-face aromatic interactions between the triazine and phenanthroline moieties of neighboring ligands contributed to the stabilization of an unusual M_6L_4 S_4-symmetric scalenohedron over a higher-symmetry pseudo-octahedral structure.[361] Finally, with Siegel and Baldridge we reported the assembly of an S_{10}-symmetric, 5-fold interlocked [2]catenane, from Cu^I, a corannulene-based penta-aniline and 2-formyl-6-methylpyridine.[362] DFT calculations indicate that inter-ligand aromatic interactions between corannulene units are a key driving force for the interlocking of the two 5-fold symmetric cages.

This section highlights the critical role geometric and steric factors, as well as the enhancement of noncovalent interactions, have in controlling the final structure observed in self-assembly processes. Although a sizeable amount of work has already been conducted in this area, these examples also illustrate that much space remains to be explored. Fujita's contributions, especially those involving the use of bis-monodentate ligands with Pd^{II} metal centers, may inspire similar systematic studies focusing on small changes to one geometric feature of other classes of ligand, so leading to the discovery of general design principles for complex architectures.

8. Conclusion and Outlook

As we have detailed in this review, recent years have seen the rapid development of many new approaches to the construction of metal-organic structures beyond the Platonic solids. The advent of new applications for supramolecular cages, including catalysis,[363-369] sensing,[370-372] molecular separations,[373] and in biology,[374] has provided strong motivation for this development.

As detailed in Section 2, incorporating multiple different building blocks into the same structure is an effective way of increasing complexity. However, ensuring that mixed-component structures are formed selectively, and that narcissistic sorting is prevented, remains challenging. The six methods we outlined for driving heteroleptic architecture formation are variations on the theme of careful ligand selection and pairing. Recent efforts have demonstrated the reliability of heteroleptic approaches for the assembly of coordination cages, producing targeted structures across a range of ligand classes.[62,73,82,83,87,89,90,96,107,128,375]

Similarly, as noted in Section 6, an understanding of ligand coordination preferences can now allow the rational design of new heterometallic architectures. Employing metal ions that form coordination bonds to ligands with differing kinetic lability also provides a useful method of design. However, other methods of producing multimetallic architectures have been less thoroughly investigated, providing scope for future enquiry.

The principles of ligand flexibility, solvent effects, and templation detailed in Sections 4 and 5 are well established, and many early examples of complex architectures depend on these approaches. They can be unpredictable, however, and although serendipitous results are plentiful, targeted design from first principles remains a challenge. The factors that drive the formation of particular structures can be difficult to decipher, even after discovery. Key

106

exceptions include groundbreaking work by Ward *et al*., involving the thorough investigation of the self-assembly processes of flexible di- and tri-topic pyrazolyl-pyridine-based ligands and octahedral metal centers, which led to several new classes of structures.[186-196]

The reduced symmetry-ligand and geometry-analysis approaches of Sections 3 and 7 have benefited greatly from recent advances. As with heteroleptic approaches, it appears intuitive that reducing the symmetry of a ligand or building block should result in a self-assembled structure of reduced symmetry or increased complexity. Experience has shown that it can be challenging to obtain single structures, as opposed to intractable mixtures, however. Recent work has nonetheless clarified under which circumstances a reduction in the symmetry of ligands can result in the formation of a single, complex, architecture, as opposed to many of them.

Finally, we note that computational methods, including evolutionary algorithms[376] and machine learning,[377] are playing an increasing role in the discovery of new supramolecular cage structures,[378–380] and the rationalization of their applications, such as catalytic activity.[381] The recent implementation of high-throughput synthetic screening, using automation, has also vastly increased the capacity for exploring a large chemical space rapidly.[382–384] The advent of artificial intelligence, in particular machine learning, and automated synthetic methods may thus play a key role in the structural prediction, and subsequent synthesis, of a broad range of low-symmetry metal-organic polyhedral capsules.

9. References

1. Chakrabarty, R; Mukherjee, P. S.; Stang, P. J. Supramolecular Coordination: Self-Assembly of Finite Two- and Three-Dimensional Ensembles. *Chem. Rev.* **2011**, *111*, 6810–6918.

2. Yamashina, M.; Tanaka, Y.; Lavendomme, R.; Ronson, T. K.; Pittelkow, M.; Nitschke, J. R. An Antiaromatic-walled Nanospace. *Nature* **2019**, *574*, 511–515.

3. Sun, Y.; Chen, C.; Liu, J.; Stang, P. J. Recent Developments in the Construction and Applications of Platinum-based Metallacycles and Metallacages *via* Coordination. *Chem. Soc. Rev.* **2020**, *49*, 3889–3919.

4. Pan, M.; Wu, K.; Zhang, J.-H.; Su, C.-Y. Chiral Metal–Organic Cages/Containers (MOCs): From Structural and Stereochemical Design to Applications. *Coord. Chem. Rev.* **2019**, *378*, 333–349.

5. Yoshizawa, M.; Klosterman, J. K.; Fujita, M. Functional Molecular Flasks: New Properties and Reactions within Discrete, Self-Assembled Hosts. *Angew. Chem., Int. Ed.* **2009**, *48*, 3418–3438.

6. Ahmad, N.; Younus, H. A.; Chughtai, A. H.; Verpoort, F. Metal–Organic Molecular Cages: Applications of Biochemical Implications. *Chem. Soc. Rev.* **2015**, *44*, 9–25.

7. Yamashina, M.; Sartin, M. M.; Sei, Y.; Akita, M.; Takeuchi, S.; Tahara, T.; Yoshizawa, M. Preparation of Highly Fluorescent Host–Guest Complexes with Tunable Color upon Encapsulation. *J. Am. Chem. Soc.* **2015**, *137*, 9266–9269.

8. Ronson, T. K.; Meng, W.; Nitschke, J. R. Design Principles for the Optimization of Guest Binding in Aromatic-Paneled $Fe^{II}_4L_6$ Cages. *J. Am. Chem. Soc.* **2017**, *139*, 9698–9707.

9. Yoshizawa, M.; Kusukawa, T.; Fujita, M.; Yamaguchi, K. Ship-in-a-Bottle Synthesis of Otherwise Labile Cyclic Trimers of Siloxanes in a Self-Assembled Coordination Cage. *J. Am. Chem. Soc.* **2000**, *122*, 6311–6312.

10. Takezawa, H.; Murase, T.; Fujita, M. Temporary and Permanent Trapping of the Metastable Twisted Conformer of an Overcrowded Chromic Alkene via Encapsulation. *J. Am. Chem. Soc.* **2012**, *134*, 17420–17423.

11. Wang, K.; Jordan, J. H.; Hu, X.-Y.; Wang, L. Supramolecular Strategies for Controlling Reactivity within Confined Nanospaces. *Angew. Chem., Int. Ed.* **2020**, *59*, 13712–13721.

12. Dong, V. M.; Fiedler, D.; Carl, B.; Bergman, R. G.; Raymond, K. N. Molecular Recognition and Stabilization of Iminium Ions in Water. *J. Am. Chem. Soc.* **2006**, *128*, 14464–14465.

13. Pluth, M. D.; Bergman, R. G.; Raymond, K. N. Making Amines Strong Bases: Thermodynamic Stabilization of Protonated Guests in a Highly-Charged Supramolecular Host. *J. Am. Chem. Soc.* **2007**, *129*, 11459–11467.

14. Fang, Y.; Powell, J. A.; Li, E.; Wang, Q.; Perry, Z.; Kirchon, A.; Yang, X.; Xiao, Z.; Zhu, C.; Zhang, L.; Huang, F.; Zhou, H.-C. Catalytic Reactions within the Cavity of Coordination Cages. *Chem. Soc. Rev.* **2019**, *48*, 4707–4730.

15. Brown, C. J.; Toste, F. D.; Bergman, R. G.; Raymond, K. N. Supramolecular Catalysis in Metal-Ligand Cluster Hosts. *Chem. Rev.* **2015**, *115*, 3012–3035.

16. Pluth, M. D.; Bergman, R. G.; Raymond, K. N. Acid Catalysis in Basic Solution: A Supramolecular Host Promotes Orthoformate Hydrolysis. *Science* **2007**, *316*, 85–88.

17. Kaphan, D. M.; Levin, M. D.; Bergman, R. G.; Raymond, K. N.; Toste, F. D. A Supramolecular Microenvironment Strategy for Transition Metal Catalysis. *Science* **2015**, *350*, 1235–1238.

18. Yoshizawa, M.; Tamura, M.; Fujita, M. Diels-Alder in Aqueous Molecular Hosts: Unusual Regioselectivity and Efficient Catalysis. *Science* **2006**, *312*, 251–254.

19. Cullen, W.; Misuraca, M. C.; Hunter, C. A.; Williams, N. H.; Ward, M. D. Highly Efficient Catalysis of the Kemp Elimination in the Cavity of a Cubic Coordination Cage. *Nat. Chem.* **2016**, *8*, 231–236.

20. Zhang, D.; Ronson, T. K. ; Nitschke, J. R. Functional Capsules via Subcomponent Self-Assembly. *Acc. Chem. Res.* **2018**, *51*, 2423–2436.

21. Caulder, D. L.; Brückner, C.; Powers, R. E.; König, S.; Parac, T. N.; Leary, J. A.; Raymond, K. N. Design, Formation and Properties of Tetrahedral M_4L_4 and M_4L_6 Supramolecular Clusters. *J. Am. Chem. Soc.* **2001**, *123*, 8923–8938.

22. Bilbeisi, R. A.; Clegg, J. K.; Elgrishi, N.; de Hatten, X.; Devillard, M.; Breiner, B.; Mal, P.; Nitschke, J. R. Subcomponent Self-Assembly and Guest-Binding Properties of Face-Capped $Fe_4L_4^{8+}$ Capsules. *J. Am. Chem. Soc.* **2012**, *134*, 5110–5119.

23. Yan, L.-L.; Tan, C.-H.; Zhang, G.-L.; Zhou, L.-P.; Bünzli, J.-C.; Sun. Q.-F. Stereocontrolled Self-Assembly and Self-Sorting of Luminescent Europium Tetrahedral Cages. *J. Am. Chem. Soc.* **2015**, *137*, 8550–8555.

24. Howlader, P.; Zangrando, E.; Mukherjee, P. S. Self-Assembly of Enantiopure Pd_{12} Tetrahedral Homochiral Nanocages with Tetrazole Linkers and Chiral Recognition. *J. Am. Chem. Soc.* **2020**, *142*, 9070–9078.

25. Meng, W.; Breiner, B.; Rissanen, K.; Thoburn, J. D.; Clegg, J. K.; Nitschke, J. R. A Self-Assembled M_8L_6 Cubic Cage that Selectively Encapsulates Large Aromatic Guests. *Angew. Chem., Int. Ed.* **2011**, *50*, 3479–3483.

26. Otte, M.; Kuijpers, P. F.; Troeppner, O.; Ivanović-Burmazović, I.; Reek, J. N. H.; de Bruin, B. Encapsulated Cobalt-Porphyrin as a Catalyst for Size-Selective Radical-type Cyclopropanation Reactions. *Chem. Eur. J.* **2014**, *20*, 4880–4884.

27. Zhou, X.-P.; Wu, Y.; Li, D. Polyhedral Metal-Imidazolate Cages: Control of Self-Assembly and Cage to Cage Transformation. *J. Am. Chem. Soc.* **2013**, *135*, 16062–16065.

28. Browne, C.; Brenet, S.; Clegg, J. K.; Nitschke, J. R. Solvent-Dependent Host-Guest Chemistry of an Fe_8L_{12} Cubic Capsule. *Angew. Chem., Int. Ed.* **2013**, *52*, 1944–1948.

29. Fujita, M.; Oguro, D.; Miyazawa, M.; Oka, H.; Yamaguchi, K.; Ogura, K. Self-Assembly of Ten Molecules into Nanometre-Sized Organic Host Frameworks. *Nature* **1995**, *378*, 469–471.

30. Chand, D. K.; Biradha, K.; Fujita, M.; Sakamoto, S.; Yamaguchi, K. A Molecular Sphere of Octahedral Symmetry. *Chem. Commun.* **2002**, 2486–2487.

31. Suzuki, K.; Tominaga, M.; Kawano, M.; Fujita, M. Self-Assembly of an M_6L_{12} Coordination Cube. *Chem. Commun.* **2009**, 1638–1640.

32. Moon, D.; Kang, S.; Park, J.; Lee, K.; John, R. P.; Won, H.; Seong, G. H.; Kim, Y. S.; Kim, G. H.; Rhee, H.; Lah, M. S. Face-Driven Corner-Linked Octahedral Nanocages: M_6L_8 Cages Formed by C_3-Symmetric Triangular Facial Ligands Linked *via* C_4-Symmetric Square Tetratopic Pd^{II} Ions at Truncated Octahedron Corners. *J. Am. Chem. Soc.* **2006**, *128*, 3530–3531.

33. Rizzuto, F. J.; Wu, W.-Y.; Ronson, T. K.; Nitschke, J. R. Peripheral Templation Generates an M$^{II}_6L_4$ Guest-Binding Capsule. *Angew. Chem., Int. Ed.* **2016**, *55*, 7958–7962.

34. He, C.; Lin, Z.; He, Z.; Duan, C.; Xu, C.; Wang, Z.; Yan, C. Metal-Tunable Nanocages as Artificial Chemosensors. *Angew. Chem, Int. Ed.* **2008**, *47*, 877–881.

35. Mal, P.; Breiner, B.; Rissanen, K.; Nitschke, J. R. White Phosphorus is Air-Stable Within a Self-Assembled Tetrahedral Capsule. *Science* **2009**, *324*, 1697–1699.

36. Yoshizawa, M.; Miyagi, S.; Kawano, M.; Ishiguro, K.; Fujita, M. Alkane Oxidation *via* Photochemical Excitation of a Self-Assembled Molecular Cage. *J. Am. Chem. Soc.* **2004**, *126*, 9172–9173.

37. Yoshizawa, M.; Kusukawa, T.; Kawano, M.; Ohhara, T.; Tanaka, I.; Kurihara, K.; Niimura, N.; Fujita, M. Endohedral Clusterization of Ten Water Molecules into a "Molecular Ice" within the Hydrophobic Pocket of a Self-Assembled Cage. *J. Am. Chem. Soc.* **2005**, *127*, 2798–2799.

38. Pearce, N.; Champness, N. R. Metal Complexes in Supramolecular Chemistry and Self-Assembly. In *Comprehensive Coordination Chemistry III (Third Edition)*, Eds: Constable, E. C.; Parkin, G.; Que, L. Jr.; *Elsevier,* **2021**; pp. 81–98.

39. Wang, M.; Lan, W.-J.; Zheng, Y.-R.; Cook, T. R.; White, H. S.; Stang, P. J. Post-Self-Assembly Covalent Chemistry of Discrete Multicomponent Metallosupramolecular Hexagonal Prisms. *J. Am. Chem. Soc.* **2011**, *133*, 10752–10755.

40. Roberts, D. A.; Pilgrim, B. S.; Nitschke, J. R. Covalent Post-Assembly Modification in Metallosupramolecular Chemistry. *Chem. Soc. Rev.* **2018**, *47*, 626–644.

41. Zeng, H.; Stewart-Yates, L.; Casey, L. M.; Bampos, N.; Roberts, D. A. Covalent Post-Assembly Modification: A Synthetic Multipurpose Tool in Supramolecular Chemistry. *ChemPlusChem* **2020**, *85*, 1249–1269.

42. McConnell, A. J.; Wood, C. S.; Neelakandan, P. P.; Nitschke, J. R. Stimuli-Responsive Metal–Ligand Assemblies. *Chem. Rev.* **2015**, *115*, 7729–7793.

43. Han, M.; Michel, R.; He, B.; Chen, Y.-S.; Stalke, D.; John, M.; Clever, G. H. Light-Triggered Guest Uptake and Release by a Photochromic Coordination Cage. *Angew. Chem., Int. Ed.* **2013**, *52*, 1319–1323.

44. Akine, S.; Miyashita, M.; Nabeshima, T. A Metallo-Molecular Cage That Can Close the Apertures with Coordination Bonds. *J. Am. Chem. Soc.* **2017**, *139*, 4631–4634.

45. Szalóki, G.; Croué, V.; Carré, V.; Aubriet, F.; Alévêque, O.; Levillain, E.; Allain, M.; Aragó, J.; Ortí, E.; Goeb, S.; Sallé, M. Controlling the Host–Guest Interaction Mode through a Redox Stimulus. *Angew. Chem., Int. Ed.* **2017**, *56*, 16272–16276.

46. McTernan, C. T. Ronson, T. K.; Nitschke, J. R. Post-assembly Modification of Phosphine Cages Controls Host-Guest Behavior. *J. Am. Chem. Soc.* **2019**, *141*, 6837–6842.

47. Grancha, T.; Carné-Sánchez, A.; Hernández-López, L.; Albalad, J.; Imaz, I.; Juanhuix, J.; Maspoch, D. Phase Transfer of Rhodium(II)-Based Metal–Organic Polyhedra Bearing Coordinatively Bound Cargo Enables Molecular Separation. *J. Am. Chem. Soc.* **2019**, *141*, 18349–18355.

48. Nguyen, B.-N. T.; Grommet, A. B.; Tron, A.; Georges, M. C. A.; Nitschke, J. R. Heat Engine Drives Transport of an $Fe^{II}_4L_4$ Cage and Cargo. *Adv. Mater.* **2020**, *32*, 1907241.

49. Andrés, M. A.; Carné-Sánchez, A.; Sánchez-Laínez, J.; Roubeau, O.; Coronas, J.; Maspoch, D.; Gascón, I. Ultrathin Films of Porous Metal–Organic Polyhedra for Gas Separation. *Chem. Eur. J.* **2020**, *26*, 143–147.

50. Ma, L.; Haynes, C. J. E.; Grommet, A. B.; Walczak, A.; Parkins, C. C.; Doherty, C. M.; Longley, L.; Tron, A.; Stefankiewicz, A. R.; Bennett, T. D.; Nitschke, J. R. Coordination Cages as Permanently Porous Ionic Liquids. *Nat. Chem.* **2020**, *12*, 270–275.

51. Hosono, N.; Kitagawa, S. Modular Design of Porous Soft Materials via Self-Organization of Metal–Organic Cages. *Acc. Chem. Res.* **2018**, *51*, 2437–2446.

52. Gu, Y.; Alt, E. A.; Wang, H.; Li, X.; Willard, A. P.; Johnson, J. A. Photoswitching Topology in Polymer Networks with Metal–Organic Cages as Crosslinks. *Nature* **2018**, *560*, 65–69.

53. Zhukhovitskiy, A. V.; Zhong, M.; Keeler, E. G.; Michaelis, V. K.; Sun, J. E. P.; Hore, M. J. A.; Pochan, D. J.; Griffin, R. G.; Willard, A. P.; Johnson, J. A. Highly Branched and Loop-Rich Gels *via* Formation of Metal–Organic Cages Linked by Polymers. *Nat. Chem.* **2016**, *8*, 33–41.

54. Wang, Y.; Gu, Y.; Keeler, E. G.; Park, J. V.; Griffin, R. G.; Johnson, J. A. Star PolyMOCs with Diverse Structures, Dynamics, and Functions by Three-Component Assembly. *Angew. Chem., Int. Ed.* **2017**, *56*, 188–192.

55. Sutar, P.; Suresh, V. M.; Jayaramulu, K.; Hazra, A.; Maji, T. K. Binder Driven Self-Assembly of Metal-Organic Cubes Towards Functional Hydrogels. *Nat. Commun.* **2018**, *9*, 3587.

56. Ariga, K.; Shionoya, M. Nanoarchitectonics for Coordination Asymmetry and Related Chemistry. *Bull. Chem. Soc. Jpn.* **2021**, *94*, 839–859.

57. Rizzuto, F. J.; von Krbek, L. K. S.; Nitschke, J. R. Strategies for Binding Multiple Guests in Metal-Organic Cages. *Nat. Rev. Chem.* **2019**, *3*, 204–222.

58. Takezawa, H.; Shitozawa, K.; Fujita, M. Enhanced Reactivity of Twisted Amides inside a Molecular Cage. *Nat. Chem.* **2020**, *12*, 574–578.

59. Takezawa, H.; Kanda, T.; Nanjo, H.; Fujita, M. Site-Selective Functionalization of Linear Diterpenoids through U-Shaped Folding in a Confined Artificial Cavity. *J. Am. Chem. Soc.* **2019**, *141*, 5112–5115.

60. Niki, K.; Tsutsui, T.; Yamashina, M.; Akita, M.; Yoshizawa, M. Recognition and Stabilization of Unsaturated Fatty Acids by a Polyaromatic Receptor. *Angew. Chem., Int. Ed.* **2020**, *59*, 10489–10492.

61. Patrick, G. L. *An Introduction to Medicinal Chemistry*, 6th Ed.; Oxford University Press: Oxford, U.K., 2017.

62. Rizzuto, F. J.; Carpenter, J. P.; Nitschke, J. R. Multisite Binding of Drugs and Natural Products in an Entropically Favorable, Heteroleptic Receptor. *J. Am. Chem. Soc.* **2019**, *141*, 9087–9095.

63. Sawada, T.; Yoshizawa, M.; Sato, S.; Fujita, M. Minimal Nucleotide Duplex Formation in Water through Enclathration in Self-Assembled Hosts. *Nat. Chem.* **2009**, *1*, 53–56.

64. Saha, R.; Devaraj, A.; Bhattacharyya, S.; Das, S.; Zangrando, E.; Mukherjee, P. S. Unusual Behavior of Donor-Acceptor Stenhouse Adducts in Confined Space of a Water-Soluble Pd$^{II}_8$ Molecular Vessel. *J. Am. Chem. Soc.* **2019**, *141*, 8638–8645.

65. Caulder, D. L.; Raymond, K. N. Supramolecules by Design. *Acc. Chem. Res.* **1999**, *32*, 975–982.

66. Fujita, M.; Umemoto, K.; Yoshizawa, M.; Fujita, N.; Kusukawa, T.; Biradha, K. Molecular Paneling *via* Coordination. *Chem. Commun.* **2001**, 509–518.

67. Holliday, B. J.; Mirkin, C. A. Strategies for the Construction of Supramolecular Compounds through Coordination Chemistry. *Angew. Chem., Int. Ed.* **2001**, *40*, 2022–2043.

68. Farrell, J. R.; Mirkin, C. A.; Liable-Sands, L. M.; Rheingold, A. L. Strategy for Preparing Molecular Cylinders with Synthetically Programmable Structural Parameters. *J. Am. Chem. Soc.* **1998**, *120*, 11834–11835.

69. Holliday, B. J.; Farrell, J. R.; Mirkin, C. A.; Lam, K.-C.; Rheingold, A. L. Metal-Directed Assembly of Triple-Layered Fluorescent Metallocyclophanes. *J. Am. Chem. Soc.* **1999**, *121*, 6316–6317.

70. Mollick, S.; Fajal, S.; Mukherjee, S.; Ghosh, S. K. Stabilizing Metal–Organic Polyhedra (MOP): Issues and Strategies. *Chem. Asian J.* **2019**, *14*, 3096–3108.

71. Gosselin, A. J.; Rowland, C. A.; Bloch, E. D. Permanently Microporous Metal–Organic Polyhedra. *Chem. Rev.* **2020**, *120*, 8987–9014.

72. Lee, S.; Jeong, H.; Nam, D.; Lah, M. S.; Choe, W. The Rise of Metal-Organic Polyhedra. *Chem. Soc. Rev.* **2021**, *50*, 528-555.

73. Zheng, Y.-R.; Zhao, Z.; Wang, M.; Ghosh, K.; Pollock, J. B.; Cook, T. R.; Stang, P. J. A Facile Approach toward Multicomponent Supramolecular Structures: Selective Self-Assembly via Charge Separation. *J. Am. Chem. Soc.* **2010**, *132*, 16873–16882.

74. Zheng, Y.-R.; Lan, W.-J.; Wang, M.; Cook, T. R.; Stang, P. J. Designed Post-Self-Assembly Structural and Functional Modifications of a Truncated Tetrahedron. *J. Am. Chem. Soc.* **2011**, *133*, 17045–17055.

75. Zhao, Z.; Zheng, Y.-R.; Wang, M.; Pollock, J. B.; Stang, P. J. Construction of Hexagonal Prisms of Variable Size via Coordination-Driven Multicomponent Self-Assembly. *Inorg. Chem.* **2010**, *49*, 8653–8655.

76. Yan, X.; Cook, T. R.; Wang, P.; Huang, F.; Stang, P. J. Highly Emissive Platinum(II) Metallacages. *Nat. Chem.* **2015**, *7*, 342–348.

77. Chen, C.; Sun, Y.; Zhao, Y.; VanderLinden, R. T.; Tuo, W.; Zhang, F.; Zhang, S.; Sepehrpour, H.; Yan, C.; Wang, J.; Li, D.; Stang, P. J. Anthracene-Induced Formation of Highly Twisted Metallacycle and its Crystal Structure and Tunable Assembly Behaviors. *PNAS* **2021**, *118*, e2102602118.

78. Sun, Y.; Zhang, F.; Jiang, S.; Wang, Z.; Ni, R.; Wang, H.; Zhou, W.; Li, X.; Stang, P. J. Assembly of Metallacages into Soft Suprastructures with Dimensions of up to Micrometers and the Formation of Composite Materials. *J. Am. Chem. Soc.* **2018**, *140*, 17297–17307.

79. He, W.; Liu, F.; Duan, C.; Guo, Z.; Zhou, S.; Liu, Y.; Zhu, L. Construction of a Square-Planar Molecular Box: Self-Assembly of Palladium(II) Complexes of 3,6,9,16,19,22-Hexaazatricyclo[22.2.2.$2^{11,14}$]triacon-11,13,24,26(1),27,29-hexaene through Hydrogen-Bonding Interactions. *Inorg. Chem.* **2001**, *40*, 7065–7071.

80. Hou, Y.; Zhang, Z.; Lu, S.; Yuan, J.; Zhu, Q.; Chen, W.-P.; Ling, S.; Li, X.; Zheng, Y.-Z.; Zhu, K.; Zhang, M. Highly Emissive Perylene Diimide-Based Metallacages and their Host-Guest Chemistry for Information Encryption. *J. Am. Chem. Soc.* **2020**, *142*, 18763–18768.

81. Mirtschin, S.; Slabon-Turski, A.; Scopelliti, R.; Velders, A. H.; Severin, K. A Coordination Cage with an Adaptable Cavity Size. *J. Am. Chem. Soc.* **2010**, *132*, 14004–14005.

82. Schmittel, M.; He, B.; Mal, P. Supramolecular Multicomponent Self-Assembly of Shape-Adaptive Nanoprisms: Wrapping up C_{60} with Three Porphyrin Units. *Org. Lett.* **2008**, *10*, 2513–2516.

83. Goswami, A.; Saha, S.; Biswas, P. K.; Schmittel, M. (Nano)mechanical Motion Triggered by Metal Coordination: from Functional Devices to Networked Multicomponent Catalytic Machinery. *Chem. Rev.* **2020**, *120*, 125–199.

84. Yoshizawa, M.; Nagao, M.; Kumazawa, K.; Fujita, M. Side Chain-Directed Complementary *cis*-Coordination of Two Pyridines on Pd(II); Selective Multicomponent Assembly of Square-, Rectangular-, and Trigonal Prism-Shaped Molecules. *J. Organomet. Chem.* **2005**, *690*, 5383–5388.

85. Zhu, R.; Bloch, W. M.; Holstein, J. J.; Mandal, S.; Schäfer, L. V.; Clever, G. H. Donor-Site-Directed Rational Assembly of Heteroleptic *cis*-[Pd$_2$L$_2$L'$_2$] Coordination Cages from Picolyl Ligands. *Chem. Eur. J.* **2018**, *24*, 12976–12982.

86. Chen, B.; Horiuchi, S.; Holstein, J. J.; Tessarolo, J.; Clever, G. H. Tunable Fullerene Affinity of Cages, Bowls and Rings Assembled by Pd^{II} Coordination Sphere Engineering. *Chem. Eur. J.* **2019**, *25*, 14921–14927.

87. Jayamurugan, G.; Roberts, D. A.; Ronson, T. K.; Nitschke, J. R. Selective *Endo* and *Exo* Binding of Mono- and Ditopic Ligands to a Rhomboidal Diporphyrin Prism. *Angew. Chem., Int. Ed.* **2015**, *54*, 7539–7543.

88. Kaeser, A.; Mohankumar, M.; Mohanraj, J.; Monti, F.; Holler, M.; Cid, J.-J.; Moudam, O.; Nierengarten, I.; Karmazin-Brelot, L.; Duhayon, C.; Delavaux-Nicot, B.; Armaroli, N.; Nierengarten, J.-F. Heteroleptic Copper(I) Complexes Prepared from Phenanthroline and Bis-Phosphine Ligands. *Inorg. Chem.* **2013**, *52*, 12140–12151.

89. Baxter, P.; Lehn, J.-M.; DeCian, A.; Fischer, J. Multicomponent Self-Assembly: Spontaneous Formation of a Cylindrical Complex from Five Ligands and Six Metal Ions. *Angew. Chem., Int. Ed.* **1993**, *32*, 69–72.

90. Baxter, P. N. W.; Lehn, J.-M., Kneisel, B. O.; Baum, G.; Fenske, D. The Designed Self-Assembly of Multicomponent and Multicompartmental Cylindrical Nanoarchitectures. *Chem. Eur. J.* **1999**, *5*, 113–120.

91. Han, M.; Engelhard, D. M.; Clever, G. H. Self-assembled Coordination Cages based on Banana-Shaped Ligands. *Chem. Soc. Rev.* **2014**, *43*, 1848–1860.

92. Löffler, S.; Lübben, J.; Krause, L.; Stalke, D.; Dittrich, B.; Clever, G. H. Triggered Exchange of Anionic for Neutral Guests inside a Cationic Coordination Cage. *J. Am. Chem. Soc.* **2015**, *137*, 1060–1063.

93. Preston, D.; Lewis, J. E. M.; Crowley, J. D. Multicavity $[Pd_nL_4]^{2n+}$ Cages with Controlled Segregated Binding of Different Guests. *J. Am. Chem. Soc.* **2017**, *139*, 2379–2386.

94. Freye, S.; Hey, J.; Torras-Galán, A.; Stalke, D.; Herbst-Irmer, R.; John, M.; Clever, G. H. Allosteric Binding of Halide Anions by a New Dimeric Interpenetrated Coordination Cage. *Angew. Chem., Int. Ed.* **2012**, *51*, 2191–2194.

95. Regeni, I.; Chen, B.; Frank, M.; Baksi, A.; Holstein, J. J.; Clever, G. H. Coal-Tar Dye-based Coordination Cages and Helicates. *Angew. Chem., Int. Ed.* **2021**, *60*, 5673–5678.

96. Bloch, W. M.; Abe, Y.; Holstein, J. J.; Wandtke, C. M.; Dittrich, B.; Clever, G. H. Geometric Complementarity in Assembly and Guest Recognition of a Bent Heteroleptic *cis*-$[Pd_2L^A_2L^B_2]$ Coordination Cage. *J. Am. Chem. Soc.* **2016**, *138*, 13750–13755.

97. Pullen, S.; Tessarolo, J.; Clever, G. H. Increasing Structural and Functional Complexity in Self-Assembled Coordination Cages. *Chem. Sci*. **2021**, *12*, 7269–7293.

98. Bloch, W. M.; Holstein, J. J.; Hiller, W.; Clever, G. H. Morphological Control of Heteroleptic *cis*- and *trans*-$Pd_2L_2L'_2$ Cages. *Angew. Chem., Int. Ed.* **2017**, *56*, 8285–8289.

99. Wu, K.; Zhang, B.; Drechsler, C.; Holstein, J. J.; Clever, G. H. Backbone-Bridging Promotes Diversity in Heteroleptic Cages. *Angew. Chem., Int. Ed.* **2021**, *60*, 6403–6407.

100. Frank, M.; Johnstone, M. D.; Clever, G. H. Interpenetrated Cage Structures. *Chem. Eur. J.* **2016**, *22*, 14104–14125.

101. Schulte, T. R.; Holstein, J. J.; Schneider, L.; Adam, A.; Haberhauer, G.; Clever, G. H. A New Mechanically-Interlocked [Pd$_2$L$_4$] Cage Motif by Dimerization of two Peptide-Based Lemniscates. *Angew. Chem., Int. Ed.* **2020**, *59*, 22489–22493.

102. Li, R.-L.; Tessarolo, J.; Lee, H.; Clever, G. H. Multi-Stimuli Control over Assembly and Guest Binding in Metallo-Supramolecular Hosts Based on Dithienylethene Photoswitches. *J. Am. Chem. Soc.* **2021**, *143*, 3865–3873.

103. Tessarolo, J.; Lee, H.; Sakuda, E.; Umakoshi, K.; Clever, G. H. Integrative Assembly of Heteroleptic Tetrahedra Controlled by Backbone Steric Bulk. *J. Am. Chem. Soc.* **2021**, *143*, 6339–6344.

104. Sudan, S.; Li, R.-J.; Jansze, S. M.; Platzek, A.; Rudolf, R.; Clever, G. H.; Fadaei-Tirani, F.; Scopelliti, R.; Severin, K. Identification of a Heteroleptic Pd$_6$L$_6$L'$_6$ Coordination Cage by Screening of a Virtual Combinatorial Library. *J. Am. Chem. Soc.* **2021**, *143*, 1773–1778.

105. Sun, Q.-F.; Sato, S.; Fujita, M. An M$_{12}$(L^1)$_{12}$(L^2)$_{12}$ Cantellated Tetrahedron: A Case Study on Mixed-Ligand Self-Assembly. *Angew. Chem., Int. Ed.* **2014**, *53*, 13510–13513.

106. Benkhäuser, C.; Lützen, A. Self-Assembly of Heteroleptic Dinuclear Metallosupramolecular Kites from Multivalent Ligands via Social Self-Sorting. *Beilstein J. Org. Chem.* **2015**, *11*, 693–700.

107. Ronson, T. K.; Roberts, D. A.; Black, S. P.; Nitschke, J. R. Stacking Interactions Drive Selective Self-Assembly and Self-Sorting of Pyrene-Based M$^{II}_4$L$_6$ Architectures. *J. Am. Chem. Soc.* **2015**, *137*, 14502–14512.

108. Zhang, D.; Ronson, T. K.; Xu, L.; Nitschke, J. R. Transformation Network Culminating in a Heteroleptic Cd$_6$L$_6$L'$_2$ Twisted Trigonal Prism. *J. Am. Chem. Soc.* **2020**, *142*, 9152–9157.

109. Lee, H.; Noh, T. H.; Jung, O.-S. Construction of Hetero-Four-Layered Tripalladium(II) Cyclophanes by Transannular π$\cdots$π Interactions. *Angew. Chem., Int. Ed.* **2016**, *55*, 1005–1009.

110. Iseki, S.; Nonomura, K.; Kishida, S.; Ogata, D.; Yuasa, J. Zinc-Ion-Stabilized Charge-Transfer Interactions Drive Self-Complementary or Complementary Molecular Recognition. *J. Am. Chem. Soc.* **2020**, *142*, 15842–15851.

111. Kumazawa, K.; Biradha, K.; Kusukawa, T.; Okano, T.; Fujita, M. Multicomponent Assembly of a Pyrazine-Pillared Coordination Cage That Selectively Binds Planar Guests by Intercalation. *Angew. Chem., Int. Ed.* **2003**, *42*, 3909–3913.

112. Olenyuk, B.; Whiteford, J. A.; Fechtenkötter, A.; Stang, P. J. Self-Assembly of Nanoscale Cuboctahedra by Coordination Chemistry. *Nature* **1999**, *398*, 796–799.

113. Schweiger, M.; Seidel, S. R.; Schmitz, M.; Stang, P. J. Rational Design of Chiral Nanoscale Adamantanoids. *Org. Lett.* **2000**, *2*, 1255–1257.

114. Crowley, J. D.; Steele, I. M.; Bosnich, B. Molecular Recognition – Allosterism Generated by Weak Host-Guest Interactions in Molecular Rectangles. *Eur. J. Inorg. Chem.* **2005**, *2005*, 3907–3917.

115. Yamaki, Y.; Nakamura, T.; Suzuki, S.; Yamamura, M.; Minoura, M.; Nabeshima, T. A Self-Assembled Rectangular Host with Terpyridine-Platinum(II) Moieties that Binds Unsubstituted Pentacene in Solution. *Eur. J. Org. Chem.* **2016**, *2016*, 1678–1683.

116. Chan. A. K.-W.; Lam, W. H.; Tanaka, Y.; Wong, K. M.-C.; Yam, V. W.-W. Multiaddressable Molecular Rectangles with Reversible Host-Guest Interactions: Modulation of pH-Controlled Guest Release and Capture. *PNAS* **2015**, *112*, 690–695.

117. Preston, D.; Kruger, P. E. Using Complementary Ligand Denticity to Direct Metallosupramolecular Structure about Metal Ions with Square-Planar Geometry. *ChemPlusChem* **2020**, *85*, 454–465.

118. Samanta, D.; Shanmugaraju, S.; Joshi, S. A.; Patil, Y. P.; Nethaji, M.; Mukherjee, P. S. Pillar Height Dependent Formation of Unprecedented Pd_8 Molecular Swing and Pd_6 Molecular Boat via Multicomponent Self-Assembly. *Chem. Commun.* **2012**, *48*, 2298–2300.

119. Samanta, D.; Mukherjee, P. S. Multicomponent Self-Sorting of a Pd_7 Molecular Boat and its use in Catalytic Knoevenagel Condensation. *Chem. Commun.* **2013**, *49*, 4307–4309.

120. García-Simón, C.; Gramage-Doria, R.; Raoufmoghaddam, S.; Parella, T.; Costas, M.; Ribas, X.; Reek, J. N. H. Enantioselective Hydroformylation by a Rh-Catalyst Entrapped in a Supramolecular Metallocage. *J. Am. Chem. Soc.* **2015**, *137*, 2680–2687.

121. García-Simón, C.; Garcia-Borràs, M.; Gómez, L.; Parella, T.; Osuna, S.; Juanhuix, J.; Imaz, I.; Maspoch, D.; Costas, M.; Ribas, X. Sponge-Like Molecular Cage for Purification of Fullerenes. *Nat. Commun.* **2014**, *5*, 5557.

122. Fuertes-Espinosa, C.; García-Simón, C.; Pujals, M.; Garcia-Borràs, M.; Gómez, L.; Parella, T.; Juanhuix, J.; Imaz, I.; Maspoch, D.; Costas, M.; Ribas, X. Supramolecular Fullerene Sponges as Catalytic Masks for Regioselective Functionalisation of C_{60}. *Chem* **2020**, *6*, 169–186.

123. Fuertes-Espinosa, C.; Murillo, J.; Soto, M. E.; Ceron, M. R.; Morales-Martínez, R.; Rodríguez-Fortea, A.; Poblet, J. M.; Echegoyen, L.; Ribas, X. Highly Selective Encapsulation and Purification of U-Based C_{78}-EMFs within a Supramolecular Nanocapsule. *Nanoscale* **2019**, *11*, 23035–23041.

124. Ubasart, E.; Borodin, O.; Fuertes-Espinosa, C.; Xu, Y.; García-Simón, C.; Gómez, L.; Juanhuix, J.; Gándara, F.; Imaz, I.; Maspoch, D.; von Delius, M.; Ribas, X. A Three-Shell Supramolecular Complex Enables the Symmetry-Mismatched Chemo- and Regioselective Bis-Functionalization of C_{60}. *Nat. Chem.* **2021**, *13*, 420–427.

125. Zhang, L.; Lin, Y.-J.; Li, Z.-H.; Jin G.-X. Rational Design of Polynuclear Organometallic Assemblies from a Simple Heteromultifunctional Ligand. *J. Am. Chem. Soc.* **2015**, *137*, 13670–13678.

126. Zhang, L.; Lin, Y.-J.; Li, Z.-H., Stoddart, J. F.; Jin, G.-X. Coordination-Driven Selective Formation of D_2 Symmetric Octanuclear Organometallic Cages. *Chem. Eur. J.* **2021**, *27*, 9524–9528.

127. Lavendomme, R.; Ronson, T. K.; Nitschke, J. R. Metal and Organic Templates Together Control the Size of Covalent Macrocycles and Cages. *J. Am. Chem. Soc.* **2019**, *141*, 12147–12158.

128. Preston, D.; Barnsley, J. E.; Gordon, K. C.; Crowley, J. D. Controlled Formation of Heteroleptic $[Pd_2(L_a)_2(L_b)_2]^{4+}$ Cages. *J. Am. Chem. Soc.* **2016**, *138*, 10578–10585.

129. Chepelin, O.; Ujma, J.; Barran, P. E.; Lusby, P. J. Sequential, Kinetically Controlled Synthesis of Multicomponent Stereoisomeric Assemblies. *Angew. Chem., Int. Ed.* **2012**, *51*, 4194–4197.

130. Lewis, J. E. M.; Crowley, J. D. Metallo-Supramolecular Self-Assembly with Reduced Symmetry Ligands. *ChemPlusChem* **2020**, *85*, 815–827.

131. McMorran, D. A.; Steel, P. J. The First Coordinatively Saturated, Quadruply Stranded Helicate and Its Encapsulation of a Hexafluorophosphate Anion. *Angew. Chem., Int. Ed.* **1998**, *37*, 3295–3297.

132. Schmidt, A.; Casini, A.; Kühn, F. E. Self-Assembled M_2L_4 Coordination Cages: Synthesis and Potential Applications. *Coord. Chem. Rev.* **2014**, *275*, 19–36.

133. Lewis, J. E. M.; Tarzia, A.; White, A. J. P.; Jelfs, K. E. Conformational Control of Pd_2L_4 Assemblies with Unsymmetrical Ligands. *Chem. Sci.* **2020**, *11*, 677–683.

134. Ogata, D.; Yuasa, J. Dynamic Open Coordination Cage from Nonsymmetrical Imidazole-Pyridine Ditopic Ligands for Turn-On/Off Anion Binding. *Angew. Chem., Int. Ed.* **2019**, *58*, 18424–18428.

135. Sen, S. K.; Natarajan, R. Influence of Conformational Change and Interligand Hydrogen Bonding in a Chiral Metal-Organic Cage. *Inorg. Chem.* **2019**, *58*, 7180–7188.

136. Mishra, S. S.; Kompella, S. V. K.; Krishnaswamy, S.; Balasubramanian, S.; Chand, D. K. Low-Symmetry Self-Assembled Coordination Complexes with Exclusive Diastereoselectivity: Experimental and Computational Studies. *Inorg. Chem.* **2020**, *59*, 12884–12894.

137. Lewis, J. E. M. Multi-functional, Low Symmetry Pd_2L_4 Nanocage Libraries. *Chem. Eur. J.* **2021**, *27*, 4454–4460.

138. Lisboa, L. S.; Findlay, J. A.; Wright, L. J.; Hartinger, C. G.; Crowley, J. D. A Reduced-Symmetry Heterobimetallic $[PdPtL_4]^{4+}$ Cage: Assembly, Guest Binding, and Stimulus-Induced Switching. *Angew. Chem., Int. Ed.* **2020**, *59*, 11101–11107.

139. Markwell-Heys, A. W.; Schneider, M. L.; Madridejos, J. M. L.; Metha, G. F.; Bloch W. M. Self-Sorting of Porous $Cu_4L_2L'_2$ Metal–Organic Cages Composed of Isomerisable Ligands. *Chem. Commun.* **2021**, *57*, 2915–2918.

140. Young, M. C.; Holloway, L. R.; Johnson, A. M.; Hooley, R. J. A Supramolecular Sorting Hat: Stereocontrol in Metal-Ligand Self-Assembly by Complementary Hydrogen Bonding. *Angew. Chem.*, *Int. Ed.* **2014**, *53*, 9832–9836.

141. Holloway, L. R.; Bogie, P. M.; Lyon, Y.; Julian, R. R.; Hooley, R. J. Stereoselective Postassembly CH Oxidation of Self-Assembled Metal-Ligand Cage Complexes. *Inorg. Chem.* **2017**, *56*, 11435–11442.

142. da Camara, B.; Dietz, P. C.; Chalek, K. R.; Mueller, L. J.; Hooley, R. J. Selective, Cofactor-Mediated Catalytic Oxidation of Alkanethiols in a Self-Assembled Cage Host. *Chem. Commun.* **2020**, *56*, 14263–14266.

143. Ngai, C.; Bogie, P. M.; Holloway, L. R.; Dietz, P. C.; Mueller, L. J.; Hooley, R. J. Cofactor-Mediated Nucleophilic Substitution Catalyzed by a Self-Assembled Holoenzyme Mimic. *J. Org. Chem.* **2019**, *84*, 12000–12008.

144. Holloway, L. R.; Bogie, P. M.; Lyon, Y.; Ngai, C.; Miller, T. F.; Julian, R. R.; Hooley, R. J. Tandem Reactivity of a Self-Assembled Cage Catalyst with Endohedral Acid Groups. *J. Am. Chem. Soc.* **2018**, *140*, 8078–8081.

145. Wang, X.; Huang, J.; Xiang, S.; Liu, Y.; Zhang, J.; Eichhöfer, A.; Fenske, D.; Bai, S.; Su, C.-Y. Discrete Ag_6L_6 Coordination Nanotubular Structures Based on a T-Shaped Pyridyl Diphosphine. *Chem. Commun.* **2011**, *47*, 3849–3851.

146. Hang, X.; Liu, B.; Zhu, X.; Wang, S.; Han, H.; Liao, W.; Liu, Y.; Hu, C. Discrete {Ni_{40}} Coordination Cage: A Calixarene-Based Johnson-Type (J_{17}) Hexadecahedron. *J. Am. Chem. Soc.* **2016**, *138*, 2969–2972.

147. Zhang, Q.; Jiang, F.; Huang, Y.; Wu, M.; Hong, M. Coordination-Driven Face-Directed Self-Assembly of a M_9L_6 Hexahedral Nanocage from Octahedral Ni(II) Ions and Asymmetric Hydrazone Ligands. *Cryst. Growth Des.* **2009**, *9*, 28–31.

148. Sun, B.; Wang, M.; Lou, Z.; Huang, M.; Xu, C.; Li, X.; Chen, L.-J.; Yu, Y.; Davis, G. L.; Xu, B.; Yang, H.-B.; Li, X. From Ring-in-Ring to Sphere-in-Sphere: Self-Assembly of Discrete 2D and 3D Architectures with Increasing Stability. *J. Am. Chem. Soc.* **2015**, *137*, 1556–1564.

149. Song, B.; Zhang, Z.; Wang, K.; Hsu, C.-H.; Bolarinwa, O.; Wang, J.; Li, Y.; Yin, G.-Q.; Rivera, E.; Yang, H.-B.; Liu, C.; Xu, B.; Li, X. Direct Self-Assembly of a 2D and 3D Star of David. *Angew. Chem., Int. Ed.* **2017**, *56*, 5258–5262.

150. Sun, Q.-F.; Murase, T.; Sato, S.; Fujita, M. A Sphere-in-Sphere Complex by Orthogonal Self-Assembly. *Angew. Chem.*, *Int. Ed.* **2011**, *50*, 10318–10321.

151. Wang, H.; Zhou, L.-P.; Zheng, Y.; Wang, K.; Song, B.; Yan, X.; Wojtas, L.; Wang, X.-Q.; Jiang, X.; Wang, M.; Sun, Q.-F.; Xu, B.; Yang, H.-B.; Sue, A. C.-H.; Chan, Y.-T.; Sessler, J. L.; Jiao, Y.; Stang, P. J.; Li, X. Double-Layered Supramolecular Prisms Self-Assembled by Geometrically Non-equivalent Tetratopic Subunits. *Angew. Chem.*, *Int. Ed.* **2021**, *60*, 1298–1305.

152. Shi, J.; Li, Y.; Jiang, X.; Yu, H.; Li, J.; Zhang, H.; Trainer, D. J.; Hla, S. W.; Wang, H.; Wang, M.; Li, X. Self-Assembly of Metallo-Supramolecules with Dissymmetrical Ligands and Characterization by Scanning Tunneling Microscopy. *J. Am. Chem. Soc.* **2021**, *143*, 1224–1234.

153. Wang, H.; Liu, C.-H.; Wang, K.; Wang, M.; Yu, H.; Kandapal, S.; Brzozowski, R.; Xu, B.; Wang, M.; Lu, S.; Hao, X.-Q.; Eswara, P.; Nieh, M.-P.; Cai, J.; Li, X. Assembling Pentatopic Terpyridine Ligands with Three Types of Coordination Moieties into a Giant Supramolecular Hexagonal Prism: Synthesis, Self-Assembly, Characterization and Antimicrobial Study. *J. Am. Chem. Soc.* **2019**, *141*, 16108–16116.

154. Wang, H.; Qian, X.; Wang, K.; Su, M.; Haoyang, W.-W.; Jiang, X.; Brzozowski, R.; Wang, M.; Gao, X.; Li, Y.; Xu, B.; Eswara, P.; Hao, X.-Q.; Gong, W.; Hou, J.-L.; Cai, J.; Li, X. Supramolecular Kandinsky Circles with High Antibacterial Activity. *Nat. Commun.* **2018**, *9*, 1815.

155. Sun, Q.-F.; Sato, S.; Fujita, M. An $M_{18}L_{24}$ Stellated Cuboctahedron through Post-Stellation of an $M_{12}L_{24}$ Core. *Nat. Chem.* **2012**, *4*, 330–333.

156. Tominaga, M.; Suzuki, K.; Kawano, M.; Kusukawa, T.; Ozeki, T.; Sakamoto, S.; Yamaguchi, K.; Fujita, M. Finite, Spherical Coordination Networks that Self-Organize from 36 Small Components. *Angew. Chem., Int. Ed.* **2004**, *43*, 5621–5625.

157. Sato, S.; Ishido, Y.; Fujita, M. Remarkable Stabilization of $M_{12}L_{24}$ Spherical Frameworks through the Cooperation of 48 Pd(II)-Pyridine Interactions. *J. Am. Chem. Soc.* **2009**, *131*, 6064–6065.

158. Fox, O. D.; Drew, M. G. B.; Beer, P. D. Resorcarene-Based Nanoarchitectures: Metal-Directed Assembly of a Molecular Loop and Tetrahedron. *Angew. Chem., Int. Ed.* **2000**, *39*, 135–140.

159. Zhong, Z.; Ikeda, A.; Shinkai, S.; Sakamoto, S.; Yamaguchi, K. Creation of Novel Chiral Cryptophanes by a Self-Assembling Method Utilizing a Pyridyl-Pd(II) Interaction. *Org. Lett.* **2001**, *3*, 1085–1087.

160. McKinlay, R. M.; Cave, G. W. V.; Atwood, J. L. Supramolecular Blueprint Approach to Metal-Coordinated Capsules. *PNAS* **2005**, *102*, 5944–5948.

161. Dalgarno, S. J.; Power, N. P.; Atwood, J. L. Metallo-Supramolecular Capsules. *Coord. Chem. Rev.* **2008**, *252*, 825–841.

162. Pei, W.-Y; Yang, J.; Wu, H.; Zhou, W.; Yang, Y.-W.; Ma, J.-F. A Calix[4]resorcinarene-Based Giant Coordination Cage: Controlled Assembly and Iodine Uptake. *Chem. Commun.* **2020**, *56*, 2491–2494.

163. Pasquale, S.; Sattin, S.; Escudero-Adán, E. C.; Martínez-Belmonte, M.; de Mendoza, J. Giant Regular Polyhedra from Calixarene Carboxylates and Uranyl. *Nat. Commun.* **2012**, *3*, 785.

164. Kuijpers, P. F.; Otte, M.; Dürr, M.; Ivanović-Burmazović, I.; Reek, J. N. H.; de Bruin, B. A Self-Assembled Molecular Cage for Substrate-Selective Epoxidation Reactions in Aqueous Media. *ACS Catal.* **2016**, *6*, 3106–3112.

165. Rizzuto, F. J.; Ramsay, W. J.; Nitschke, J. R. Otherwise Unstable Structures Self-Assemble in the Cavities of Cuboctahedral Coordination Cages. *J. Am. Chem. Soc.* **2018**, *140*, 11502–11509.

166. von Krbek, L. K. S.; Roberts, D. A.; Pilgrim, B. S.; Schalley, C. A.; Nitschke, J. R. Multivalent Crown Ether Receptors Enable Allosteric Regulation of Anion Exchange in an Fe_4L_6 Tetrahedron. *Angew. Chem., Int. Ed.* **2018**, *57*, 14121–14124.

167. Yang, D.; Greenfield, J. L.; Ronson, T. K.; von Krbek, L. K. S.; Yu, L.; Nitschke, J. R. La^{III} and Zn^{II} Cooperatively Template a Metal-Organic Capsule. *J. Am. Chem. Soc.* **2020**, *142*, 19856–19861.

168. Sumby, C. J.; Hardie, M. J. Capsules and Star-Burst Polyhedra: An [Ag$_2$L$_2$] Capsule and a Tetrahedral [Ag$_4$L$_4$] Metallosupramolecular Prism with Cyclotriveratrylene-Type Ligands. *Angew. Chem.*, *Int. Ed.* **2005**, *44*, 6395–6399.

169. Ronson, T. K.; Fisher, J.; Harding, L. P.; Hardie, M. J. Star-Burst Prisms with Cyclotriveratrylene-Type Ligands: A [Pd$_6$L$_8$]$^{12+}$ Stella Octangular Structure. *Angew. Chem.*, *Int. Ed.* **2007**, *46*, 9086–9088.

170. Ronson, T. K.; Fisher, J.; Harding, L. P.; Rizkallah, P. J.; Warren, J. E.; Hardie, M. J. Stellated Polyhedral Assembly of a Topologically Complicated Pd$_4$L$_4$ 'Solomon Cube'. *Nat. Chem.* **2009**, *1*, 212–216.

171. Pentecost, C. D.; Chichak, K. S.; Peters, A. J.; Cave, G. W. V.; Cantrill, S. J.; Stoddart, J. F. A Molecular Solomon Link. *Angew. Chem., Int. Ed.* **2007**, *46*, 218–222.

172. Forgan, R. S.; Sauvage, J.-P.; Stoddart, J. F. Chemical Topology: Complex Molecular Knots, Links, and Entanglements. *Chem. Rev.* **2011**, *111*, 5434–5464.

173. Yang, H.; McLaughlin, C. K.; Aldaye, F. A.; Hamblin, G. D.; Rys, A. Z.; Rouiller, I.; Sleiman, H. F. Metal-Nucleic Acid Cages. *Nat. Chem.* **2009**, *1*, 390–396.

174. Aldaye, F. A.; Sleiman, H. F. Modular Access to Structurally Switchable 3D Discrete DNA Assemblies. *J. Am. Chem. Soc.* **2007**, *129*, 13376–13377.

175. Zimmermann, J.; Cebulla, M. P. J.; Mönninghoff, S.; von Kiedrowski, G. Self-Assembly of a DNA Dodecahedron from 20 Trisoligonucleotides with C_{3h} Linkers. *Angew. Chem., Int. Ed.* **2008**, *47*, 3626–3630.

176. Bhatia, D.; Mehtab, S.; Krishnan, R.; Indi, S. S.; Basu, A.; Krishnan, Y. Icosahedral DNA Nanocapsules by Modular Assembly. *Angew. Chem., Int. Ed.* **2009**, *48*, 4134–4137.

177. Seeman, N. C.; Sleiman, H. F. DNA Nanotechnology. *Nat. Rev. Mater.* **2018**, *3*, 17068.

178. Bujold, K. E.; Hsu, J. C. C.; Sleiman, H. F. Optimized DNA "Nanosuitcases" for Encapsulation and Conditional Release of siRNA. *J. Am. Chem. Soc.* **2016**, *138*, 14030–14038.

179. Paul, R. L.; Bell, Z. R.; Jeffery, J. C.; McCleverty, J. A.; Ward, M. D. Anion-Templated Self-Assembly of Tetrahedral Cage Complexes of Cobalt(II) with Bridging Ligands Containing Two Bidentate Pyrazolyl-Pyridine Binding Sites. *PNAS* **2002**, *99*, 4883–4888.

180. Fleming, J. S.; Mann, K. L. V.; Carraz, C.-A.; Psillakis, E.; Jeffery, J. C.; McCleverty, J. A.; Ward, M. D. Anion-Templated Assembly of a Supramolecular Cage Complex. *Angew. Chem., Int. Ed.* **1998**, *37*, 1279–1281.

181. Hall, B. R.; Manck, L. E.; Tidmarsh, I. S.; Stephenson, A.; Taylor, B. F.; Blaikie, E. J.; Vander Griend, D. A.; Ward, M. D. Structures, Host-Guest Chemistry and Mechanism of Stepwise Self-Assembly of M_4L_6 Tetrahedral Cage Complexes. *Dalton Trans.* **2011**, *40*, 12132–12145.

182. Bolliger, J. L.; Ronson, T. K.; Ogawa, M.; Nitschke, J. R. Solvent Effects upon Guest Binding and Dynamics of a $Fe^{II}_4L_4$ Cage. *J. Am. Chem. Soc.* **2014**, *136*, 14545–14553.

183. Roy, B.; Zangrando, E.; Mukherjee, P. S. Self-Assembly of a Redox Active Water Soluble Pd_6L_8 'Molecular Dice'. *Chem Commun.* **2016**, *52*, 4489–4492.

184. Zhang, D.; Ronson, T. K.; Mosquera, J.; Martinez, A.; Guy, L.; Nitschke, J. R. Anion Binding in Water Drives Structural Adaptation in an Azaphosphatrane-Functionalized $Fe^{II}_4L_4$ Tetrahedron. *J. Am. Chem. Soc.* **2017**, *139*, 6574–6577.

185. Mosquera, J.; Szyszko, B.; Ho, S. K. Y.; Nitschke, J. R. Sequence-Selective Encapsulation and Protection of Long Peptides by a Self-Assembled $Fe^{II}_8L_6$ Cubic Cage. *Nat. Commun.* **2017**, *8*, 14882.

186. Bell, Z. R.; Harding, L. P.; Ward, M. D. Self-Assembly of a Molecular M_8L_{12} Cube having S_6 Symmetry. *Chem. Commun.* **2003**, 2432–2433.

187. Tidmarsh, I. S.; Faust, T. B.; Adams, H.; Harding, L. P.; Russo, L.; Clegg, W.; Ward, M. D. Octanuclear Cubic Coordination Cages. *J. Am. Chem. Soc.* **2008**, *130*, 15167–15175.

188. Najar, A. M.; Tidmarsh, I. S.; Adams, H.; Ward, M. D. Cubes, Squares, and Books: A Simple Transition Metal/Bridging Ligand Combination Can Lead to a Surprising Range of Structural Types with the Same Metal/Ligand Proportions. *Inorg. Chem.* **2009**, *48*, 11871–11881.

189. Argent, S. P.; Adams, H.; Harding, L. P.; Ward, M. D. A Closed Molecular Cube and an Open Book: Two Different Products from Assembly of the Same Metal Salt and Bridging Ligand. *Dalton Trans.* **2006**, 542–544.

190. Stephenson, A.; Ward, M. D. An Octanuclear Coordination Cage with a 'Cuneane' Core – A Topological Isomer of a Cubic Cage. *Dalton Trans.* **2011**, *40*, 7824–7826.

191. Stephenson, A.; Argent, S. P.; Riis-Johannessen, T.; Tidmarsh, I. S.; Ward, M. D. Structures and Dynamic Behavior of Large Polyhedral Coordination Cages: An Unusual Cage-to-Cage Interconversion. *J. Am. Chem. Soc.* **2011**, *133*, 858–870.

192. Al-Rasbi, N. K.; Tidmarsh, I. S.; Argent, S. P.; Adams, H.; Harding, L. P.; Ward, M. D. Mixed-Ligand Molecular Paneling: Dodecanuclear Cuboctahedral Coordination Cages Based on a Combination of Edge-Bridging and Face-Capping Ligands. *J. Am. Chem. Soc.* **2008**, *130*, 11641–11649.

193. Argent, S. P.; Adams, H.; Riis-Johannessen, T.; Jeffery, J. C.; Harding, L. P.; Mamula, O.; Ward, M. D. Coordination Chemistry of Tetradentate N-Donor Ligands Containing Two Pyrazolyl-Pyridine Units Separated by a 1,8-Naphthyl Space: Dodecanuclear and Tetranuclear Coordination Cages and Cyclic Helicates. *Inorg. Chem.* **2006**, *45*, 3905–3919.

194. Bell, Z. R.; Jeffery, J. C.; McCleverty, J. A.; Ward, M. D. Assembly of a Truncated-Tetrahedral Chiral $[M_{12}(\mu\text{-}L)_{18}]^{24+}$ Cage. *Angew. Chem., Int. Ed.* **2002**, *41*, 2515–2518.

195. Stephenson, A.; Sykes, D.; Ward, M. D. Cu_{12} and Cd_{16} Coordination Cages and their Cu_3 and Cd_3 Subcomponents, and the Role of Inter-Ligand π-Stacking in Stabilising Cage Complexes. *Dalton Trans.* **2013**, *42*, 6756–6767.

196. Argent, S. P.; Jackson, F. C.; Chan, H. M.; Meyrick, S.; Taylor, C. G. P.; Ronson, T. K.; Rourke, J. P.; Ward, M. D. A Family of Diastereomeric Dodecanuclear Coordination Cages

Based on Inversion of Chirality of Individual Triangular Cyclic Helicate Faces. *Chem. Sci.* **2020**, *11*, 10167–10174.

197. Sham, K.-C.; Yiu, S.-M.; Kwong, H.-L. Dodecanuclear Hexagonal-Prismatic $M_{12}L_{18}$ Coordination Cages by Subcomponent Self-Assembly. *Inorg. Chem.* **2013**, *52*, 5648–5650.

198. Su, C.-Y.; Smith, M. D.; zur Loye, H.-C. Columnar Supramolecular Architecture Self-Assembled from S_4-Symmetric Coordination Nanotubes Encapsulating Neutral Guest Molecules. *Angew. Chem., Int. Ed.* **2003**, *42*, 4085–4089.

199. Zhang, Y.; Ali, B.; Wu, J.; Guo, M.; Yu, Y.; Liu, Z.; Tang, J. Construction of Metallosupramolecular Coordination Complexes: from Lanthanide Helicates to Octahedral Cages Showing Single-Molecule Magnet Behavior. *Inorg. Chem.* **2019**, *58*, 3167–3174.

200. Gianneschi, N. C.; Masar, M. S.; Mirkin, C. A. Development of a Coordination Chemistry-Based Approach for Functional Supramolecular Structures. *Acc. Chem. Res.* **2005**, *38*, 825–837.

201. Mendez-Arroyo, J.; d'Aquino, A. I.; Chinen, A. B.; Manraj, Y. D.; Mirkin, C. A. Reversible and Selective Encapsulation of Dextromethorphan and β-Estradiol Using an Asymmetric Molecular Capsule Assembled via the Weak-Link Approach. *J. Am. Chem. Soc.* **2017**, *139*, 1368–1371.

202. Mosquera, J.; Ronson, T. K.; Nitschke, J. R. Subcomponent Flexibility Enables Conversion between D_4-Symmetric $Cd^{II}_8L_8$ and T-Symmetric $Cd^{II}_4L_4$ Assemblies. *J. Am. Chem. Soc.* **2016**, *138*, 1812–1815.

203. Chen, Q.; Jiang, F.; Yuan, D.; Lyu, G.; Chen, L.; Hong, M. A Controllable and Dynamic Assembly System Based on Discrete Metallocages. *Chem. Sci.* **2014**, *5*, 483–488.

204. Zhao, L.; Wei, J.; Zhang, J.; He, C.; Duan, C. Encapsulation of a Quinhydrone Cofactor in the Inner Pocket of Cobalt Triangular Prisms: Combined Light-Driven Reduction of Protons and Hydrogenation of Nitrobenzene. *Angew. Chem., Int. Ed.* **2017**, *56*, 15284–15288.

205. Liu, Y.; Lin, Z.; He, C.; Zhao, L.; Duan, C. A Symmetry-Controlled and Face-Driven Approach for the Assembly of Cerium-Based Molecular Polyhedra. *Dalton Trans.* **2010**, *39*, 11122–11125.

206. Jiao, Y.; Zhang, J.; Zhang, L.; Lin, Z.; He, C.; Duan, C. Metal-Organic Polyhedra Containing 36 and 24 Folds of Amide Groups for Selective Luminescent Recognition of Natural Disaccharides. *Chem. Commun.* **2012**, *48*, 6022–6024.

207. Zhao, L.; Qu, S.; He, C.; Zhang, R.; Duan, C. Face-driven Octanuclear Cerium(IV) Luminescence Polyhedra: Synthesis and Luminescent Sensing Natural Saccharides. *Chem. Commun.* **2011**, *47*, 9387–9389.

208. Cai, L.-X.; Yan, D.-N.; Cheng, P.-M.; Xuan, J.-J.; Li, S.-C.; Zhou, L.-P.; Tian, C.-B.; Sun, Q.-F. Controlled Self-Assembly and Multistimuli-Responsive Interconversions of Three Conjoined Twin-Cages. *J. Am. Chem. Soc.* **2021**, *143*, 2016–2024.

209. Cheng, P.-M.; Cai, L.-X.; Li, S.-C.; Hu, S.-J.; Yan, D.-N.; Zhou, L.-P.; Sun, Q.-F. Guest-Reaction Driven Cage to Conjoined Twin-Cage Mitosis-Like Host Transformation. *Angew. Chem., Int. Ed.* **2020**, 5*9*, 23569–23573.

210. Xuan, W.; Zhang, M.; Liu, Y.; Chen, Z.; Cui, Y. A Chiral Quadruple-Stranded Helicate Cage for Enantioselective Recognition and Separation. *J. Am. Chem. Soc.* **2012**, *134*, 6904–6907.

211. Luo, D.; Wang, X.-Z.; Yang, C.; Zhou, X.-P.; Li, D. Self-Assembly of Chiral Metal-Organic Tetartoid. *J. Am. Chem. Soc.* **2018**, *140*, 118–121.

212. Luo, D.; Zhou, X.-P.; Li, D. Beyond Molecules: Mesoporous Supramolecular Frameworks Self-Assembled from Coordination Cages and Inorganic Anions. *Angew. Chem., Int. Ed.* **2015**, *54*, 6190–6195.

213. Wang, X.-Z.; Sun, M.-Y.; Zheng, J.; Luo, D.; Qi, L.; Zhou, X.-P.; Li, D. Coordination-Driven Self-Assembly of $M_{10}L_8$ Metal-Organic Bi-Capped Square Antiprisms with Adaptable Cavities. *Dalton Trans.* **2019**, *48*, 17713–17717.

214. Lai, Y.-L.; Wang, X.-Z.; Dai, R.-R.; Huang, Y.-L.; Zhou, X.-C.; Zhou, X.-P.; Li, D. Self-Assembly of Mixed-Valence and Heterometallic Metallocycles: Efficient Catalysts for the Oxidation of Alcohols to Aldehydes in Ambient Air. *Dalton Trans.* **2020**, *49*, 7304–7308.

215. Lai, Y.-L.; Wang, X.-Z.; Zhou, X.-C.; Dai, R.-R.; Zhou. X.-P.; Li, D. Self-assembly of a Mixed Valence Copper Triangular Prism and Transformation to Cage Triggered by an External Stimulus. *Inorg. Chem.* **2020**, *59*, 17374–17378.

216. Samanta, D.; Mukherjee, S.; Patil, Y. P.; Mukherjee, P. S. Self-Assembled Pd_6 Open Cage with Triimidazole Walls and the Use of its Confined Nanospace for Catalytic Knoevenagel- and Diels-Alder Reactions in Aqueous Medium. *Chem. Eur. J.* **2012**, *18*, 12322–12329.

217. Fujita, M.; Yu, S.-Y.; Kusukawa, T.; Funaki, H.; Ogura, K.; Yamaguchi, K. Self-Assembly of Nanometer-Sized Macrotricyclic Complexes from Ten Small Component Molecules. *Angew. Chem., Int. Ed.* **1998**, *37*, 2082–2085.

218. Canton, M.; Grommet, A. B.; Pesce, L.; Gemen, J.; Li, S.; Diskin-Posner, Y.; Credi, A.; Pavan, G. M.; Andréasson, J.; Klajn, R. Improving Fatigue Resistance of Dihydropyrene by Encapsulation within a Coordination Cage. *J. Am. Chem. Soc.* **2020**, *142*, 14557–14565.

219. Pesce, L.; Perego, C.; Grommet, A. B.; Klajn, R.; Pavan, G. M. Molecular Factors Controlling the Isomerization of Azobenzenes in the Cavity of a Flexible Coordination Cage. *J. Am. Chem. Soc.* **2020**, *142*, 9792–9802.

220. Samanta, D.; Galaktionova, D.; Gemen, J.; Shimon, L. J. W.; Diskin-Posner, Y.; Avram, L.; Král, P.; Klajn, R. Reversible Chromism of Spiropyran in the Cavity of a Flexible Coordination Cage. *Nat. Commun.* **2018**, *9*, 641.

221. Samanta, D.; Gemen, J.; Chu, Z.; Diskin-Posner, Y.; Shimon, L. J. W.; Klajn, R. Reversible Photoswitching of Encapsulated Azobenzenes in Water. *PNAS* **2018**, *115*, 9379–9384.

222. Fujita, N.; Biradha, K.; Fujita, M.; Sakamoto, S.; Yamaguchi, K. A Porphyrin Prism: Structural Switching Triggered by Guest Inclusion. *Angew. Chem., Int. Ed.* **2001**, *40*, 1718–1721.

223. Bar, A. K.; Mohapatra, S.; Zangrando, E.; Mukherjee, P. S. A Series of Trifacial Pd_6 Molecular Barrels with Porphyrin Walls. *Chem. Eur. J.* **2012**, *18*, 9571–9579.

224. Roy, B.; Ghosh, A. K.; Srivastava, S.; D'Silva, P.; Mukherjee, P. S. A Pd_8 Tetrafacial Molecular Barrel as Carrier for Water Insoluble Fluorophore. *J. Am. Chem. Soc.* **2015**, *137*, 11916–11919.

225. Argent, S. P.; Greenaway, A.; Gimenez-Lopez, M. D. C.; Lewis, W.; Nowell, H.; Khlobystov, A. N.; Blake, A. J.; Champness, N. R.; Schröder, M. High-Nuclearity Metal-Organic Nanospheres: A Cd_{66} Ball. *J. Am. Chem. Soc.* **2012**, *134*, 55–58.

226. Tashiro, S.; Tominaga, M.; Kusukawa, T.; Kawano, M.; Sakamoto, S.; Yamaguchi, K.; Fujita, M. Pd^{II}-Directed Dynamic Assembly of a Dodecapyridine Ligand into End-Capped and Open Tubes: The Importance of Kinetic Control in Self-Assembly. *Angew. Chem., Int. Ed.* **2003**, *42*, 3267–3270.

227. Bandi, S.; Pal, A. K.; Hanan, G. S.; Chand, D. K. Stoichiometrically Controlled Revocable Self-Assembled 'Spiro' versus Quadruple-Stranded 'Double-Decker' Type Coordination Cages. *Chem. Eur. J.* **2014**, *20*, 13122–13126.

228. Zarra, S.; Clegg, J. K.; Nitschke, J. R. Selective Assembly and Disassembly of a Water-Soluble $Fe_{10}L_{15}$ Prism. *Angew. Chem., Int. Ed.* **2013**, *52*, 4837–4840.

229. Kieffer, M.; Pilgrim, B. S.; Ronson, T. K.; Roberts, D. A.; Aleksanyan, M.; Nitschke, J. R. Perfluorinated Ligands Induce Meridional Metal Stereochemistry to Generate M_8L_{12}, $M_{10}L_{15}$, and $M_{12}L_{18}$ Prisms. *J. Am. Chem. Soc.* **2016**, *138*, 6813–6821.

230. Metherell, A. J.; Ward, M. D. Geometric Isomerism in Coordination Cages Based on Tris-chelate Vertices: a Tool to Control both Assembly and Host/Guest Chemistry. *Dalton Trans.* **2016**, *45*, 16096–16111.

231. Castilla, A. M.; Ramsay, W. J.; Nitschke, J. R. Stereochemistry in Subcomponent Self-Assembly. *Acc. Chem. Res.* **2014**, *47*, 2063–2073.

232. Carpenter, J. P.; McTernan, C. T.; Greenfield, J. L.; Lavendomme, R.; Ronson, T. K.; Nitschke, J. R. Controlling the Shape and Chirality of an Eight-Crossing Molecular Knot. *Chem* **2021**, *7*, 1534–1543.

233. Kilbas, B.; Mirtschin, S.; Scopelliti, R.; Severin, K. A Solvent-Responsive Coordination Cage. *Chem. Sci.* **2012**, *3*, 701–704.

234. Lu, X.; Li, X.; Guo, K.; Xie, T.-Z.; Moorefield, C. N.; Wesdemiotis, C.; Newkome, G. R. Probing a Hidden World of Molecular Self-Assembly: Concentration-Dependent, Three-Dimensional Supramolecular Interconversions. *J. Am. Chem. Soc.* **2014**, *136*, 18149–18155.

235. Xie, T.-Z.; Endres, K. J.; Guo, Z.; Ludlow, J. M. III; Moorefield, C. N.; Saunders, M. J.; Wesdemiotis, C.; Newkome, G. R. Controlled Interconversion of Superposed-Bistriangle, Octahedron, and Cuboctahedron Cages Constructed Using a Single, Terpyridinyl-Based Polyligand and Zn^{2+}. *J. Am. Chem. Soc.* **2016**, *138*, 12344–12347.

236. Endo, K.; Ube, H.; Shionoya, M. Multi-Stimuli-Responsive Interconversion between Bowl- and Capsule-Shaped Self-Assembled Zinc(II) Complexes. *J. Am. Chem. Soc.* **2020**, *142*, 407–416.

237. Nakamura, T.; Ube, H.; Shiro, M.; Shionoya, M. A Self-Assembled Multiporphyrin Cage Complex through Three Different Zinc(II) Center Formation under Well-Balanced Aqueous Conditions. *Angew. Chem., Int. Ed.* **2013**, *52*, 720–723.

238. Rizzuto, F. J.; Pröhm, P.; Plajer, A. J.; Greenfield, J. L.; Nitschke, J. R. Hydrogen-Bond-Assisted Symmetry Breaking in a Network of Chiral Metal-Organic Assemblies. *J. Am. Chem. Soc.* **2019**, *141*, 1707–1715.

239. Sørensen, A.; Castilla, A. M.; Ronson, T. K.; Pittelkow, M.; Nitschke, J. R. Chemical Signals Turn on Guest Binding through Structural Reconfiguration of Triangular Helicates. *Angew. Chem., Int. Ed.* **2013**, *52*, 11273–11277.

240. Zhan, Y.-Y.; Kojima, T.; Ishii, K.; Takahashi, S.; Haketa, Y.; Maeda, H.; Uchiyama, S.; Hiraoka, S. Temperature-controlled Repeatable Scrambling and Induced-Sorting of Building Blocks between Cubic Assemblies. *Nat. Commun.* **2019**, *10*, 1440.

241. Yoshizawa, M.; Nakagawa, J.; Kumazawa, K.; Nagao, M.; Kawano, M.; Ozeki, T.; Fujita, M. Discrete Stacking of Large Aromatic Molecules within Organic-Pillared Coordination Cages. *Angew. Chem., Int. Ed.* **2005**, *44*, 1810–1813.

242. Wang, S.; Sawada, T.; Ohara, K.; Yamaguchi, K.; Fujita, M. Capsule-Capsule Conversion by Guest Encapsulation. *Angew. Chem., Int. Ed.* **2016**, *55*, 2063–2066.

243. Wang, S.; Sawada, T.; Fujita, M. Capsule-Bowl Conversion Triggered by a Guest Reaction. *Chem. Commun.* **2016**, *52*, 11653–11656.

244. Hiraoka, S.; Fujita, M. Guest-Selected Formation of Pd(II)-Linked Cages from a Prototypical Dynamic Library. *J. Am. Chem. Soc.* **1999**, *121*, 10239–10240.

245. Wood, D. M.; Meng, W.; Ronson, T. K.; Stefankiewicz, A. R.; Sanders, J. K. M.; Nitschke, J. R. Guest-Induced Transformation of a Porphyrin-Edged $Fe^{II}_4L_6$ Capsule into a $Cu^IFe^{II}_2L_4$ Fullerene Receptor. *Angew. Chem., Int. Ed.* **2015**, *54*, 3988–3992.

246. Rizzuto, F. J.; Nitschke, J. R. Stereochemical Plasticity Modulates Cooperative Binding in a $Co^{II}_{12}L_6$ Cuboctahedron. *Nat. Chem.* **2017**, *9*, 903–908.

247. Müller, I. M.; Möller, D. Rational Design of a Coordination Cage with a Trigonal-Bipyramidal Shape Constructed from 33 Building Units. *Angew. Chem., Int. Ed.* **2005**, *44*, 2969–2973.

248. Guo, J.; Chang, Q.; Liu, Z.; Wang, Y.; Liu, C.; Wang, M.; Huang, D.; Chen, G.; Zhao, H.; Wang, W.; Fang, X. How to Not Build a Cage: Endohedral Functionalization of Polyoxometalate-Based Metal-Organic Polyhedra. *Chem. Sci.* **2021**, *12*, 7361–7368.

249. Paterson, B. M.; White, K. F.; White, J. M.; Abrahams, B. F.; Donnelly, P. S. Guest-induced Assembly of Bis(thiosemicarbazonato) Zinc(II) Coordination Nanotubes. *Angew. Chem., Int. Ed.* **2017**, *56*, 8370–8374.

250. Yamashina, M.; Yuki, T.; Sei, Y.; Akita, M.; Yoshizawa, M. Anisotropic Expansion of an M_2L_4 Coordination Capsule: Host Capability and Frame Rearrangement. *Chem. Eur. J.* **2015**, *21*, 4200–4204.

251. Tsutsui, T.; Catti, L.; Yoza, K.; Yoshizawa, M. An Atropisomeric M_2L_4 Cage Mixture Displaying Guest-Induced Convergence and Strong Guest Emission in Water. *Chem. Sci.* **2020**, *11*, 8145–8150.

252. Riddell, I. A.; Smulders, M. M. J.; Clegg, J. K.; Hristova, Y. R.; Breiner, B.; Thoburn, J. D.; Nitschke, J. R. Anion-Induced Reconstitution of a Self-Assembling System to Express a Chloride-Binding $Co_{10}L_{15}$ Pentagonal Prism. *Nat. Chem.* **2012**, *4*, 751–756.

253. Ayme, J.-F.; Beves, J. E.; Campbell, C. J.; Gil-Ramírez, G.; Leigh, D. A.; Stephens, A. J. Strong and Selective Anion Binding within the Central Cavity of Molecular Knots and Links. *J. Am. Chem. Soc.* **2015**, *137*, 9812–9815.

254. Zhang, L.; Stephens, A. J.; Lemonnier, J.-F.; Pirvu, L.; Vitorica-Yrezabal, I. J.; Robinson, C. J.; Leigh, D. A. Coordination Chemistry of a Molecular Pentafoil Knot. *J. Am. Chem. Soc.* **2019**, *141*, 3952–3958.

255. Marcos, V.; Stephens, A. J.; Jaramillo-Garcia, J.; Nussbaumer, A. L.; Woltering, S. L.; Valero, A.; Lemonnier, J.-F.; Vitorica-Yrezabal, I. J.; Leigh, D. A. Allosteric Initiation and Regulation of Catalysis with a Molecular Knot. *Science* **2016**, *352*, 1555−1559.

256. Riddell, I. A.; Hristova, Y. R.; Clegg, J. K.; Wood, C. S.; Breiner, B.; Nitschke, J. R. Five Discrete Multinuclear Metal-Organic Assemblies from One Ligand: Deciphering the Effects of Different Templates. *J. Am. Chem. Soc.* **2013**, *135*, 2723–2733.

257. Riddell, I. A.; Ronson, T. K.; Clegg, J. K.; Wood, C. S.; Bilbeisi, R. A.; Nitschke, J. R. Cation- and Anion-Exchanges Induce Multiple Distinct Rearrangements within Metallosupramolecular Architectures. *J. Am. Chem. Soc.* **2014**, *136*, 9491–9498.

258. Riddell, I. A.; Ronson, T. K.; Nitschke, J. R. Mutual Stabilisation between $M^{II}_4L_6$ Tetrahedra and $M^{II}X_4^{2-}$ Metallate Guests. *Chem. Sci.* **2015**, *6*, 3533–3537.

259. Haynes, C. J. E.; Zhu, J.; Chimerel, C.; Hernández-Ainsa, S.; Riddell, I. A.; Ronson, T. K.; Keyser, U. F.; Nitschke, J. R. Blockable $Zn_{10}L_{15}$ Ion Channels through Subcomponent Self-Assembly. *Angew. Chem., Int. Ed.* **2017**, *56*, 15388–15392.

260. Chifotides, H. T.; Giles, I. D.; Dunbar, K. R. Supramolecular Architectures with π-Acidic 3,6-Bis(2-pyridyl)-1,2,4,5-tetrazine Cavities: Role of Anion-π Interactions in the Remarkable Stability of Fe(II) Metallacycles in Solution. *J. Am. Chem. Soc.* **2013**, *135*, 3039–3055.

261. Yu, H.-J.; Liu, Z.-M.; Pan, M.; Wu, K.; Wei, Z.-W.; Xu, Y.-W.; Fan, Y.-N.; Wang, H.-P.; Su, C.-Y. Elucidating Anion-Dependent Formation and Conversion of Pd_2L_4 and Pd_3L_6 Metal-Organic Cages by Complementary Techniques. *Eur. J. Inorg. Chem.* **2018**, *2018*, 80–85.

262. Klein, C.; Gütz, C.; Bogner, M.; Topić, F.; Rissanen, K.; Lützen, A. A New Structural Motif for an Enantiomerically Pure Metallosupramolecular Pd_4L_8 Aggregate by Anion Templating. *Angew. Chem.*, *Int. Ed.* **2014**, *53*, 3739–3742.

263. Sun, X.; Johnson, D. W.; Caulder, D. L.; Raymond, K. N.; Wong, E. H. Rational Design and Assembly of $M_2M'_3L_6$ Supramolecular Clusters with C_{3h} Symmetry by Exploiting Incommensurate Symmetry Numbers. *J. Am. Chem. Soc.* **2001**, *123*, 2752–2763.

264. Sun, X.; Johnson, D. W.; Caulder, D. L.; Powers, R. E.; Raymond, K. N.; Wong, E. H. Exploiting Incommensurate Symmetry Numbers: Rational Design and Assembly of $M_2M'_3L_6$ Supramolecular Clusters with C_{3h} Symmetry. *Angew. Chem., Int. Ed.* **1999**, *38*, 1303–1307.

265. Wu, H.-B.; Wang, Q.-M. Construction of Heterometallic Cages with Tripodal Metalloligands. *Angew. Chem., Int. Ed.* **2009**, *48*, 7343–7345.

266. Li, X.; Wu, J.; He, C.; Zhang, R.; Duan, C. Multicomponent Self-Assembly of a Pentanuclear Ir-Zn Heterometal-Organic Polyhedron for Carbon Dioxide Fixation and Sulfite Sequestration. *Chem. Commun.* **2016**, *52*, 5104–5107.

267. Li, X.; Wu, J.; Chen, L.; Zhong, X.; He, C.; Zhang, R.; Duan, C. Engineering an Iridium-Containing Metal-Organic Molecular Capsule for Induced-Fit Geometrical Conversion and Dual Catalysis. *Chem. Commun.* **2016**, *52*, 9628–9631.

268. Sanz, S.; O'Connor, H. M.; Martí-Centelles, V.; Comar, P.; Pitak, M. B.; Coles, S. J.; Lorusso, G.; Palacios, E.; Evangelisti, M.; Baldansuren, A.; Chilton, N. F.; Weihe, H.; McInnes, E. J. L.; Lusby, P. J.; Piligkos, S.; Brechin, E. K. $[M^{III}_2M^{II}_3]^{n+}$ Trigonal Bipyramidal Cages Based on Diamagnetic and Paramagnetic Metalloligands. *Chem. Sci.* **2017**, *8*, 5526–5535.

269. Garrison, J. C.; Panzner, M. J.; Custer, P. D.; Reddy, D. V.; Rinaldi, P. L.; Tessier, C. A.; Youngs, W. J. Synthesis and Characterization of a Trigonal Bipyramidal Supramolecular Cage Based Upon Rhodium and Platinum Metal Centers. *Chem. Commun.* **2006**, 4644–4646.

270. Hardy, M.; Struch, N.; Holstein, J. J.; Schnakenburg, G.; Wagner, N.; Engeser, M.; Beck, J.; Clever, G. H.; Lützen, A. Dynamic Complex-to-Complex Transformations of Heterobimetallic Systems Influence the Cage Structure or Spin State of Iron(II) Ions. *Angew. Chem., Int. Ed.* **2020**, *59*, 3195–3200.

271. Smulders, M. M. J.; Jiménez, A.; Nitschke, J. R. Integrative Self-Sorting Synthesis of a $Fe_8Pt_6L_{24}$ Cubic Cage. *Angew. Chem., Int. Ed.* **2012**, *51*, 6681–6685.

272. Preston, D.; Sutton, J. J.; Gordon, K. C.; Crowley, J. D. A Nona-nuclear Heterometallic Pd_3Pt_6 "Donut"-Shaped Cage: Molecular Recognition and Photocatalysis. *Angew. Chem., Int. Ed.* **2018**, *57*, 8659–8663.

273. Metherell, A. J.; Ward, M. D. Stepwise Synthesis of a Ru_4Cd_4 Coordination Cage Using Inert and Labile Subcomponents: Introduction of Redox Activity at Specific Sites. *Chem. Commun.* **2014**, *50*, 6330–6332.

274. Metherell, A. J.; Ward, M. D. Stepwise Assembly of an Adamantoid Ru_4Ag_6 Cage by Control of Metal Coordination Geometry at Specific Sites. *Chem. Commun.* **2014**, *50*, 10979–10982.

275. Wragg, A. B.; Metherell, A. J.; Cullen, W.; Ward, M. D. Stepwise Assembly of Mixed-Metal Coordination Cages Containing both Kinetically Inert and Kinetically Labile Metal Ions: Introduction of Metal-Centred Redox and Photophysical Activity at Specific Sites. *Dalton Trans.* **2015**, *44*, 17939–17949.

276. Metherell, A. J.; Ward, M. D. Imposing Control on Self-Assembly: Rational Design and Synthesis of a Mixed-Metal, Mixed-Ligand Coordination Cage Containing Four Types of Component. *Chem. Sci.* **2016**, *7*, 910–915.

277. Metherell, A. J.; Cullen, W.; Stephenson, A.; Hunter, C. A.; Ward, M. D. *Fac* and *mer* Isomers of Ru(II) Tris(pyrazolyl-pyridine) Complexes as Models for the Vertices of Coordination Cages: Structural Characterisation and Hydrogen-bonding Characteristics. *Dalton Trans.* **2014**, *43*, 71–84.

278. Li, H.; Han, Y.-F., Lin, Y.-J.; Guo, Z.-W.; Jin, G.-X. Stepwise Construction of Discrete Heterometallic Coordination Cages Based on Self-Sorting Strategy. *J. Am. Chem. Soc.* **2014**, *136*, 2982–2985.

279. Li, J.-R.; Zhou, H.-C. Bridging-Ligand-Substitution Strategy for the Preparation of Metal–Organic Polyhedra. *Nat. Chem.* **2010**, *2*, 893–898.

280. Tranchemontagne, D. J.; Ni, Z.; O'Keeffe, M.; Yaghi, O. M. Reticular Chemistry of Metal–Organic Polyhedra. *Angew. Chem.*, *Int. Ed.* **2008**, *47*, 5136–5147.

281. Byrne, K.; Zubair, M.; Zhu, N.; Zhou, X.-P.; Fox, D. S.; Zhang, H.; Twamley, B.; Lennox, M. J.; Düren, T.; Schmitt, W. Ultra-Large Supramolecular Coordination Cages Composed of Endohedral Archimedean and Platonic Bodies. *Nat. Commun.* **2017**, *8*, 15268.

282. Carpenter, J. P.; McTernan, C. T.; Ronson, T. K.; Nitschke, J. R. Anion Pairs Template a Trigonal Prism with Disilver Vertices. *J. Am. Chem. Soc.* **2019**, *141*, 11409–11413.

283. Fatila, E. M.; Twum, E. B.; Karty, J. A.; Flood, A. H. Ion Pairing and Co-facial Stacking Drive High-Fidelity Bisulfate Assembly with Cyanostar Macrocyclic Hosts. *Chem. Eur. J.* **2017**, *23*, 10652–10662.

284. Minisci, F.; Citterio, A.; Giordano, C. Electron-Transfer Processes: Peroxydisulfate, a Useful and Versatile Reagent in Organic Chemistry. *Acc. Chem. Res.* **1983**, *16*, 27–32.

285. Wood, C. S.; Ronson, T. K.; Belenguer, A. M.; Holstein, J. J.; Nitschke, J. R. Two-Stage Directed Self-Assembly of a Cyclic [3]Catenane. *Nat. Chem.* **2015**, *7*, 354–358.

286. Wang, Z.; Su, H.-F.; Tan, Y.-Z.; Schein, S.; Lin, S.-C.; Liu, W.; Wang, S.-A.; Wang, W.-G.; Tung, C.-H.; Sun, D.; Zheng, L.-S. Assembly of Silver Trigons into a Buckyball-like Ag_{180} Nanocage. *PNAS* **2017**, *114*, 12132–12137.

287. McTernan, C. T.; Ronson, T. K.; Nitschke, J. R. Selective Anion Binding Drives the Formation of $Ag^I_8L_6$ and $Ag^I_{12}L_6$ Six-Stranded Helicates. *J. Am. Chem. Soc.* **2021**, *143*, 664–670.

288. Zhu, Z.-Z.; Tian, C.-B.; Sun, Q.-F. Coordination-Assembled Molecular Cages with Metal Cluster Nodes. *Chem. Rec.* **2021**, 21, 498–522.

289. Gong, Y.; Tao, Y.; Xu, N.; Sun, C.; Wang, X.; Su, Z. Two Polyoxovanadate-based Metal-Organic Polyhedra with Undiscovered "Near-miss Johnson Solid" Geometry. *Chem. Commun.* **2019**, *55*, 10701–10704.

290. Bao, S.-J.; Xu, Z.-M.; Ju, Y.; Song, Y.-L.; Wang, H.; Niu, Z.; Li, X.; Braunstein, P.; Lang, J.-P. The Covalent and Coordination Co-driven Assembly of Supramolecular Octahedral Cages with Controllable Degree of Distortion. *J. Am. Chem. Soc.* **2020**, *142*, 13356–13361.

291. Howlader, P.; Bhandari, P.; Chakraborty, D.; Clegg, J. K.; Mukherjee, P. S. Self-Assembly of a Pd_8 Macrocycle and Pd_{12} Homochiral Tetrahedral Cages Using Poly(tetrazolate) Linkers. *Inorg. Chem.* **2020**, *59*, 15454–15459.

292. Jiao, J.; Tan, C.; Li, Z.; Liu, Y.; Han, X.; Cui, Y. Design and Assembly of Chiral Coordination Cages for Asymmetric Sequential Reactions. *J. Am. Chem. Soc.* **2018**, *140*, 2251–2259.

293. Tandon, S.; Steuber, F. W.; Kathalikkattil, A. C.; Venkatesan, M.; Watson, G. W.; Schmitt, W. Modulating Structural and Electronic Properties of Rare Archimedean and Johnson-Type Mn Cages. *Inorg. Chem.* **2021**, *60*, 8388–8393.

294. Altmann, P. J.; Pöthig, A. Pillarplexes: A Metal-Organic Class of Supramolecular Hosts. *J. Am. Chem. Soc.* **2016**, *138*, 13171–13174.

295. Altmann, P. J.; Pöthig, A. A pH-Dependent, Mechanically Interlocked Switch: Organometallic [2]Rotaxane vs. Organic [3]Rotaxane. *Angew. Chem., Int. Ed.* **2017**, *56*, 15733–15736.

296. Hiraoka, S.; Harano, K.; Tanaka, T.; Shiro, M.; Shionoya, M. Quantitative Formation of Sandwich-Shaped Trinuclear Silver(I) Complexes and Dynamic Nature of Their $P \rightleftharpoons M$ Flip Motion in Solution. *Angew. Chem., Int. Ed.* **2003**, *42*, 5182–5185.

297. Sun, Q.-F.; Iwasa, J.; Ogawa, D.; Ishido, Y.; Sato, S.; Ozeki, T.; Sei, Y.; Yamaguchi, K.; Fujita, M. Self-Assembled $M_{24}L_{48}$ Polyhedra and Their Sharp Structural Switch upon Subtle Ligand Variation. *Science* **2010**, *328*, 1144–1147.

298. Fujita, D.; Ueda, Y.; Sato, S.; Yokoyama, H.; Mizuno, N.; Kumasaka, T.; Fujita, M. Self-Assembly of $M_{30}L_{60}$ Icosidodecahedron. *Chem* **2016**, *1*, 91–101.

299. Bunzen, J.; Iwasa, J.; Bonakdarzadeh, P.; Numata, E.; Rissanen, K.; Sato, S.; Fujita, M. Self-Assembly of $M_{24}L_{48}$ Polyhedra Based on Empirical Prediction. *Angew. Chem., Int. Ed.* **2012**, *51*, 3161–3163.

300. Harris, K.; Fujita, D.; Fujita, M. Giant Hollow M_nL_{2n} Spherical Complexes: Structure, Functionalisation and Applications. *Chem. Commun.* **2013**, *49*, 6703–6712.

301. Saha, S.; Regeni, I.; Clever, G. H. Structure Relationships between Bis-Monodentate Ligands and Coordination Driven Self-Assemblies. *Coord. Chem. Rev.* **2018**, *374*, 1–14.

302. Suzuki, K.; Kawano, M.; Fujita, M. Solvato-Controlled Assembly of Pd_3L_6 and Pd_4L_8 Coordination "Boxes". *Angew. Chem., Int. Ed.* **2007**, *46*, 2819–2822.

303. Kishida, N.; Matsumoto, K.; Tanaka, Y.; Akita, M.; Sakurai, H.; Yoshizawa, M. Anisotropic Contraction of a Polyaromatic Capsule and its Cavity-Induced Compression Effect. *J. Am. Chem. Soc.* **2020**, *142*, 9599–9603.

304. Fujita, D.; Ueda, Y.; Sato, S.; Mizuno, N.; Kumasaka, T.; Fujita, M. Self-Assembly of Tetravalent Goldberg Polyhedra from 144 Small Components. *Nature* **2016**, *540*, 563–566.

305. Malay, A. D.; Miyazaki, N.; Biela, A.; Chakraborti, S.; Majsterkiewicz, K.; Stupka, I.; Kaplan, C. S.; Kowalczyk, A.; Piette, B. M. A. G.; Hochberg, G. K. A.; Wu, D.; Wrobel, T. P.; Fineberg, A.; Kushwah, M. S.; Kelemen, M.; Vavpetič, P.; Pelicon, P.; Kukura, P.; Benesch, J. L. P.; Iwasaki, K.; Heddle, J. G. An Ultra-stable Gold-coordinated Protein Cage Displaying Reversible Assembly. *Nature* **2019**, *569*, 438–442.

306. Liu, D.; Chen, M.; Li, K.; Li, Z.; Huang, J.; Wang, J.; Jiang, Z.; Zhang, Z.; Xie, T.; Newkome, G. R.; Wang, P. Giant Truncated Metallo-Tetrahedron with Unexpected Supramolecular Aggregation Induced Emission Enhancement. *J. Am. Chem. Soc.* **2020**, *142*, 7987–7994.

307. Liu, D.; Chen, M.; Li, Y.; Shen, Y.; Huang, J.; Yang, X.; Jiang, Z.; Li, X.; Newkome, G. R.; Wang, P. Vertical Assembly of Giant Double- and Triple-Decker Spoked Wheel Supramolecular Structures. *Angew. Chem., Int. Ed.* **2018**, *57*, 14116–14120.

308. Barrow, S. J.; Kasera, S.; Rowland, M. J.; del Barrio, J.; Scherman, O. A. Cucurbituril-Based Molecular Recognition. *Chem. Rev.* **2015**, *115*, 12320–12406.

309. Ogoshi, T.; Yamagishi, T.-A.; Nakamoto, Y. Pillar-Shaped Macrocyclic Hosts Pillar[n]arenes: New Key Players for Supramolecular Chemistry. *Chem. Rev.* **2016**, *116*, 7937–8002.

310. Rieth, S.; Hermann, K.; Wang, B.-Y.; Badjić, J. D. Controlling the Dynamics of Molecular Encapsulation and Gating. *Chem. Soc. Rev.* **2011**, *40*, 1609–1622.

311. Sakata, Y.; Murata, C.; Akine, S. Anion-Capped Metallohost Allows Extremely Slow Guest Uptake and On-Demand Acceleration of Guest Exchange. *Nat. Commun.* **2017**, *8*, 16005.

312. Bivaud, S.; Balandier, J.-Y.; Chas, M.; Allain, M.; Goeb, S.; Sallé, M. A Metal-Directed Self-Assembled Electroactive Cage with Bis(pyrrolo)tetrathiafulvalene (BPTTF) Side Walls. *J. Am. Chem. Soc.* **2012**, *134*, 11968–11970.

313. Caskey, D. C.; Yamamoto, T.; Addicott, C.; Shoemaker, R. K.; Vacek, J.; Hawkridge, A. M.; Muddiman, D. C.; Kottas, G. S.; Michl, J.; Stang, P. J. Coordination-Driven Face-Directed Self-Assembly of Trigonal Prisms. Face-Based Conformational Chirality. *J. Am. Chem. Soc.* **2008**, *130*, 7620–7628.

314. Chang, X.; Lin, S.; Wang, G.; Shang, C.; Wang, Z.; Liu, K.; Fang, Y.; Stang, P. J. Self-Assembled Perylene Bisimide-Cored Trigonal Prism as an Electron-Deficient Host for C_{60} and C_{70} Driven by "Like Dissolves Like". *J. Am. Chem. Soc.* **2020**, *142*, 15950–15960.

315. Bhat, I. A.; Jain, R.; Siddiqui, M. M.; Saini, D. K.; Mukherjee, P. S. Water-Soluble Pd_8L_4 Self-Assembled Molecular Barrel as an Aqueous Carrier for Hydrophobic Curcumin. *Inorg. Chem.* **2017**, *56*, 5352–5360.

316. Bhandari, P.; Modak, R.; Bhattacharyya, S.; Zangrando, E.; Mukherjee, P. S. Self-Assembly of Octanuclear Pt^{II}/Pd^{II} Coordination Barrels and Uncommon Structural Isomerization of a Photochromic Guest in Molecular Space. *JACS Au*, **2021**, *1*, 2242–2248.

317. Goeb, S.; Bivaud, S.; Croué, V.; Vajpayee, V.; Allain, M.; Sallé, M. A Self-Assembled Electro-Active M_8L_4 Cage Based on Tetrathiafulvalene Ligands. *Materials* **2014**, *7*, 611–622.

318. Bhattacharyya, S.; Venkateswarulu, M.; Sahoo, J.; Zangrando, E.; De, M.; Mukherjee, P. S. Self-Assembled Pt^{II}_8 Metallosupramolecular Tubular Cage as Dual Warhead Antibacterial Agent in Water. *Inorg. Chem.* **2020**, *59*, 12690–12699.

319. Cecot, G.; Marmier, M.; Geremia, S.; De Zorzi, R.; Vologzhanina, A. V.; Pattison, P.; Solari, E.; Fadaei Tirani, F.; Scopelliti, R.; Severin, K. The Intricate Structural Chemistry of $M^{II}_{2n}L_n$-Type Assemblies. *J. Am. Chem. Soc.* **2017**, *139*, 8371–8381.

320. Tang, J.-H.; Ni, R.; He, Y.-Q.; Vanderlinden, R. T.; Li, Y.; Shi, B.; Li, Z.-Y.; Wang, H.; Li, X.; Sun, Y.; Zhong, Y.-W.; Stang, P. J. Metal–Organic Pt(II) Hexagonal-Prism Macrocycles and their Photophysical Properties. *Inorg. Chem.* **2019**, 58, 13376–13381.

321. Yang, J.; Bhadbhade, M.; Donald, W. A.; Iranmanesh, H.; Moore, E. G.; Yan, H.; Beves, J. E. Self-assembled Supramolecular Cages Containing Ruthenium(II) Polypyridyl Complexes. *Chem. Commun.* **2015**, *51*, 4465–4468.

322. Yamanoi, Y.; Sakamoto, Y.; Kusukawa, T.; Fujita, M.; Sakamoto, S.; Yamaguchi, K. Dynamic Assembly of Coordination Boxes from (en)Pd(II) Unit and a Rectangular Panel-Like Ligand: NMR, CSI-MS, and X-ray Studies. *J. Am. Chem. Soc.* **2001**, *123*, 980–981.

323. Cecot, G.; Alameddine, B.; Prior, S.; De Zorzi, R.; Geremia, S.; Scopelliti, R.; Fadaei, F. T.; Solari, E.; Severin, K. Large Heterometallic Coordination Cages with Gyrobifastigium-Like Geometry. *Chem. Commun.* **2016**, *52*, 11243–11246.

324. Howlader, P.; Mondal, B.; Purba, P. C.; Zangrando, E.; Mukherjee, P. S. Self-Assembled Pd(II) Barrels as Containers for Transient Merocyanine Form and Reverse Thermochromism of Spiropyran. *J. Am. Chem. Soc.* **2018**, *140*, 7952–7960.

325. Cecot, G.; Doll, M. T.; Planes, O. M.; Ramorini, A.; Scopelliti, R.; Fadaei-Tirani, F.; Severin, K. Cages vs. Prisms: Controlling the Formation of Metallosupramolecular Architectures with Ligand Side-Chains. *Eur. J. Inorg. Chem.* **2019**, 2972–2976.

326. Bhat, I. A.; Devaraj, A.; Zangrando, E.; Mukherjee, P. S. A Discrete Self-Assembled Pd_{12} Triangular Orthobicupola Cage and its Use for Intramolecular Cycloaddition. *Chem. Eur. J.* **2018**, *24*, 13938–13946.

327. Bhattacharyya, S.; Ali, S. R.; Venkateswarulu, M.; Howlader, P.; Zangrando, E.; De, M.; Mukherjee, P. S. Self-Assembled Pd_{12} Coordination Cage as Photoregulated Oxidase-Like Nanozyme. *J. Am. Chem. Soc.* **2020**, *142*, 18981–18989.

328. Aggarwal, B. B.; Kumar, A.; Bharti, A. C. Anticancer Potential of Curcumin: Preclinical and Clinical Studies. *Anticancer Res.* **2003**, *23*, 363-398.

329. Priyadarsini, K. I. Photophysics, Photochemistry and Photobiology of Curcumin: Studies from Organic Solutions, Bio-mimetics and Living Cells. *J. Photochem. Photobiol., C* **2009**, *10*, 81–95.

330. Anand, P.; Kunnumakkara, A. B.; Newman, R. A.; Aggarwal, B. B. Bioavailability of Curcumin: Problems and Promises. *Mol. Pharmaceutics* **2007**, *4*, 807–818.

331. Howlader, P.; Das, P.; Zangrando, E.; Mukherjee, P. S. Urea-Functionalized Self-Assembled Molecular Prism for Heterogeneous Catalysis in Water. *J. Am. Chem. Soc.* **2016**, *138*, 1668–1676.

332. Mu, C.; Zhang, Z.; Hou, Y.; Liu, H.; Ma, L.; Li, X.; Ling, S.; He, G.; Zhang, M. Tetraphenylethylene-Based Multicomponent Emissive Metallacages as Solid-State Fluorescent Materials. *Angew. Chem., Int. Ed.* **2021**, *60*, 12293–12297.

333. Meng, W.; Clegg, J. K.; Nitschke, J. R. Transformative Binding and Release of Gold Guests from a Self-Assembled Cu_8L_4 Tube. *Angew. Chem., Int. Ed.* **2012**, *51*, 1881–1884.

334. Meng, W.; League, A. B.; Ronson, T. K.; Clegg, J. K.; Isley, W. C.; Semrouni, D.; Gagliardi, L.; Cramer, C. J.; Nitschke, J. R. Empirical and Theoretical Insights into the Structural Features and Host-Guest Chemistry of M_8L_4 Tube Architectures. *J. Am. Chem. Soc.* **2014**, *136*, 3972–3980.

335. Cook, T. R.; Zheng, Y.-R.; Stang, P. J. Metal–Organic Frameworks and Self-Assembled Supramolecular Coordination Complexes: Comparing and Contrasting the Design, Synthesis, and Functionality of Metal–Organic Materials. *Chem. Rev.* **2013**, *113*, 734–777.

336. Bivaud, S.; Goeb, S.; Croué, V.; Dron, P. I.; Allain, M.; Sallé, M. Self-Assembled Containers Based on Extended Tetrathiafulvalene. *J. Am. Chem. Soc.* **2013**, *135*, 10018–10021.

337. Bivaud, S.; Goeb, S.; Croué, V.; Allain, M.; Pop, F.; Sallé, M. Tuning the Size of a Redox-Active Tetrathiafulvalene-Based Self-Assembled Ring. *Beilstein J. Org. Chem.* **2015**, *11*, 966–971.

338. Szalóki, G.; Krykun, S.; Croué, V.; Allain, M.; Morille, Y.; Aubriet, F.; Carré, V.; Voitenko, Z.; Goeb, S.; Sallé, M. Redox-Driven Transformation of a Discrete Molecular Cage into an Infinite 3D Coordination Polymer. *Chem. Eur. J.* **2018**, *24*, 11273–11277.

339. Croué V.; Goeb, S.; Szalóki, G.; Allain, M.; Sallé, M. Reversible Guest Uptake/Release by Redox-Controlled Assembly/Disassembly of a Coordination Cage. *Angew. Chem., Int. Ed.* **2016**, *55*, 1746–1750.

340. Zhu, R.; Regeni, I.; Holstein, J. J.; Dittrich, B.; Simon, M.; Prévost, S.; Gradzielski, M.; Clever, G. H. Catenation and Aggregation of Multi-Cavity Coordination Cages. *Angew. Chem., Int. Ed.* **2018**, *57*, 13652–13656.

341. Yazaki, K.; Akita, M.; Prusty, S.; Chand, D. K.; Kikuchi, T.; Sato, H.; Yoshizawa, M. Polyaromatic Molecular Peanuts. *Nat. Commun.* **2017**, *8*, 15914.

342. Matsumoto, K.; Kusaba, S.; Tanaka, Y.; Sei, Y.; Akita, M.; Aritani, K.; Haga, M.-a.; Yoshizawa, M. A Peanut-Shaped Polyaromatic Capsule: Solvent-Dependent Transformation and Electronic Properties of a Non-Contacted Fullerene Dimer. *Angew. Chem., Int. Ed.* **2019**, *58*, 8463–8467.

343. Samantray, S.; Krishnaswamy, S.; Chand, D. K. Self-Assembled Conjoined-Cages. *Nat. Commun.* **2020**, *11*, 880.

344. Aoyagi, M.; Biradha, K.; Fujita, M. Quantitative Formation of Coordination Nanotubes Templated by Rodlike Guests. *J. Am. Chem. Soc.* **1999**, *121*, 7457–7458.

345. Aoyagi, M.; Tashiro, S.; Tominaga, M.; Biradha, K.; Fujita, M. Spectroscopic and Crystallographic Studies on the Stability of Self-Assembled Coordination Nanotubes. *Chem. Commun.* **2002**, 2036–2037.

346. Yamaguchi, T.; Tashiro, S.; Tominaga, M.; Kawano, M.; Ozeki, T.; Fujita, M. A 3.5-nm Coordination Nanotube. *J. Am. Chem. Soc.* **2004**, *126*, 10818–10819.

347. Takeda, N.; Umemoto, K.; Yamaguchi, K.; Fujita, M. A Nanometre-sized Hexahedral Coordination Capsule Assembled from 24 Components. *Nature* **1999**, *398*, 794–796.

348. Umemoto, K.; Tsukui, H.; Kusukawa, T.; Biradha, K.; Fujita, M. Molecular Paneling by Coordination: An $M_{15}L_6$ Hexahedral Molecular Capsule having Clefts for Reversible Guest Inclusion. *Angew. Chem., Int. Ed.* **2001**, *40*, 2620–2622.

349. Umemoto, K.; Yamaguchi, K.; Fujita, M. Molecular Paneling via Coordination: Guest-Controlled Assembly of Open Cone and Tetrahedron Structures from Eight Metals and Four Ligands. *J. Am. Chem. Soc.* **2000**, *122*, 7150–7151.

350. Bhat, I. A.; Zangrando, E.; Mukherjee, P. S. Coordination-Driven Self-Assembly of Discrete Molecular Nanotubular Architectures. *Inorg. Chem.* **2019**, *58*, 11172–11179.

351. Bhat, I. A.; Samanta, D.; Mukherjee, P. S. A Pd_{24} Pregnant Molecular Nanoball: Self-Templated Stellation by Precise Mapping of Coordination Sites. *J. Am. Chem. Soc.* **2015**, *137*, 9497–9502.

352. Jeong, K. S.; Kim, Y. S.; Kim, Y. J.; Lee, E.; Yoon, J. H.; Park, W. H.; Park, Y. W.; Jeon, S.-J.; Kim, Z. H.; Kim, J.; Jeong, N. Lanthanitin: A Chiral Nanoball Encapsulating 18 Lanthanum Ions by Ferritin-Like Assembly. *Angew. Chem., Int. Ed.* **2006**, *45*, 8134–8138.

353. He, C.; Wang, J.; Zhao, L.; Liu, T.; Zhang, J.; Duan, C. A Photoactive Basket-Like Metal-Organic Tetragon Worked as an Enzymatic Molecular Flask for Light Driven H_2 Production. *Chem. Commun.* **2013**, *49*, 627–629.

354. Xu, J.; Raymond, K. N. Lord of the Rings: An Octameric Lanthanum Pyrazolonate Cluster. *Angew. Chem., Int. Ed.* **2000**, *39*, 2745–2747.

355. Tan, Y. B.; Okayasu, Y.; Katao, S.; Nishikawa, Y.; Asanoma, F.; Yamada, M.; Yuasa, J.; Kawai, T. Visible Circularly Polarized Luminescence of Octanuclear Circular Eu(III) Helicate. *J. Am. Chem. Soc.* **2020**, *142*, 17653–17661.

356. Johnson, D. W.; Xu, J.; Saalfrank, R. W.; Raymond, K. N. Self-Assembly of a Three-Dimensional $[Ga_6(L^2)_6]$ Metal-Ligand "Cylinder". *Angew. Chem., Int. Ed.* **1999**, *38*, 2882–2885.

357. Saalfrank, R. W.; Glaser, H.; Demleitner, B.; Hampel, F.; Chowdhry, M. M.; Schünemann, V.; Trautwein, A. X.; Vaughan, G. B. M.; Yeh, R.; Davis, A. V.; Raymond, K. N. Self-Assembly of Tetrahedral and Trigonal Antiprismatic Clusters $[Fe_4(L^4)_4]$ and $[Fe_6(L^5)_6]$ on the Basis of Trigonal Tris-Bidentate Chelators. *Chem. Eur. J.* **2002**, *8*, 493–497.

358. Chen, B.; Holstein, J. J.; Horiuchi, S.; Hiller, W. G.; Clever, G. H. Pd(II) Coordination Sphere Engineering: Pyridine Cages, Quinoline Bowls, and Heteroleptic Pills Binding One or Two Fullerenes. *J. Am. Chem. Soc.* **2019**, *141*, 8907–8913.

359. Bar, A. K.; Chakrabarty, R.; Mostafa, G.; Mukherjee, P. S. Self-assembly of a Nanoscopic $Pt_{12}Fe_{12}$ Heterometallic Open Molecular Box Containing Six Porphyrin Walls. *Angew. Chem., Int. Ed.* **2008**, *47*, 8455–8459.

360. Tang, X.; Chu, D.; Gong, W.; Cui, Y.; Liu, Y. Metal-Organic Cages with Missing Linker Defects. *Angew. Chem., Int. Ed.* **2021**, *60*, 9099–9105.

361. Rizzuto, F. J.; Kieffer, M.; Nitschke, J. R. Quantified Structural Speciation in Self-Sorted $Co^{II}_6L_4$ Cage Systems. *Chem. Sci.* **2018**, *9*, 1925–1930.

362. Ronson, T. K.; Wang, Y.; Baldridge, K.; Siegel, J. S.; Nitschke, J. R. An S_{10}-Symmetric 5-Fold Interlocked [2]Catenane. *J. Am. Chem. Soc.* **2020**, *142*, 10267–10272.

363. Jing, X.; He, C.; Zhao, L.; Duan, C. Photochemical Properties of Host–Guest Supramolecular Systems with Structurally Confined Metal–Organic Capsules. *Acc. Chem. Res.* **2019**, *52*, 100–109.

364. Wang, Q.-Q.; Gonell, S.; Leenders, S. H. A. M.; Dürr, M.; Ivanović-Burmazović, I.; Reek, J. N. H. Self-Assembled Nanospheres with Multiple Endohedral Binding Sites Pre-Organize Catalysts and Substrates for Highly Efficient Reactions. *Nat. Chem.* **2016**, *8*, 225–230.

365. Liu, W.; Stoddart, J. F. Emergent Behaviour in Nanoconfined Molecular Containers. *Chem* **2021**, *7*, 919–947.

366. Wang, Y.; Sun, Y.; Shi, P.; Sartin, M. M.; Lin, X.; Zhang, P.; Fang, H.; Peng, P.; Tian, Z.; Cao, X. Chaperone-Like Chiral Cages for Catalyzing Enantioselective Supramolecular Polymerization. *Chem. Sci.* **2019**, *10*, 8076–8082.

367. Li, L.; Yang, L.; Li, X.; Wang, J.; Liu, X.; He, C. Supramolecular Catalysis of Acyl Transfer within Zinc Porphyrin-Based Metal–Organic Cages. *Inorg. Chem.* **2021**, *60*, 8802–8810.

368. Ikbal, S. A.; Colomban, C.; Zhang, D.; Delecluse, M.; Brotin, T.; Dufaud, V.; Dutasta, J.-P.; Sorokin, A. B.; Martinez, A. Bioinspired Oxidation of Methane in the Confined Spaces of Molecular Cages. *Inorg. Chem.* **2019**, *58*, 7220–7228.

369. Syntrivanis, L.-D.; Némethová, I.; Schmid, D.; Levi, S.; Prescimone, A.; Bissegger, F.; Major, D. T.; Tiefenbacher, K. Four-Step Access to the Sesquiterpene Natural Product Presilphiperfolan-1β-ol and Unnatural Derivatives via Supramolecular Catalysis. *J. Am. Chem. Soc.* **2020**, *142*, 5894–5900.

370. Wu, G.; Chen, Y.; Fang, S.; Tong, L.; Shen, L.; Ge, C.; Pan, Y.; Shi, X.; Li, H. A Self-Assembled Cage for Wide-Scope Chiral Recognition in Water. *Angew. Chem., Int. Ed.* **2021**, *60*, 16594–16599.

371. Jia, C.; Zuo, W.; Yang, D.; Chen, Y.; Cao, L.; Custelcean, R.; Hostaš, J.; Hobza, P.; Glaser, R.; Wang, Y.-Y.; Yang, X.-J.; Wu, B. Selective Binding of Choline by a Phosphate-Coordination-Based Triple Helicate Featuring an Aromatic Box. *Nat. Commun.* **2017**, *8*, 938.

372. Jia, F.; Hupatz, H.; Yang, L.-P.; Schröder, H. V.; Li, D.-H.; Xin, S.; Lentz, D.; Witte, F.; Xie, X.; Paulus, B.; Schalley, C. A.; Jiang, W. Naphthocage: A Flexible yet Extremely Strong Binder for Singly Charged Organic Cations. *J. Am. Chem. Soc.* **2019**, *141*, 4468–4473.

373. Chen, G.-H.; He, Y.-P.; Liang, F.-P.; Zhang, L.; Zhang, J. A Green Separation Process of Ag via a $Ti_4(embonate)_6$ Cage. *Dalton Trans.* **2020**, *49*, 17194–17199.

374. Sepehrpour, H.; Fu, W.; Sun, Y.; Stang, P. J. Biomedically Relevant Self-Assembled Metallacycles and Metallacages. *J. Am. Chem. Soc.* **2019**, *141*, 14005–14020.

375. Bloch, W. M.; Clever, G. H. Integrative Self-Sorting of Coordination Cages Based on 'Naked' Metal Ions. *Chem. Commun*. **2017**, *53*, 8506–8516.

376. Berardo, E.; Turcani, L.; Miklitz, M.; Jelfs, K. E. An Evolutionary Algorithm for the Discovery of Porous Organic Cages. *Chem. Sci.* **2018**, *9*, 8513–8527.

377. Turcani, L.; Greenaway, R. L.; Jelfs, K. E. Machine Learning for Organic Cage Property Prediction. *Chem. Mater.* **2019**, *31*, 714–727.

378. Berardo, E.; Greenaway, R. L.; Turcani, L.; Alston, B. M.; Bennison, M. J.; Miklitz, M.; Clowes, R.; Briggs, M. E.; Cooper, A. I.; Jelfs, K. E. Computationally-Inspired Discovery of an Unsymmetrical Porous Organic Cage. *Nanoscale* **2018**, *10*, 22381–22388.

379. Abet, V.; Szczypiński, F. T.; Little, M. A.; Santolini, V.; Jones, C. D.; Evans, R.; Wilson, C.; Wu, X.; Thorne, M. F.; Bennison, M. J.; Cui, P.; Cooper, A. I.; Jelfs, K. E.; Slater, A. G.

Inducing Social Self-Sorting in Organic Cages to Tune the Shape of the Internal Cavity. *Angew. Chem., Int. Ed.* **2020**, *59*, 16755–16763.

380. Tarzia, A.; Lewis, J. E. M.; Jelfs, K. E. High-throughput Computational Evaluation of Low Symmetry Pd_2L_4 Cages to Aid in System Design. *Angew. Chem., Int. Ed.* **2021**, *60*, 20879–20887.

381. Young, T. A.; Martí-Centelles, V.; Wang, J.; Lusby, P. J.; Duarte, F. Rationalizing the Activity of an "Artificial Diels-Alderase": Establishing Efficient and Accurate Protocols for Calculating Supramolecular Catalysis. *J. Am. Chem. Soc.* **2020**, *142*, 1300–1310.

382. Greenaway, R. L.; Jelfs, K. E. High-Throughput Approaches for the Discovery of Supramolecular Organic Cages. *ChemPlusChem* **2020**, *85*, 1813–1823.

383. Porwol, L.; Kowalski, D. J.; Henson, A.; Long, D.-L.; Bell, N. L.; Cronin, L. An Autonomous Chemical Robot Discovers the Rules of Inorganic Coordination Chemistry without Prior Knowledge. *Angew. Chem., Int. Ed.* **2020**, *59*, 11256–11261.

384. Greenaway, R. L.; Santolini, V.; Bennison, M. J.; Alston, B. M.; Pugh, C. J.; Little, M. A.; Miklitz, M.; Eden-Rump, E. G. B.; Clowes, R.; Shakil, A.; Cuthbertson, H. J.; Armstrong, H.; Briggs, M. E.; Jelfs, K. E.; Cooper, A. I. High-Throughput Discovery of Organic Cages and Catenanes Using Computational Screening Fused with Robotic Synthesis. *Nat. Commun.* **2018**, *9*, 2849.

Acknowledgements:

Author Biographies:

Dr. Charlie McTernan

Charlie studied Chemistry (MChem) at Hertford College, University of Oxford. His Part II project was conducted under the supervision of Prof. Tim Donohoe, investigating the synthesis of isoquinoline motifs using palladium-catalyzed α-arylation. He joined Prof. David Leigh's group in 2013, funded by a University of Manchester Dean's Faculty Award. His doctoral research included the synthesis of artificial molecular machines, switchable catalysts, and rotaxanes. In 2017 he joined the Nitschke Research Group, then in 2018 he began his Leverhulme Early Career Research Fellowship, jointly funded by the Isaac Newton Trust, and joined Sidney Sussex College as a Research Fellow, where he investigated the synthesis and post-assembly modification of diverse metal-organic capsules, and ways to tie molecular knots in single molecules. In 2021, he started his independent career at the Francis Crick Institute and King's College London, exploring how interlocked architectures and metal-organic capsules can be applied in biological settings.

Jack Davies

Jack received an MChem from the University of Manchester in 2018. During this time, he completed an internship at Nanoco Technologies, and a year-long industrial placement in medicinal chemistry at F. Hoffmann-La Roche. His final year research project was in the field of metallosupramolecular chemistry, conducted under the supervision of Dr. Imogen Riddell. In 2018 he began doctoral research in the group of Prof. Jonathan Nitschke at the University of Cambridge.

Prof. Jonathan Nitschke

Jonathan R. Nitschke was born in Syracuse, New York, USA. He received his Bachelor of Arts in chemistry from Williams College in 1995, remaining confused to this day as to whether chemistry is an art, and his doctorate from the University of California, Berkeley, in 2001, under the supervision of T. Don Tilley. He then undertook postdoctoral studies with Jean-Marie Lehn in Strasbourg, and in 2003 he started his independent research career as a Maître-assistant (fixed-term PI) in the Organic Chemistry Department of the University of Geneva. In 2007, he was appointed University Lecturer at Cambridge, where he has been a full professor since 2014. His research program investigates the self-assembly of complex, functional structures from simple molecular precursors and metal ions.